POLITECNICO DI MILANO

SCUOLA DI INGEGNERIA DEI PROCESSI INDUSTRIALI

DIPARTIMENTO DI CHIMICA, MATERIALI E INGEGNERIA CHIMICA
"GIULIO NATTA"

LAUREA SPECIALISTICA
INGEGNERIA DEI MATERIALI

"STRENGTH IMPROVEMENT OF ADHESIVE JOINTS THROUGH AIR PLASMA TREATMENT OPTIMIZATION"

Tutor for Politecnico di Milano:
Prof. Roberto FRASSINE

Co-tutor:
Prof. Luca ANDENA

Co-tutor for Imperial College of London:
Prof. Bamber K. R. BLACKMAN

Co-tutor for Politecnico di Torino:
Prof. Giovanni CAMINO

Thesis by:
Marco BONAITI
750399

ACADEMIC YEAR 2010/2011

Preface

During the last decades, the growing use of adhesion as a bonding mechanism has strongly contributed to its scientific development. Ever more demanding applications and advance in adhesives technologies raised the interest over the study of adhesion mechanisms and improvements in their mechanical performances.

Enormous steps have been made in recent years, justified by the deepening of adhesion understanding, made possible by new investigating techniques.
In shoes production, in particular, the role of adhesion is becoming more and more important since adhesives are beginning to outperform traditional mechanical junctions, such as seams. This trend justifies the studies in adhesion improvement in shoes sector and, therefore, this thesis.

Together with the technical goal of the thesis, a primary role of this work has been the acquisition and implementation of engineer forma mentis. This has been chief driver in approaching new problems through uncertainties, hypothesis, data, solutions and opportunities.

The thesis project, the first steps and most of technical experiment of this work have been performed at the Department of Mechanics of the Imperial College of London.

Figures index

Tables index

Abstract

The work investigated the many aspects concerning the establishment and improvement of adhesive phenomena through the optimization of a forced air plasma to treat polymeric joints typically adopted in shoe production. Polyamide 12 and ethylene vinyl acetate substrates have been jointed with monocomponent polyurethane glue. Two different types of EVA have been investigated: an unfilled copolymer and a blend containing fillers; a third foamed version has been assessed with certain limitations. Surface energy analyses have been performed on all adherends through the mean of contact angles measurements with four high surface tension liquids; Owen-Wendt-Rabel-Kaelble interpolation method has been used to assess both polar and dispersive components of surface energies of all polymers. The effect on surface energy originated by different cleaning procedures has also been investigated: polishing (up to 0.25 μm roughness), dry tissue wiping and deep detergent cleaning have been assessed. Plasma treatment parameters optimization has been carried out through water contact angle minimization: the number of plasma passes and the distance of the substrate from the plasma torch have been varied to obtain the highest surface energies for all polymers. 90° fixed arm peel tests have been performed on 12 different junctions: PA 12 has been bonded with two unfoamed EVAs using PU adhesive; plasma treatment has been varied obtaining four level of intensity. The high temperature induced by the plasma treatment has also been used to prepare junctions without glue, exploiting polymer diffusive phenomena. Fracture mechanic testing has been used to characterize adhesive fracture energy of joints. Double Lap Joint tests have been performed to assess shear adhesive properties of foamed EVA - PA 12 joints and to compare them with the peel tests results.

Finally, adhesive fracture energy results have been compared with surface measurements.

Abstract in italiano

Nel lavoro sono stati studiati i principali aspetti riguardanti l'instaurazione e il rafforzamento di fenomeni adesivi attraverso l'ottimizzazione di un trattamento al plasma ad aria forzata. Substrati di poliammide 12 (PA) ed etilen-vinilacetato (EVA), tipicamente utilizzati nella produzione di scarpe, sono stati incollati con adesivo poliuretanico monocomponente. Sono stati esaminati due EVA: un copolimero non caricato e un blend caricato; un'ulteriore terza versione espansa è stata analizzata sotto alcuni aspetti. Quattro liquidi ad alta tensione superficiale sono stati utilizzati, attraverso il metodo dell'angolo di contatto, per valutare le energie superficiali di tutti gli aderendi; sfruttando il metodo d'interpolazione di Owen-Wendt-Rabel-Kaelble è stato possibile valutare sia la componente polare dell'energia superficiale che quella dispersiva. È stato studiato in che modo tre differenti tipi di pulizia (lucidatura fino a 0.25μm, per mezzo di un panno secco e tramite detergente) influenzassero l'energia superficiale. È stata condotta un'ottimizzazione dei parametri di trattamento al plasma attraverso una minimizzazione dell'angolo di contatto dell'acqua: sono stati variati il numero di passate del plasma e la distanza tra il substrato e la pistola in modo da ottenere la massima energia superficiale per tutti i substrati. Prove di peeling a 90° sono state condotte su 12 tipi di giunti differenti: il PA è stato incollato con le due versioni non espanse di EVA tramite l'adesivo poliuretanico; la potenza del trattamento al plasma è stata variata in modo da ottenere quattro livelli di intensità. L'alta temperatura indotta dal plasma è stata inoltre utilizzata per preparare giunzioni adesive senza poliuretano, sfruttando fenomeni diffusivi. La meccanica della frattura è stata utilizzata per caratterizzare l'energia di frattura adesiva dei giunti. Prove di taglio su giunti a doppia sovrapposizione sono state condotte per valutare le proprietà adesive di giunzioni PA 12/EVA-espanso e i risultati sono stati comparati con quelli ottenuti dalle prove di peel.

In ultimo, le energie di frattura adesiva sono state confrontate con i valori di energia superficiale ottenuti in precedenza dagli stessi trattamenti al plasma.

Ampio estratto in italiano

La tesi ha approfondito diversi aspetti riguardanti l'instaurazione e il rafforzamento di fenomeni adesivi in un giunto tipicamente utilizzato nella produzione di scarpe: l'incollaggio tra una suola e il relativo corpo della calzatura. Il lavoro è stato svolto in collaborazione con Nike, che ha fornito i materiali: una poliammide 12 (PA) e una versione espansa di un copolimero etilen-vinilacetato (EVA). Vista la natura cellulare dell'EVA, che ha creato difficoltà con alcuni tipi di test, il produttore ha fornito due ulteriori versioni non espanse dello stesso materiale. La seconda versione rispecchia la stessa composizione chimica del primo EVA, ma in forma non espansa, mentre il terzo copolimero, oltre a non essere espanso, è anche privo di fillers (è stato in questo modo possibile valutare anche l'effetto delle cariche sull'adesione).

Lo scopo del lavoro è l'incremento della resistenza a frattura di giunti PA-EVA e la misurazione delle loro proprietà meccaniche. Il miglioramento delle proprietà adesive degli aderendi è stato implementato attraverso l'ottimizzazione di un trattamento al plasma ad aria forzata sui polimeri da collegare. A questo scopo sono stati eseguiti diversi tipi di prove, sia di tipo meccanico sia di analisi di superfice: questo breve estratto ripercorre sinteticamente le premesse, le ipotesi, le analisi e i risultati cui si è giunti durante il lavoro.

La prima parte della tesi si è concentrata sull'analisi delle energie superficiali di tutti gli aderendi. Uno dei requisiti fondamentali perché s'instaurino forze adesive tra due materiali è che si stabilisca tra essi un intimo contatto, in grado di promuovere la formazione di interazioni intermolecolari. Nella grande maggioranza delle applicazioni adesive questo fine è raggiunto utilizzando una sostanza inizialmente fluida per unire due substrati solidi. A questo fluido si richiede dapprima la capacità di penetrare nelle micro cavità e negli interstizi superficiali degli aderendi solidi in modo da favorire l'instaurazione di forze attrattive e in seguito l'indurimento necessario a garantire resistenza strutturale al giunto. Un requisito fondamentale perché questo processo avvenga è che l'adesivo, durante la fase di applicazione da fluido, sia in grado di bagnare completamente la superfice del solido. Il processo fisico di interazione tra un liquido e un solido è controllato dall' energia superficiale: essa rappresenta il lavoro termodinamico necessario per aumentare la superfice di una sostanza di una quantità unitaria. È necessario che il solido possegga un'energia di superficie superiore del liquido perché questo spanda liberamente sulla sua superfice una volta depositato. Le misure di energia superficiale consentono non solo di stabilire se un adesivo bagni bene un determinato aderendo, ma anche di confrontare differenti trattamenti per valutarne il migliore.

Il metodo più comune per la misura dell'energia superficiale si basa l'angolo di contatto che s'instaura tra un liquido e un solido quando una goccia è depositata su un substrato. Attraverso la deposizione di differenti liquidi è possibile valutare non solo l'intensità ma anche la natura delle forze intermolecolari presenti su una superficie, che ne determinano l'energia superficiale. La maggior parte degli autori divide queste forze in una componente polare e una dispersiva dove la prima rappresenta le interazioni dovute a gruppi polari e la seconda indica tutte le altre. Il metodo di analisi sviluppato da Owen-Wendt-Kaelble-Rabel ha permesso di interpolare linearmente i dati ottenuti da una serie di misurazioni di angoli di contatto con liquidi differenti e di ottenere in questo modo una precisa misura delle componenti dell'energia superficiale di tutti i polimeri analizzati. Al set di cinque liquidi inizialmente scelto (acqua, glicerina, diiodometano, formammide e glicole etilenico) è stata sottratta la glicerina, poiché le interpolazioni lineari hanno da subito evidenziato la sua incompatibilità con gli altri liquidi, dovuta alla sua elevata viscosità. La prima analisi di energia superficiale ha riguardato le superfici lucidate dei polimeri: una serie di dischi abrasivi è stata utilizzata per rimuovere le disomogeneità superficiali di dimensioni maggiori mentre particelle di diamante dal diametro di 0.25 μm sono state utilizzate per la lucidatura finale. I valori ottenuti mostrano che la poliammide e le due versioni non espanse di EVA hanno una simile energia superficiale (30 - 40 mJ/m^2), nonostante gli EVA abbiano una componente polare trascurabile, mentre questa vale circa 7 mJ/m^2 per la poliammide. Non è stato invece possibile svolgere un'analisi accurata sull' EVA cellulare: esso è costituito da un cuore espanso e da uno strato superficiale non espanso. L'analisi di energia superficiale del cuore espanso non è stata possibile a causa della sua natura cellulare mentre lo strato superficiale presenta un'elevata disomogeneità che non può essere eliminata con il processo di lucidatura.

Un secondo studio ha poi riguardato gli effetti sull'energia superficiale degli aderendi derivanti da differenti tipi di pulizia; è infatti noto che la presenza di sporcizia o contaminazioni modifica le proprietà adesive di un substrato. Si è scelto di studiare due diversi tipi di pulizia, una semplice rimozione della polvere con un panno secco e un lavaggio più intenso con un tipico detergente per piatti: questo studio è stato importante anche per quanto riguarda il miglioramento del processo tecnologico d'incollaggio. I risultati ottenuti mostrano che, nonostante non siano presenti significative differenze nel valore totale dell'energia di superficie, la lucidatura è stato l'unico processo che ha messo in evidenza una spiccata componente polare nella poliammide.

La seconda parte della tesi ha riguardato l'ottimizzazione dei parametri di trattamento dei polimeri per mezzo di un plasma ad aria forzata. Lo scopo del processo è stato quello di individuare il miglior set di condizioni di trattamento in modo da ottenere il valore più alto

possibile di energia superficiale per ognuno dei polimeri analizzati. Il primo parametro su cui è possibile agire è la distanza della sorgente di plasma dalla superficie da trattare. Studi precedenti hanno dimostrato che nel caso della poliammide una distanza di 10mm permette un trattamento ideale mentre per quanto riguarda gli EVA sono state esaminate distanze di trattamento di 5, 10, 15 e 20 mm. La durata del trattamento è stato il secondo parametro su cui si è potuto agire per modulare l'intensità del plasma: siccome la dimensione della sorgente non è sufficiente per trattare tutta l'area d'incollaggio contemporaneamente la durata del trattamento è stata regolata variando la velocità con cui si è spostata la sorgente sul substrato e il numero di passate effettuate. Studi precedenti hanno dimostrato che una velocità di 10mm/s permette un trattamento adeguato mentre il numero di passate è stato variato, per tutti e tre i polimeri analizzati, da 1 a 4. Ulteriori passate hanno provocato la comparsa di fenomeni degradativi sulle superfici, dovute all'eccessivo calore sviluppato dal plasma. La valutazione completa dell'energia superficiale per ognuna delle differenti condizioni di trattamento previste avrebbe richiesto molto tempo visto l'elevato numero di angoli di contatto che si sarebbero dovuti misurare; è stato quindi deciso di ottimizzare la sperimentazione utilizzando soltanto l'acqua. In Figura 1 un grafico esemplificativo mostra l'andamento dell'angolo di contatto in funzione del numero di passate e della distanza del substrato dalla sorgente:
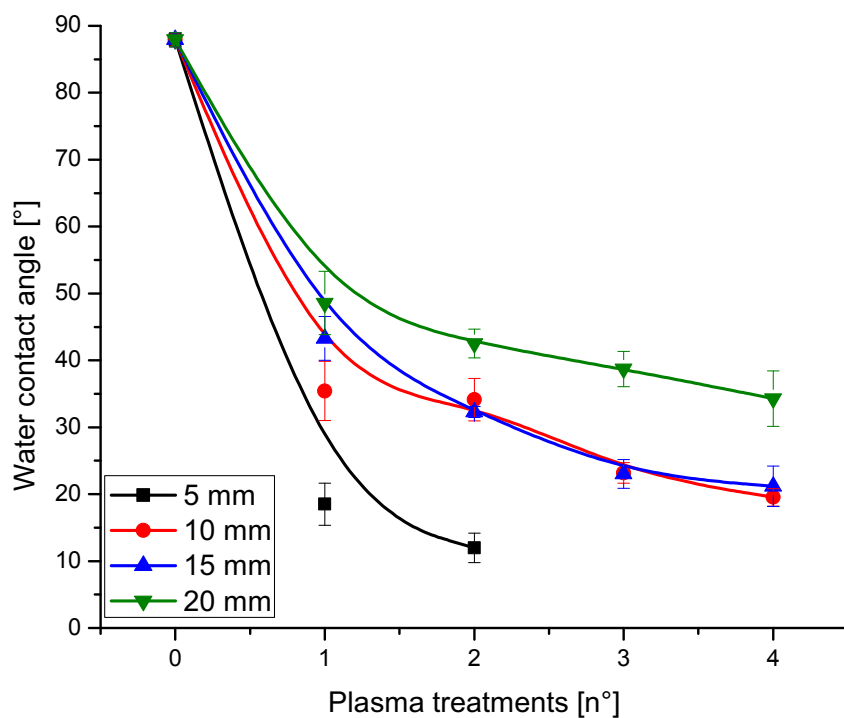
Figura 1: angolo di contatto dell'acqua in funzione del n° di passate (EVA caricato, pulito con detergente)

In Figura 1 si può osservare come l'angolo di contatto minimo sia stato raggiunto dopo 2 passate ad una distanza di 5 mm. In questo caso non è stato possibile proseguire con una

terza passata alla stessa distanza a causa della comparsa di fenomeni degradativi. Analisi complete con il metodo OWRK sono state eseguite nelle condizioni di minimo angolo di contatto dell'acqua per valutare le componenti polari e dispersive. In Tabella 1 un estratto esemplificativo dei risultati ottenuti, in questo caso relativamente all'EVA caricato.

EVA caricato

Iniziale (lucidato)				5 mm x 2 passate			Δ percentuale		
γ_S^P	γ_S^D	γ_S^{tot}		γ_S^P	γ_S^D	γ_S^{tot}	γ_S^P	γ_S^D	γ_S^{tot}
$[mJ/m^2]$	$[mJ/m^2]$	$[mJ/m^2]$		$[mJ/m^2]$	$[mJ/m^2]$	$[mJ/m^2]$	[%]	[%]	[%]
1.45	31.64	33.09	*Panno secco*	41.47	30.36	71.83	+2760 %	-4.0 %	+117.1 %
			Detergente	44.35	27.14	71.49	+2958 %	-14.2 %	+116.0 %

Tabella 1: confronto tra l'energia superficiale iniziale e quella rilevata dopo il trattamento al plasma più efficace (EVA caricato).

Come mostrano i risultati in Tabella 1 il trattamento al plasma è estremamente efficace nell'incrementare le energie superficiali dell'EVA caricato, e lo stesso si riscontra per gli altri polimeri analizzati. In particolare si verifica che l'aumento è dovuto all'incremento della parte polare dell'energia di superficie, dovuta all'instaurazione sulla stessa di gruppi polari.

Una volta stabilite le condizioni di trattamento che hanno consentito i valori maggiori di energia superficiale, sono stati eseguiti dei test meccanici per valutare la resistenza a frattura dei giunti. I primi test eseguiti sono stati di peeling a 90°, dove una parte del giunto viene fissata e l'altro aderendo viene sollecitato in trazione (modo I) fino alla frattura, che poi propaga lungo tutta l'interfaccia tra i due materiali. Questo tipo di configurazione, che riproduce una delle situazioni di frattura più comuni per questo tipo di giunti, necessita che almeno uno dei due materiali sia flessibile. Siccome né la poliammide né la forma espansa dell'EVA sono sufficientemente flessibili nella geometria in cui sono stati forniti, non è stato possibile realizzare delle prove di peeling su giunti composti da questi due materiali. La poliammide è stata quindi giuntata con i due diversi tipi di etilen-vinilacetato non espansi attraverso un adesivo poliuretanico monocomponente solitamente utilizzato per questo tipo di applicazioni: variando i parametri di trattamento sono stati realizzati 8 differenti tipi di provini con adesivo. Diversi tentativi sono stati inoltre condotti per collegare i polimeri sfruttando fenomeni diffusivi superficiali, senza ricorrere pertanto all'uso di adesivi: ulteriori 4 tipi di giunti sono stati realizzati a questo scopo.

I provini collegati con adesivo poliuretanico, preparati per entrambi gli EVA non espansi, sono stati trattati con 4 intensità differenti di plasma. Oltre a quelli realizzati senza

trattamento alcuno e a quelli trattati in modo da ottenere il più alto valore di energia superficiale (secondo le analisi spiegate in precedenza) sono stati realizzati anche altri provini rispettivamente con un trattamento più intenso di quest'ultimo e uno meno intenso. E' stato possibile verificare un incremento della resistenza a frattura in tutti i giunti realizzati con polimeri trattati al plasma rispetto a quelli non processati. In particolare si è appurato che le condizioni in cui si è constatato il miglioramento maggiore sono state quelle ottenute dai provini realizzati con il trattamento meno intenso. I due trattamenti più aggressivi hanno prodotto invece campioni leggermente meno resistenti di quest'ultimo, sebbene migliori di quelli non trattati.

Per quanto riguarda invece i giunti realizzati senza adesivo si è cercato di sfruttare l'innalzamento della temperatura degli aderendi causato dal trattamento al plasma per promuovere fenomeni diffusivi e favorire l'adesione. Purtroppo nessuno dei provini realizzati senza adesivo ha garantito un soddisfacente livello di adesione. Alcuni dei risultati più rilevanti ottenuti dalle prove di peeling a 90° sono riassunti in Tabella 2.

	Materiali nel giunto		Distanza	Passate	Adesivo	Forza di peel [N/cm]	En. frattura adesiva [J/m²]
1a	PA / EVA caricato	PA	10 mm	4 pas.	PU	**1.68**	**94.95 ± 8.69**
		EVA	5 mm	2 pas.			
1b	PA / EVA non car.	PA	10 mm	4 pas.	PU	**1.48**	**92.79 ± 8.79**
		EVA	5 mm	2 pas.			
2a	PA / EVA caricato	PA	5 mm	4 pas.	-	**-**	**-**
		EVA	5 mm	2 pas.			
2b	PA / EVA non car.	PA	5 mm	4 pas.	-	**-**	**-**
		EVA	5 mm	2 pas.			
3a	PA / EVA caricato	PA	5 mm	4 pas.	PU	**1.72**	**97.14 ± 10.3**
		EVA	5 mm	2 pas.			
3b	PA / EVA non car.	PA	5 mm	4 pas.	PU	**1.32**	**87.20 ± 11.2**
		EVA	5 mm	2 pas.			
4a	PA / EVA caricato	PA	-	-	PU	**1.43**	**82.86 ± 11.5**
		EVA	-	-			
4b	PA / EVA non car.	PA	-	-	PU	**0.647**	**47.20 ± 8.19**
		EVA	-	-			
5a	PA / EVA caricato	PA	10 mm	1 pas.	PU	**1.96**	**109.2 ± 10.5**
		EVA	10 mm	1 pas.			
5b	PA / EVA non car.	PA	10 mm	1 pas.	PU	**1.90**	**119.5 ± 15.3**
		EVA	10 mm	1 pas.			
6a	PA / EVA caricato	PA	10 mm	1 pas.	-	**≈ 0**	**≈ 0**
		EVA	10 mm	1 pas.			
6b	PA / EVA non car.	PA	10 mm	1 pas.	-	**≈ 0**	**≈ 0**
		EVA	10 mm	1 pas.			

Tabella 2: descrizione delle condizioni di pretrattamento e incollaggio dei provini
per i peeling test e principali risultati ottenuti.

Sono state infine condotte prove di taglio su giunti a doppia sovrapposizione. Con questa configurazione sono stati preparati 2 set di provini accoppiando la poliammide con le due versioni, espanso e non espanso, di EVA caricato. Le prove hanno dimostrato che i due polimeri hanno comportamenti simili.

Infine, il tentativo di stabilire una correlazione diretta tra l'energia superficiale di un'aderendo e la sua resistenza alla frattura adesiva non ha dato risultati completamente soddisfacenti.

I. CHAPTER: INTRODUCTION

I.1 _Introduction_

The main goal of this work was to improve adhesive bonding between two polymers through surface treatment optimization and to test the mechanical strength improvements obtained. This analysis has been carried out with the collaboration of Nike, leader in the market of shoes, which supplied the materials: a polyamide (PA) and a foamed ethylene - vinylacetate (EVA). To adequately test some mechanical features of the junction also the unfoamed version of the EVA has been studied, and to assess possible effects on bonding due to blend fillers another unfilled version of the same material has been included in the analysis.

The bonding enhancement process was mainly obtained through the optimization of a forced air plasma treatment. To establish the best plasma treatment conditions, surface characterization was the first step. Initially it has been kept into consideration the factory environment of production, providing analyses of different surface cleaning methods. Later, the parameters of the plasma treatment have been optimized to obtain the highest wettability of the substrates to bond. The investigation of such surface has been carried out through sophisticate adherend analysis, which allowed calculating precise data on their surface energies.

Once best conditions to enhance polymers wettability were established, mechanical investigations have been carried out to test whether the results of the air plasma treatment optimization resembled the ones obtained with real junctions. Polyurethane adhesive has been used to bond the adherends and peel tests on the unfoamed polymers have been exploited to determine truthful and reproducible data on the joint resistance. Junctions with no adhesives, based on the diffusive mechanisms boosted by the increase in temperature induced by the plasma have also been investigated. These experimentations allowed assessing the bonding improvement due to plasma treatment. At last, adhesive shear tests have been carried out, to compare different materials and ascertain to what extent forced air plasma treatment should be used to improve adhesive bonding in shoe soles.

II.   CHAPTER: THEORETHICAL BACKGROUND

II.1   *Adhesion*

In materials science *adhesion* refers to the entirety of physical and chemical phenomena established in the molecular attraction between two different materials put in direct contact. The term *cohesion* instead refers to the all the complex system of phenomena involved in the attraction between molecules of the same type.

According to a simple definition by *Comyn* [1] an *adhesive* is a "material which when applied to the surface of other materials can join them together and resist separation" and the correlated word *adherend* or *substrate* are used instead to indicate the "bodies or materials to be bonded by the adhesive".

Some of the important reasons for choosing adhesives over mechanical bonding methods may include:

- Improved stress distribution over bonded region, thus preventing localization of stresses and stress concentration;
- Ability to join dissimilar and similar materials together, thus resulting in flexibility in engineering design;
- Significant weight reduction due to absence of heavy mechanical fasteners;
- Reduction in costs (and in some cases improved service life) [2].

It is widely recognized that to establish a strong adhesion between two materials an intimate molecular contact is necessary (although sometimes insufficient). Developing adhesion science and studying its mechanisms *Kinloch* [3] and *Comyn* [1] have indicated some basic requirements that an adhesive substance and its adhesive environment and application should meet in order to obtain an effectively joint system:

- The adhesive must wet the surface, *i.e.* it must spread on the substrate with contact angle approaching zero;
- When applied, the adhesive should have a relatively low viscosity;
- After the application the adhesive should harden to a cohesively strong solid (this process can take place through several different chemical or physical activities);
- The bonding process should be carried out in a way that adhesive and substrate are brought together facilitating the displacement of any trapped air;

Although the coexistence of several different phenomena and mechanisms involved in any adhesive system (which will be explained later) is widely accepted, in most of them the

factor playing the most important role is the degree of the intermolecular forces.

Intermolecular forces are weak electrostatic interactions between two or more molecules (which in the case of adhesives are different). The energy of these bonding is generally up to around 40 kJ/mol, therefore much lower than interatomic forces. The most common type of physical attractive forces are Van der Waals forces, attributed mostly to the subsequent effects [4]:

- London forces (or dispersion forces), which arise from quantum induced instantaneous polarization of molecules; they are always present and they usually represent the main part of total interactions in condensed matter.
- Dipole-dipole forces, which arise between permanent electrostatic dipoles.
- Debye forces, which arise from interactions between a permanent dipole and an induced dipole on a polarizable molecule.
- Hydrogen bond, which are a particular case of dipole-dipole interactions between a hydrogen atom and a second, small and strongly electronegative atom such as fluorine, oxygen or nitrogen atom.

In practice most adhesive materials are polymeric therefore most bonds involve intermolecular forces but in few cases chemical bonding may be due also to covalent bonds or even ionic bonds. Covalent bond is a chemical bonding characterized by the sharing of pairs of electrons between atoms. The stable balance of attractive and repulsive forces between atoms when they share electrons is known as covalent bonding but when one of the atom sharing the electron pair attracts it more than the other an electrostatic attraction between the formed ions may occur, introducing a certain degree of ionic bond.[5]

II.2 *Surface energy*

Surface tension is a direct way to measure the extent of intermolecular forces. According to *Kinloch* [3] "the tension in surface layers is the result of the attraction of the bulk material for the surface layer and this attraction tend to reduce the number of molecules in the surface region resulting in an increase in intermolecular distance; this increase requires work to be done, and returns work to the system upon a return to normal configuration".

The determination of the surface free energy of a solid substrate is a rather complex process and, for many adhesive bonding situations, it is not strictly necessary as the determination of the contact angle may sometimes suffice [6]. Measurements of contact angles are usually a starting point to determinate the surface energy of a substrate.

Apart from being important for the evaluation of the surface free energy the contact angle is important also to evaluate the wetting equilibrium. This is because, as said previously, an

important requisite to establish a strong bond is to create an intimate contact between the substrate and the adhesive liquid *i.e.* the liquid must spread on the solid surface freely.

II.2.1   Contact angle

It has been observed that if a drop of a liquid placed on a solid surface does not spread but reaches an equilibrium state it remains on the surface as a drop with a certain contact angle θ between the solid and the liquid phases.

Such phenomenon has firstly been analysed by Young [7] using simple planar geometry and obtaining the equation:

$$\gamma_{SA} = \gamma_{SL} + \gamma_{LA} \cos\theta \qquad (II.2,1)$$

The geometrical equilibrium in shown in Figure II.1, where γ_{SA}, γ_{SL} and γ_{LA} represented the free energies of the solid-air, solid-liquid and liquid-air interfaces.
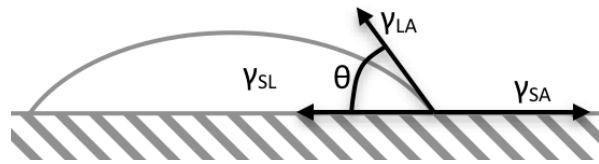
Figure II.1: shape exhibited by a drop in equilibrium with an angle theta on a solid surface.

Many authors, including *Bangham*, *Razouk* and later *Boyd* and *Livingston* (as reported by *Fox et al.* [6]) pointed out that equation II.2,1 was incorrect because γ_{LA} can be altered by adsorption of vapour on the solid. This is because generally the solid is contaminated with a fully developed adsorbed film in equilibrium with the saturated vapour of the liquid, which (especially if soluble or capillary active) diminishes the energy of the free liquid surface.

Naming γ_{S0} the free surface energy of a solid in a vacuum, γ_{SV^0} the one in saturated vapour and γ_{SV} the one in vapour at a pressure *p*, the correct statement of equation (II.2, 1) is, in the case of saturated vapour:

$$\gamma_{SV^0} = \gamma_{SL} + \gamma_{LV^0} \cos\theta_E \qquad (II.2,2)$$

while for system where the contact angle does not change with time, in case of a vapour at a partial pressure *p* inferior of the saturated pressure:

$$\gamma_{SV} = \gamma_{SL} + \gamma_{LV} \cos\theta \qquad (II.2,3)$$

The term γ_{SV} may be considerably lower than the free energy of the solid in vacuum γ_{S0}. This reduction in surface free energy of the solid when covered by a layer of vapour has been defined by the concept of "equilibrium spreading pressure", π^0, by *Bangham et al. [8]:*

$$\pi^0 = \gamma_{S0} - \gamma_{SV^0} = RT \int_0^{p_0} \Gamma d(\ln p) \qquad (II.2,4)$$

where, if the vapour obeys to the ideal gas law, p and p_0 are the vapour pressures and the equilibrium vapour pressure of the pure liquid adsorbate, R is the gas constant, T the experimental temperature and Γ is the absorption of the vapour on the surface.

For all these consideration equation (II.2, 1) can now be written as:

$$\gamma_{S0} = \gamma_{SL} + \gamma_{LV} \cos \theta + \pi^0 \qquad (II.2,5)$$

Approaching the problem using Gibbs free energy leads to the same equation, as described by *Adamson et al.* [8]; the change in surface free energy ΔG^s associated with a small displacement of the liquid causing a variation in the solid surface covered by ΔA is:

$$\Delta G^s = \Delta A(\gamma_{SL} - \gamma_{SV^0}) + \Delta A \gamma_{LV} cos(\theta - \Delta \theta) \qquad (II.2,6)$$

where γ_{SL}, γ_{LV} and γ_{SV^0} have the same meaning of before.

At equilibrium:

$$\lim_{\Delta A \to 0} \frac{\Delta G^s}{\Delta A} = 0$$

Which leads again to:

$$\gamma_{SL} - \gamma_{SV^0} + \gamma_{LV} \cos \theta = 0 \qquad (II.2,7)$$

where it is stressed the fact that the work of adhesion and the adhesion tension involve γ_{SV^0} rather than γ_{S0}.

For practical purposes it is said that a liquid is nonspreading when $\theta > 0°$ [5] (while other authors, e.g. *Adamson et al.* [8], use the expression "the liquid does not wet the solid if the contact angle is greater than 90° "). However, when $\theta = 0°$, the liquid wets the solid completely and spontaneously spreads freely over the surface while when $\theta > 90°$ drops of liquid tend to move about easily on the surface and not to enter capillary pores. The rate at which the liquid spreads or moves depends upon factors such as roughness of the surface and viscosity of the liquid among others. It is important to note that when a liquid spreads completely over a surface (*i.e.* $\theta = 0°$) equation II.2,7 ceases to hold and the imbalance of free energies comes from a spreading contribution. This term, named generally equilibrium-spreading coefficient S, can be expressed in this way

$$S = \gamma_{SV^0} - \gamma_{LV} - \gamma_{SL} \qquad (II.2,8)$$

and when it is positive the liquid spreads spontaneously on the solid surface. If this term is negative it is still possible to wet the surface, only by applying an additional pressure balancing the forces.

Poor wetting   Good wetting   Complete wetting
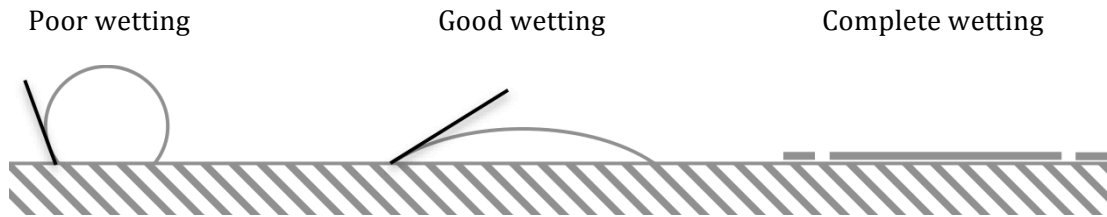
Figure II.2: different drop shapes caused by different wetting behaviours.

So far it has been discussed the case of solid-liquid-gas interfaces however it is possible to have also contact angles between a solid surface and 2 immiscible liquids. In this case more attention has to be paid to mutual saturations but these circumstances lie outside the scope of this work.

II.2.2   *Contact angle measurements*

To measure the contact angle between a liquid and a solid surface the most used methods are the sessile-drop, the sessile bubble and the Wilhelmy techniques, even if some other techniques are available and widely used. In this work only the sessile-drop method has been used to characterize the solid surfaces therefore the other main methods are only briefly described.

The capillary rise on a Wilhelmy plate allows obtaining contact angles by measurement of the height of the meniscus on a partially immersed plate and permits both static and dynamic measurements with the peculiarity that under some circumstances allows also to calculate the contact angle between the liquid and porous solids or fibers (where the sessile drop method cannot be used).

The sessile bubble method and the other methods used to evaluate also surface tension of liquids (like the analysis of hanging drops and bubbles) rely on the fact that, as said, small drop or bubbles will tend to assume a spherical shape because surface forces depend on the area (which depends on the square of the linear dimension) whereas distortion is due to a gravitational effect (therefore depending on the volume). When gravitational and surface tensional effects are comparable the shape of the bubble can be used to evaluate such outcomes.

Two other techniques, not frequently used, are interference microscopy and specular reflection. "Interference microscopy relies on interference fringe patterns produced by the edge of the drop surface to calculate the contact angle. Specular reflection uses a beam of light reflected from the liquid surface. By pivoting the beam on its axis, the orientation at which the specular reflection disappears is determined, and the contact angle established"[9].

The worldwide most used method to measure surface energy however is, as said, the sessile drop method, which has been used in this work too. Its explanation and all the technical details are explained in Chapter III.

II.2.3   *Surface energy calculation*

Surface energy of a solid can be evaluated through contact angle considering the interactions between the solid and a liquid. The interface contacts depend upon all the different types of intermolecular forces: hydrogen bonding, polar interactions, acid/base interactions and dispersive forces, called also Van der Waals forces, which include different phenomena listed in II.1.

To better characterize the nature of interactions established, many authors divide surface energy in two parts, a dispersive component and a polar one, where the former accounts for all the dispersive interactions and the latter for the others. Therefore, for both the liquid and the solid:

$$\gamma_L = \gamma_L^P + \gamma_L^D \qquad (II.2,9)$$

$$\gamma_S = \gamma_S^P + \gamma_S^D \qquad II.2,10)$$

Where the subscripts indicate the material and the superscripts distinguish between the polar (^{P}) and the dispersive (^{D}) components.

During the years, many different theories have been proposed to calculate surface energy of a solid (and its component) using the contact angle technique. These rely on the effects of different liquids (with different surface tension and a different ratio between the components) on the same solid to calculate not only its surface energy but also to separate the effects due to different components. In fact, the interactions established between solids and liquids depend upon not only the degree of such forces, but also on the type, where strongest interactions are due to similar types of forces.

The simplest theories developed are the one based only on the calculation of the total amount of interactions.

II.2.3.1   *One component theories: Zisman and EoS (Equation of State)*

The first and the simplest theory was the *Zisman* method [10] [11], which evaluated solids surface energy only as a single component using the critical surface tension of the liquid. According to Zisman, "a liquid wets a solid completely when the work of cohesion for the formation of a liquid surface W_{LL} is smaller than the work of cohesion for the formation of the interface boundary W_{SL}". As described in II.2.1, the difference between these two values is the spreading pressure S: when S is positive the solid will be completely wetted.

Since

$$W_{SL} = \gamma_L (\cos \theta + 1) \qquad (II.2,11)$$

and

$$W_{LL} = 2 \cdot \gamma_L \qquad (II.2,12)$$

for a contact angle of 0° the work of adhesion W_{SL} equals the work of cohesion W_{LL}, and thus 0° contact angle can be defined as the limiting angle for spreading, the complete wetting; (this is also because a positive spreading pressure S corresponds to a negative contact angle, which cannot be measured in practise). By plotting the $\cos \theta$ of different liquids against their surface tension *Zisman* extrapolated the value for $\cos \theta = 1$.

This approach has been abandoned for precise measurements when it has become clear that the linear relationship between $\cos \theta$ and the surface tension γ_{SL} was based on the wrong assumption that the interfacial tension was determined by the difference between the surface tensions. This applies in fact only "when the relationship between the disperse and the polar interactions is the same between the solid and the liquid" [10].

Another single component surface tension method is the Equation of State [12], which instead sought to determine the surface energy of a solid from a single contact measurement by using a liquid with known surface tension. Considering *Young*'s equation (II.2, 1) it can be seen that another relation is required to "describe the surface energy of the solid as a function of the interfacial tension solid/liquid and the surface tension of the liquid". Due to thermodynamic considerations by *Neumann* and *Sell*, there has been for some years the credence that such relation had to exist for all systems and it could have been determined empirically. Later, according to *Good* [13] "first *Morrison* shown that the theory's claimed thermodynamic derivation was erroneous. Second, *Fowkes* and *Van Oss* have shown that there are a great many cases of gross experimental disagreement between predictions from Neumann's equation and observed interfacial tensions between water and organic liquids. Third, Neumann's equation takes no account at all of hydrogen bonds or of the Lewis base nature of polar compound that form hydrogen bonds".

Although these theories are still reported as methods to measure surface energy, they should never be used for technical analysis.

II.2.3.2   Two component theories

These more precise theories account for both the components (polar and dispersive) of surface energy explained above. Most important two components theories are the Fowkes method, the Wu method and the Owens-Wendt-Rabel-Kaelble method (called hereafter OWRK), where the formers are mentioned and the latter is the one adopted for this thesis and therefore will be explained in great detail.

Both Fowkes and OWRK methods allow calculating both fraction of surface energy but while Fowkes initially determined only the disperse fraction the latter were the first to determine both the components. Main difference between two methods is that in Fowkes' one it is necessary to use at least one purely dispersive liquid to assess at first the dispersive fraction, while the polar component is calculated as a second step. In the OWRK technique instead, both parts are computed together with a single linear regression, and it is not necessary to use a purely dispersive liquid. Since it is not easy task to find a liquid with high surface energy universally considered to be completely dispersive (the differences regarding literature values for liquid surface energies will be presented later) the OWRK method has been adopted for the thesis.

Considering how Young's equation (formulated more than 200 years ago) is written today:

$$\gamma_{SV} = \gamma_{SL} + \gamma_{LV} \cos \theta \qquad (II.2,13)$$

it was informally recognized by the early 1950s that a very serious puzzle existed because it was not possible to go beyond Young's equation without dealing with an analytical relation between γ_{SV} and γ_{LV} [13]. A great deal of discussion rose around how to express γ_{SL} and the two main solutions to this problem are now embedded in the OWRK and the Wu methods.

- In OWRK method [14] γ_{SL} is evaluated as a geometric mean between the components of the surface energies of the liquid and the solid:

$$\gamma_{SL} = \gamma_S + \gamma_L - 2 \left(\sqrt{\gamma_S^D \cdot \gamma_L^D} + \sqrt{\gamma_S^P \cdot \gamma_L^P} \right) \qquad (II.2,14)$$

- In Wu method [15] instead γ_{SL} is calculated with a harmonic mean:

$$\gamma_{SL} = \gamma_S + \gamma_L - 4 \left(\frac{\gamma_S^D \cdot \gamma_L^D}{\gamma_S^D + \gamma_L^D} + \frac{\gamma_S^P \cdot \gamma_L^P}{\gamma_S^P + \gamma_L^P} \right) \qquad (II.2,15)$$

Despite the different ways of computing γ_{SL} the results given by this two methods are very similar [13], therefore there is no need to use both for the purposes of this thesis.

II.2.3.3　OWRK method

The OWRK method is an extension of an initial *Owens-Wendt* analysis where the two authors took equation $\gamma_{SL} = \gamma_S + \gamma_S - 2\left(\sqrt{\gamma_S^D \cdot \gamma_L^D} + \sqrt{\gamma_S^P \cdot \gamma_L^P}\right)$ and combined it with Young's one. The authors solved the equation system by using the contact angle of two different liquids with known disperse and polar fractions of the surface tension [14]. This approach based on only two liquids may introduce significant error if there is a problem with one of them and does not allow evaluating the precision of the analysis. To this initial approach, *Kaelble* solved the equation for combinations of two liquids and calculated the mean values of the resulting single analysis in order to reduce the error. Another approach developed by *Kinloch et al.* [16], which reduced again the error, used a matrix analysis to cross-compare all the results coming from the couple of liquids, succeeding in reducing significantly the scatter. Again, this was not enough to find if any single experimental result was probably wrong or deeply affected by error.

The solution came from *Rabel*: he made it possible to calculate the polar and disperse fractions of the surface energy with the aid of a single linear regression from the contact angle data of various liquids.

By combining equation (II.2, 14) and Young's equation it is possible to obtain:

$$\frac{(1 + \cos\theta) \cdot \gamma_L}{2\sqrt{\gamma_L^D}} = \sqrt{\gamma_S^P} \cdot \sqrt{\frac{\gamma_L^P}{\gamma_L^D}} + \sqrt{\gamma_S^D} \qquad (II.2, 16)$$

which resembles the general equation for a straight line:　$y = mx + b$:

$$\underbrace{\frac{(1 + \cos\theta) \cdot \gamma_L}{2\sqrt{\gamma_L^D}}}_{y} = \underbrace{\sqrt{\gamma_S^P}}_{m} \cdot \underbrace{\sqrt{\frac{\gamma_L^P}{\gamma_L^D}}}_{x} + \underbrace{\sqrt{\gamma_S^D}}_{q}$$

This equation can be subsequently plotted in a graph to obtain a linear regression. In Figure II.3 an example of the explained method:
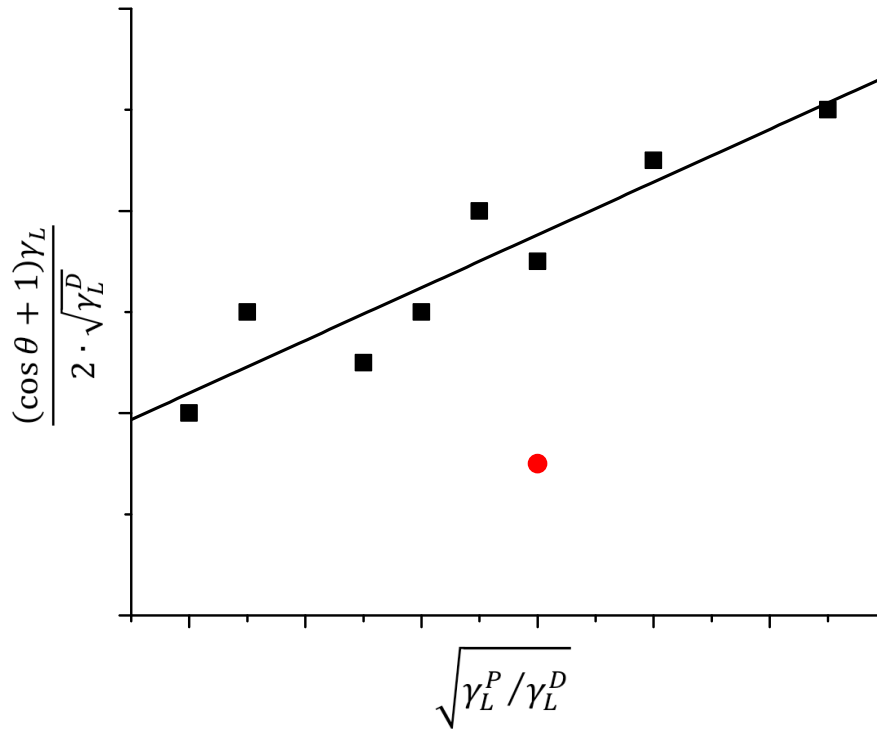
Figure II.3: example of OWRK linear fit (red point indicates a wrong data, clearly detectable).

In this case it is quite easy spotting if any point lies far from the fitting line, as for instance the red circle shown in Figure II.3. Since to each point corresponds a single liquid it is simple to recognize if there is any problem in the analysis with that liquid, which is quite important during such analysis. With the approaches explained before this was hardly possible, especially with the Owens-Wendt method, still broadly used.

II.2.3.4   Three components theories

There is also a more complicated method, which will be only briefly explained: The Van Oss method [17]. It includes the dispersive surface energy γ_L^D but subdivides the polar component as being the sum of two more specific fractions: the surface energy due to acidic interactions and the one due to basic interactions. The former theoretically describes a surface's propensity to have polar interactions with a second surface that has the ability to act basic by donating electrons (and the latter vice versa). This method is useful in particular when there is great imbalance between the acid and base component of the polar surface energy, which is not the case of polymers.

For the reasons explained above OWRK method was the most suitable for the analysis required in this work.

31

II.2.4   _Adhesive systems and adhesive mechanisms_

Adhesive joining is a common method for connecting two or more components together, and its major advantages over mechanical connections have already been explained in II.1. An adhesive joint however is a complex system, and those involved in its study should not only have an understanding of the mechanics of the joint but also some awareness of the science and chemistry of adhesion. As explained by _Devries_ [18] "the strength of an adhesive joint is a system property dependent on the properties of the adhesive, the adherend(s), and the interphase and requires an understanding of mechanics, physics and chemistry".

Even if a fundamental mechanism that determines how a material adheres to another has not yet been unambiguously identified, it is widely accepted that a certain number of different mechanisms act in different adhesive joints. Since the scope of this work is to improve the resistance of an adhesive joint, it is important to be aware of all the bonding mechanism(s) involved, in order to be able to recognize which ones are present, the ones that can be improved and the ones not involved.

According to most studies, there are six commonly recognized main mechanisms able to bond a material with another in an adhesive way. Even if the scope of this work is not to investigate all of them, a brief description of their theories will help understand why in some cases an acceptable joint strength has been achieved while in other no intimate adhesion established.

The most widely accepted jointing mechanisms are [18-20]:

- Mechanical interlocking

Mechanical interlocking might be considered as being different from chemical adhesion but this physical phenomenon acts in improving the adhesion of many joints. Many surface treatments like surface roughening and some surface modification serve the purpose of improving mechanical interlocking or even "hooking".
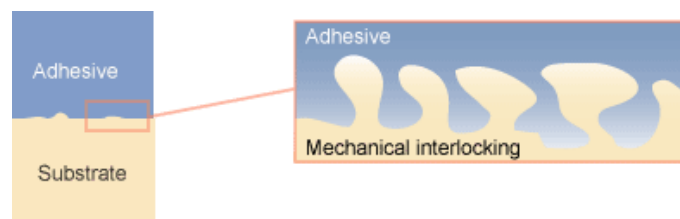
Figure II.4: microporosity/roughness of the substrate improves adhesion [18].

Mechanical interlocking theory states that good adhesion occurs only when the adhesive penetrates into pores, holes, crevices and other irregularities of the substrate, as in Figure II.4. To do this, the adhesive must not only wet the surface but also have the right viscosity

during the preparation of the joint.

Many surface pre-treatments have the scope of roughen the surface: beyond the objective of creating irregularities which can promote mechanical interlocking they result in increasing the effective contact area with the adhesive. Since strong adhesion can occur as well between smooth adherends it is clear that although mechanical interlocking promotes adhesion, it is not the only mechanism.

- Diffusion theory

The diffusion theory is based on the hypothesis that one material inter-diffuses into and with another near the surfaces. It is generally applied to polymer bonding in which "the development of a boundary layer is envisioned along which the polymer chains of the two materials are intertwined" [20]. The driving force for adhesion due to diffusion to happen is the mutual diffusion of polymer chains across the surface (or either only one polymer into the other).
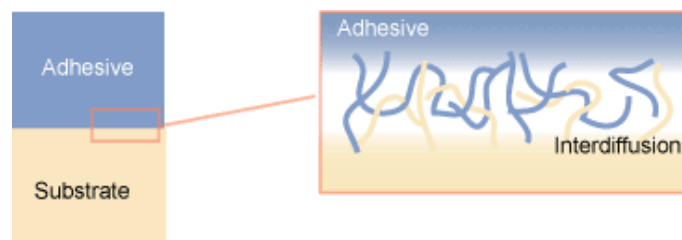
Figure II.5: interdiffusion at the interface between the two polymers [19].

This theory requires that both the adhesive and adherend are polymers mutually compatible and miscible and capable of movement: this means that this theory is supported by the important role that viscosity, temperature, and polymer type (e.g. molecular weight, chemistry and physical form) play in determining joint strength.

Self-diffusion has also been studied thoroughly and several theories have been proposed such as entanglement coupling, cooperativity, and reptation.

Polarity has been found to generally increase adhesion even if the diffusion theory "has found limited application where the polymer and adherend are not soluble or the chain movement of the polymer is constrained by its highly crosslinked, crystalline structure, or when it is below its glass transition temperature"[19].

- Absorption

Absorption mechanism involves secondary molecular forces. It comes from intimate intermolecular contact between two materials, and involves forces that develop between the atoms in the two surfaces. The forces involved include London dispersion forces, dipole-dipole interactions, hydrogen bonding or other secondary molecular forces whose strength varies from 0.1 to 10 J/mol.
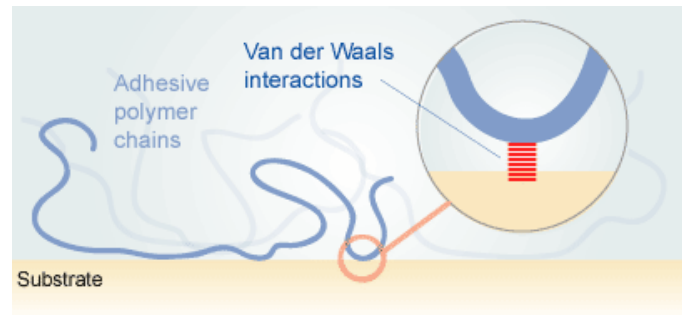
Figure II.6: establishment of Van der Waals forces between interface molecules [18].

Kinloch [21] and many others demonstrated that this is usually the most important contribution to achieve adhesion and many adhesive joints involve only the effect of these interfacial secondary forces. The theoretical degree of such forces can be higher than the values obtained from experiments: this is again due to all the irregularities (eg voids, defect, inclusions or geometrical irregularities) that may cause stress concentration during loading (as explained later in this chapter).

Especially in this case intimate contact is fundamental. This aspect has been a major topic of this work.

- Chemical reaction theory

The chemical bonding theory suggests that chemical reactions occur between the adhesive and the adherends forming primary chemical bonds. It is unlikely that this theory universally applies to all joints however it may be present in some cases. Chemical bonds are strong and make a significant contribution to the intrinsic adhesion. For example, the energies of primary chemical forces range from 60 up to 1100 KJ/mol, hence much more than secondary forces.
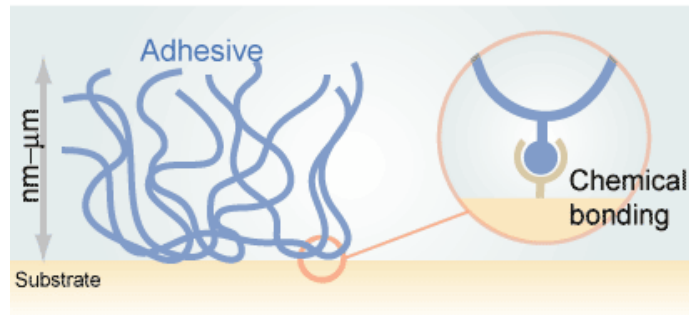
Figure II.7: primary chemical bonding between adhesive and adherend [19].

Even if this case does not apply to polymeric substrate adhesion, it is important to mention coupling agents and adhesion promoters: such molecules, *e.g.* silanes, are "bifunctional", meaning that one "end" of the molecule is intended to interact with a polymeric adhesive while the other to chemically react with atoms in the adherend surface layer (usually an oxide layer of a metal or the oxygen in ceramics).

- Electrostatic force model

This theory assumes that the electrons within the surface layers of adhesive and adherend occupy different energy levels and that electron transfer due to such difference in electronegativities occurs across the surface. This transfer generates a positive and a negative charge on the surfaces, which attract each others.

For example, when an organic polymer is brought into contact with metal, electrons are transferred from metal into polymer, creating an attracting electrical double layer (EDL).
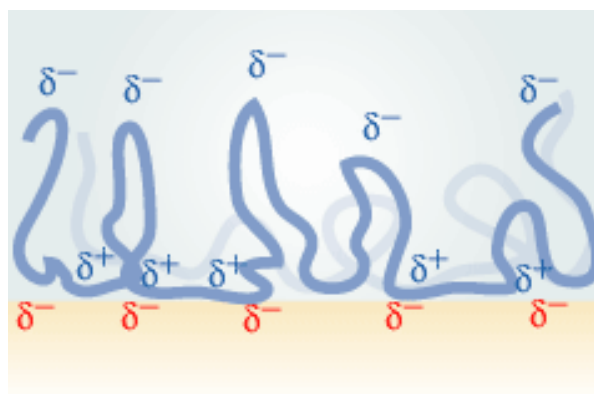
Figure II.8: electrostatic attraction between differently charged layers [19].

It is commonly recognized that the effect of electrostatic adhesion was exaggerated in the first studies and it is widely accepted now that these electrostatic forces are not primary contributors to the strength of most practical adhesive bonds.

35

- Acid-base reaction theory

According to *Devries et al.* [18] "this theory has been proposed to explain a number of observed adhesive phenomena and it is based on acid-base reaction on the surface. Initially, only *Brønsted* concept of acid and bases were considered, but the more general current theory incorporates the *Lewis* acid (electron donor-acceptor) concept. The determination of the acidity or basicity of polymers, however, is not as straightforward as might be accepted."

II.2.4.1 Correlations between adhesion and contact angle

Because adhesion, as said, is a system phenomenon, its effectiveness comes usually from a combination of some of the main mechanisms described above. This means that adhesion involves many different factors including chemical and physical properties of the materials involved, adhesive and adherend shape, joint geometry, loading rate and a wide range of environmental conditions (temperature, humidity, etc..).

In Chapter II.2 it has been said that surface energy is a common method to measure the tendency of a liquid to "wet" a surface and to evaluate the work of adhesion. However, "it is important to note that the work of adhesion, as determined by wetting experiments, represents only a small, but essential, portion of the total adhesive energy referred to in fracture mechanics" (which is described later). "the work of adhesion involved in wetting involves only surface interactions while the adhesive fracture energy includes all other dissipative mechanisms involved during fracture. Some of this mechanism may be somewhat removed from the locus of the fracture path. A one-to-one correlation has never been established between the contact angle of an adhesive in a wetting test and the subsequent strength of the adhesive bond of the cured adhesive [18]".

Despite this, a good wetting of the adhesive on the adherend during the preparation of the joint is critical for achieving an intimate contact between the parts.

II.3   *Forced air plasma treatment*

As explained in section II.1, an important requirement for each adhesively bonded surface is that it should have sufficiently high surface energy: this does not usually happen in polymers. Although many differences exists between olefins with no polar bonds and plastics with polar groups, in most polymers the existing surface energy is not enough to achieve a good adhesion. Therefore, it becomes necessary that the bonded material must be surface treated to ensure that adequate adhesion exists across the adhesive/substrate interface and to ensure sufficient long-term durability of the joint.

Main aims of surface-treatments are the following [3]:

- To remove, or prevent subsequent formation of any weak surface boundary layer on the substrate (later in this work it will be seen that in some cases a too deep surface treatment might instead induce the formation of a weak layer);
- To maximise the degree of intimate molecular contact that it is obtained between the adhesive and the substrate;
- To ensure that the level of intrinsic adhesion forces across the interface(s) are sufficient to obtain both the initial joint strength and the subsequent service life required;
- To generate a specific surface topography on the substrate;
- To assist hardening of the adhesive;
- To protect the surface of substrate prior the bonding operations.

The methods most widely used to modify surfaces of polymers are chemical treatments, electrochemical treatments, photoirradiation and plasma treatments. Chemical treatments such as oxidation, polymer grafting and etching require expensive waste disposal. In contrast, without any pollutant emission, the surface of polymers can be modified by plasmas. Plasmas are high-energy ionized gases constituted in large part by electrons and ions (but globally neutral) where the complex motes of particles are mainly due to long-range interactions (in contrast with all other forms of matter) that confers them particular physical properties. The science of plasmas is a very broad field of study but the effect of these phenomena on polymers surface treatment can be evaluated without introducing their physics, which is outside of the goal of this work.

There are two typical advantages in a mild plasma treatment for materials. One advantage is that the reaction takes place only at the material surface, without significantly changing its bulk properties. The other is that it is possible to apply it in any atmosphere, such as oxidative, reductive and inactive atmospheres. Plasma treatments have become extensively used because of their very high efficiency and operational simplicity [22].

There are many ways to produce plasma, but they all share a common principle. The plasma is generated when a voltage is induced across a non-conducting fluid: as the voltage increases the anode starts strongly attracting the electrons of the fluid (the cathode attracts the nuclei) stressing the matter between the electrodes which, as tension increases, reaches a point when the powerful electric field created is able to generate an electrical breakdown. This allows the establishment of an electric spark (in Figure III.9, next chapter, the sparks generated by the apparatus used), meaning that the fluid between the electrodes stopped being an insulator and became instead a conductor. This happens because an increasingly higher number of particles becomes ionized. The apparatus used for this work is a forced air atmospheric pressure plasma, meaning that the dielectric fluid is air and it works under atmospheric pressure (which determines the amount of particles totally present in the plasma). The technical characteristics are explained in section III.3. The interest arose over atmospheric plasma in last decades is due mainly to its versatility: change in gas species, electric current, concentration of ionic species and thus type of surface treatment can be changed to suit different requirements [23]. Forced air atmospheric pressure plasma treatment adds the simplicity of avoiding any pure gas to the added advantage of being able to treat complex shapes easily, that cannot be done with other treatment techniques like flame treatments and chemical treatments [24].

II.3.1   *Plasma treatment functioning*

In general, surface treatment with cold plasmas results in surface energy increase through the following mechanisms [25]:

1. Surface cleaning, *i.e.* removal of organic contaminations from the surfaces;
2. Ablation, or etching, of material from the surface, which can remove a weak boundary layer and increase surface area;
3. Crosslinking or branching of near-surface molecules, which can cohesively strengthen the surface layer;
4. Modification of surface-chemical structure, which can occur during plasma treatment itself, and upon re-exposure of the treated part to air, at which time residual free radicals can react with atmospheric oxygen or water vapour.

II.3.2   *Plasma effects on polymer surface*

The interaction of low-temperature air plasma (non-equilibrium plasma) with polymers causes mainly the change of surface polarity. It results, among others, in the creation of C=O, O-H and COOH groups in the oxidation process, as shown in Figure II.9 [22]:
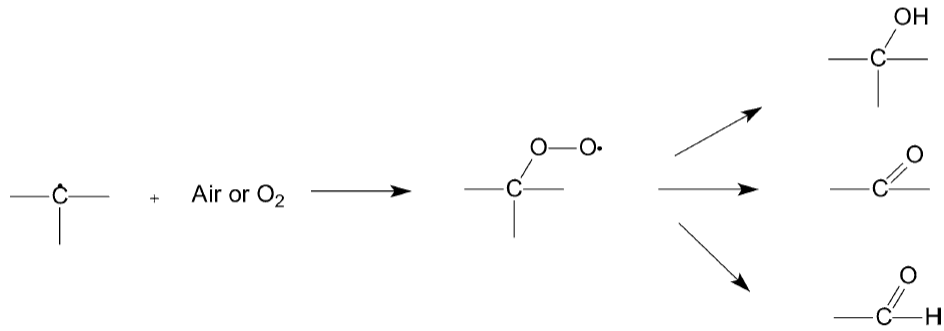
Figure II.9: mechanism for the formation of surface functional groups by atmospheric pressure plasma.

Electrons present in such plasmas are known to have kinetic energy sufficiently high for breaking up the covalent bonds and to initiate chemical reactions [26]. Specific techniques are required for understanding the mechanisms of processes caused in polymers by plasma; one of them is the measure of surface energy, where the degree of the polar fraction of surface energy is particularly affected by the plasma treatment.

II.4 *Fracture mechanics*

As the use of adhesive joints in structural components becomes more frequent, the need to define rigorous failure criteria grows more crucial. To those without a technical background mechanical testing of adhesive may appear straightforward and based on the characterization of the stresses acting on the bonded pieces, hence the maximum force that can be applied to a joint of each of the four types of loading: tension, shear, peel and cleavage [18, 27]. However, although this discipline is relatively easy to apply, it is applicable mostly to simple geometries and not capable of dealing with defects that are commonly present in adhesive joints.

This chapter focuses on a more rigorous approach, based on the fracture mechanics theory, which rather evaluates the maximum load or energy applicable to a system considering the effects of the defects it contains. Common failure criteria applied in this method are either fracture toughness (K_C) or the critical strain energy release rate (G_C) [27].

II.4.1 *Introduction to fracture mechanics*

Since all engineering components and structures contain defects it is important to assess if they affect the structural integrity of a system. Fracture mechanics is the science that evaluates the effect of such defects in a structure or a material, in relation to geometry, load applied and structural resistance. In particular, phenomenological fracture mechanics ought to predict the localization of the fracture in a loaded structure, the condition for its initiation, its mode of propagation and more importantly the effect of body's geometry [28].

Since the presence of singularities in all engineering materials is ascertained, there is the need of assessing their influence on every mechanical system. According to the most noteworthy feature of fracture mechanics, the defects normally present in a material do not reduce its ability to sustain load, but instead modify the stresses induced to the body, creating an inhomogeneous stress field near such defects [29]. When such stress concentration occurs it can give rise to propagation of the defect, *i.e.* the fracture of the component.

II.4.1.1 *Stress intensity factor*

One of the first approaches to analytically assess the extent to which the presence of a singularity influences the stress field introduced the concept of "stress concentration". Several authors (including *Irwin, Orowan, Polanyi*, earlier, and *Kirsch*, later) worked to evaluate the concentration of such stresses around many types of defects. In 1939 *Westergaard* found a relation to describe the stress field at a tip of a flat and sharp crack and

the result of stress perturbation was named "Stress intensity factor", K. *Irwin* identified 3 different "fundamental modes" of deformation and fracture: opening (mode I), in-plane shear (mode II) and out-of-plane tearing (mode III). By far, the most widely encountered in practice is mode I [30], which corresponds to normal separation of the crack under the action of tensile stresses, as shown in Figure II.10:

Mode I	Mode II	Mode III
(Opening mode)	(Sliding mode or shear mode)	(Tearing mode or out-of plane shear mode)
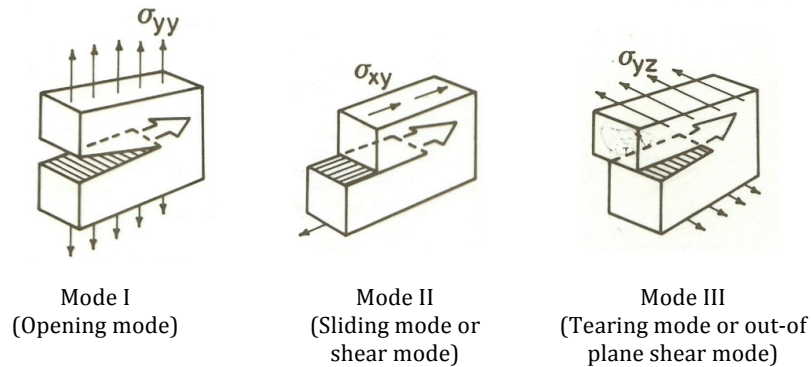
Figure II.10: fundamentals mode of fracture.

In general, the stress intensity factor depends on the applied stress, crack size and geometry, according to:

$$K = Y \cdot \sigma \sqrt{\pi \cdot a} \qquad (II.4,1)$$

where Y is called geometry factor, signifying the geometry of a crack system in a relation to the applied load, σ is the stress applied and a is the length of the crack. The stress intensity factor K defines the amplitude of the crack tip singularity and consequently the intensity of the local stress field. Local stresses are therefore proportional to K. In the vicinity of the singularity this parameter is enough to describe the crack tip condition and the use of a single-parameter for this purpose is "probably the most important concept of fracture mechanics".

In 1958 *Irwin* used this development to define a criterion for fracture based on K: fracture occurs when the stress intensity factors reaches a certain value proper of the material. This value does not depend on the geometry of the structure and the presence of singularity in the specific artefact: it is named "toughness" and it is an intrinsic property of the material. Fracture criteria based on material toughness, K_C, are nowadays proven to be effective and broadly diffused.

Unfortunately this criterion has been applied without the expected success in testing adhesive joints and in particular in peel tests, therefore other failure criteria have been used to assess joint resistance, mainly the critical strain energy release rate G_c, based on the principles firstly observed by *Griffith*.

II.4.2   *The strain energy release rate G*

(The paragraph is adapted from [30])

The very fundamentals of G_c criterion for assessing crack propagation origin from *Griffith*'s first observations. Studying glasses in the 1920's *Griffith* observed that an important difference between a cracked and an uncracked body is the additional surface associated with a crack. It is well known fact that creating new surface (new crack or crack propagation) requires energy, because surfaces carry higher energy than the body. According to *Griffith*'s hypothesis the fact that a cracked body remains stable or becomes unstable is dependent on whether the cracked body contains enough energy to afford creating additional surface while still maintaining equilibrium.
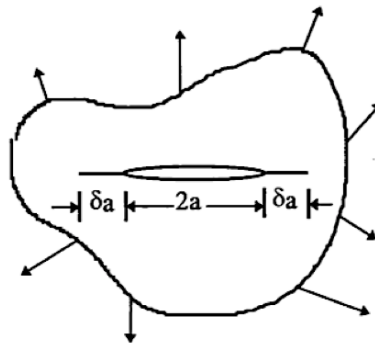
Figure II.11: equilibrium and energy balance for a cracked body (the thickness is identified with "B").

According to the law of conservation of energy the work performed per unit time by the applied load (W) must be equal to the rates of change of the internal elastic energy (U_E), plastic energy (U_P), kinetic energy (K) of the body and the energy per unit time spent increasing the crack area; in equation II.4,2 the balance: (dots refer to differentiation with respect to time)

$$\dot{W} = \dot{U}_E + \dot{U}_P + \dot{K} + \dot{\Gamma} \qquad (II.4,2)$$

In the case of interest of this work the crack grows slowly ($\dot{K} = 0$) and can be omitted. For what regards changes with respect to time, they are in this case caused by change in crack size, therefore it can be written:

$$\frac{\partial}{\partial t} = \frac{\partial}{\partial A}\frac{\partial A}{\partial t} = \dot{A}\frac{\partial}{\partial A} \qquad (II.4,3)$$

where A represents the crack area, equal to 2aB in Figure II.11 (B is the thickness and the total crack surface is twice the area of one crack surface).

Naming the potential energy

$$\Pi = U_E - W \qquad (II.4,4)$$

Equation II.4, 2 can be rewritten as

$$-\frac{\partial \Pi}{\partial A} = \frac{\partial U_P}{\partial A} + \frac{\partial \Gamma}{\partial A} \qquad (II.4,5)$$

which indicates that the reduction of potential energy is equal to the energy dissipated in plastic work and surface creation. For an ideally brittle material U_P is considered 0, therefore equation II.4, 5 can be rewritten as:

$$-\frac{\partial \Pi}{\partial A} = \frac{\partial \Gamma}{\partial A} = 2\gamma \qquad (II.4,6)$$

where γ is the energy required to form a unit of material surface area (and 2 indicates the number of faces created with a crack). The above equilibrium means that sufficient potential energy must be available in the system to overcome the surface energy of the material. In general, for an elastic body containing a crack, we can define a crack-extension force, G, per unit width of crack front:

$$G = -\frac{\partial \Pi}{\partial A} \qquad (II.4,7)$$

The total energy of the system considered contains therefore three parts:

- W   amount of work done by the applied load;

- U_E elastic energy;

- Γ energy required to form the crack surface;

$$U_{total} = (-W + U_E) + \Gamma \qquad (II.4,8)$$

According to linear elasticity theory (or to which is sometimes called *Clapeyron*'s theorem or linear elastostatics), a body under constant applied load obeys:

$$W = 2U_E \qquad (II.4,9)$$

In this case equation II.4, 7 can be rewritten as

$$G = \frac{\partial U_E}{\partial A} \qquad (II.4,10)$$

where G is usually called "strain energy release rate".

II.4.2.1   *Fracture criterion based on energy balance*

Crack extension occurs when the stress intensity factor or the strain energy release rate attain a critical value. As said, in truly brittle materials (e.g. glass or ice) the energy required for crack growth is the energy to form the new surfaces. In an engineering material instead, the energy required for a crack to grow is much larger than the surface energy. This is because plastic deformation will inevitably occur near the crack tip region and during crack

extension energy is consumed in deforming the material plastically. Considering the plastic contribute:

$$2W_f = 2(\gamma_f + \gamma_p) \qquad (II.4,11)$$

γ_p refers to the plastic work per unit area of surface created and is usually much larger than γ_f.This new definition of $2W_f$ is called R or G$_c$, and represents the resistance of the system, under the energetic view. It is common to plot the material resistance curve against the crack dimension: the driving force curse is entirely dependent on the structure geometry and loading condition, the R curve is a material property dependent mainly on temperature, environment and loading rate.

II.4.3   *Peel tests*

The analysis of peeling of laminates and adhesive joints has long history because peeling is important in many industries and products; the use of peel tests to assess these joints performances represents a natural extension of this situation and explains why such tests are so highly developed [31].
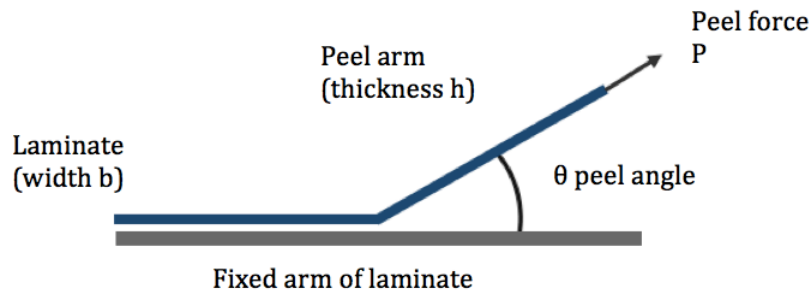
Figure II.12: peel test functioning scheme.

In Figure II.12 the basic working principle of a fixed arm peel test. A flexible material is bonded with a rigid one. The thin peeling strip in an ideal case is considered infinitely stiff in the axial direction but completely flexible in bending. This strip is peeled from the other material (which is rigid or fixed on a rigid support) by a peel force P, with a peel angle θ, ideally variable from 0° to 180°. In this thesis only fixed arm peel test with a peel angle of 90° have been performed.

II.4.3.1   *Fracture mechanics in peel tests*

According to *Kinloch et al.* [31], "some workers have analysed the peel test by considering the stress distribution around the peel, or crack front. This approach has met with little success, mainly due to the very complex stress distributions around the peel front,

especially when the crack is located at the bimaterial interface, and the difficulty of defining a failure criterion. Other have used a fracture-mechanics method and adopted a stress-intensity factor approach which is based upon a stress-singularity argument. This method has not proved to be very rewarding, mainly due to there being little physical basis for this approach in adhesive joints."

For all listed reasons most experts of peel test have adopted an approach to analyse its mechanics not based upon considering either the stress distribution around the peel front or the determination of the stress intensity factors; the approach they chose was one based upon applying a fracture-mechanics method: energy-balance approach. This means that a value of G_c is ascertained, for either cohesive fracture through the adhesive layer or along the bimaterial interphase. As explained before, the value of G_c (its curve with respect to the dimension of the crack) should be characteristic of the joint and, ideally, independent of geometric parameters such as the applied peel angle, the thickness of the flexible substrate arm(s) being peeled and the thickness of the adhesive layer. However, since the value of G_c includes plastic and viscoelastic energy dissipation which occur at the crack tip, it will be a function of the rate and temperature at which the test is conducted [31].

II.4.3.2   Peel test analysis
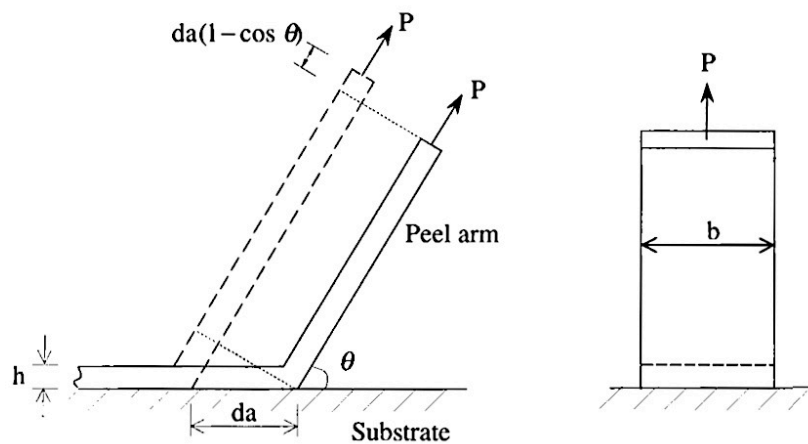
Figure II.13: peel test opening mechanism scheme [31].

As schematically shown in Figure II.13, when a critical value of P is reached the flexible strip debonds from the other adherend. Considering that this happened over a distance da, the force moves through a distance $da(1 + \cos\theta)$, performing a work $Pda(1 + \cos\theta)$. This work creates a new surface $b \cdot da$, where b is the width of the strip [31]. This gives the possibility to evaluate the input energy necessary to create a unit area:

$$G = \frac{Pda(1 - \cos\theta)}{bda} = \frac{P}{b}(1 - \cos\theta) \qquad (II.4,12)$$

It is important to note that the strip thickness does not appear in this result, nor do any material properties, but this comes from the fact that the strip was supposed to be ideal.

The test is an example of a steady-state process in that the debonding region remains the same as it grows. For this reason one would expect the load to remain constant for the whole test, and proceed with a constant speed determined by the load point. Such situation would be an example of stable propagation and would be very convenient for studying the adhesion of flexible substrates, but unfortunately this is not always the case, primarily because of the general absence of the assumptions outlined above.

As explained, an energy-based approach is commonly used to analyse peel tests. The input energy to the peel test need to be resolved into the various deformational energies: elastic, plastic and adhesive fracture energy, at least [32]:

$$G_A = \frac{dU_{ext}}{bda} + \frac{dU_s}{bda} + \frac{dU_{dt}}{bda} + \frac{dU_{db}}{bda} + \frac{dU_k}{bda} \qquad (II.4,13)$$

where G_A refers to the fracture toughness, and dU correspond to increment of external work (dU_{ext}), the change of stored strain energy (dU_s), the increment in dissipated energy (tensile, dU_{dt} and bending dU_{db}) and the increment of kinetic energy change (dU_k), respectively.

The kinetic energy term U_k is determined completely by the test speed. It can be easily included in the analysis but generally the speeds are so slow that there is little change in kinetic energy, therefore it is considered negligible.

This approach has been reported on ESIS protocol [32] in order to convert peel strength (P/b) to adhesive fracture toughness:

$$G_A = G - G_P \qquad (II.4,14)$$

G is the input energy after correction for tensile and plastic deformation in the peel arm and G_P is the plastic work in bending the peel arm. According to *Moore et al.* [32] the tensile corrections are often negligible so input energy is "G" reported in II.4,14: in order to calculate the plastic deformation energy associated with the peel arm it is first necessary to have knowledge of the tensile stress-strain characteristics of the peeled material. This will include an initial deformation but also a subsequent work hardening, plastic, deformation. The plastic arm in the peel test may then be modelled using a large-displacement beam theory modification for plastic bending. The ESIS protocol report three alternative solutions to include the stress-strain behaviour in the peel analysis:

- Bilinear stress-strain curve;
- Power law stress-strain curve;
- Digitised;

For the bilinear and power law fits a number of parameters from the stress-strain curves fits are calculated.

For the bilinear model:

$$\begin{cases} \sigma = E\varepsilon & \varepsilon \leq \varepsilon_y & (II.4,15) \\ \sigma = \sigma_y + \alpha E(\varepsilon - \varepsilon_y) & \varepsilon > \varepsilon_y & (II.4,16) \end{cases}$$

where E is the Young modulus of the first part of the curve, α is the elastic modulus ratio (after the yielding and before), σ_y is the yielding stress and ε_y the yielding deformation.

For the power-law model instead:

$$\sigma = \sigma_y \left(\frac{\varepsilon}{\varepsilon_y}\right)^N \qquad (II.4,17)$$

where N is the work hardening coefficient.
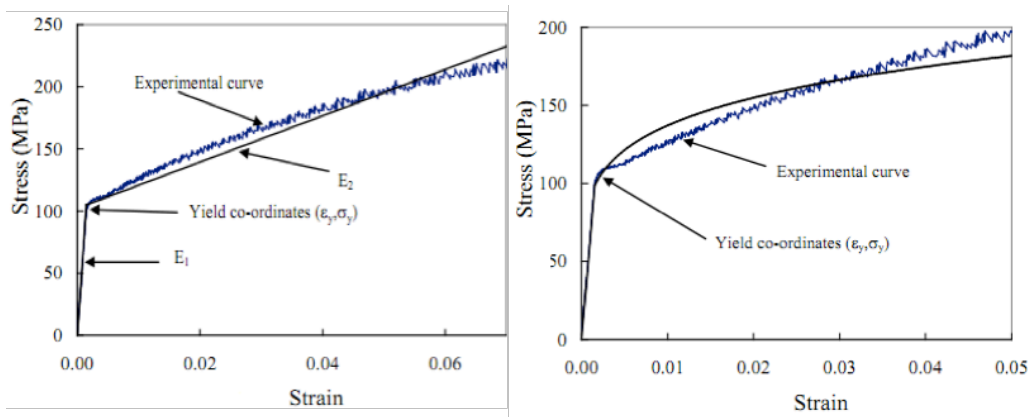
Figure II.14 a-b: example of bilinear (a) and power-law (b) fitting of a stress-strain curve [32]

The digitisation of the stress-strain behaviour requires a software package, as does the subsequent numerical analysis for calculation of G_P. This package can be downloaded from [33], and even if is the most time-consuming method, it is also the most precise. This last method has been adopted for the peel tests analysis in this thesis.

III. CHAPTER: MATERIALS AND METHODS

This chapter provides all the information on the materials necessary to thoroughly understand the work done. Explanations of the methods used to measure all data are also provided.

III.1 Materials

Main goal of this work is to optimize a plasma treatment to improve the resistance of an adhesive joint which bonds together an EVA and a PA 12 with a polyurethane adhesive.

III.1.1 Ethylene Vinyl Acetate (EVA)

Ethylene vinyl acetate is a copolymer made of ethylene and vinyl acetate where the amount of ethylene varies, in most common versions, from 60 to 98%. EVA is a thermoplastic polymer but its properties approach the ones of elastomers in softness and flexibility. Being a thermoplastic polymer its processing is easier than elastomers, making it interesting for many applications.

When VA content is below 10% the properties of EVA resemble the ones of PE except for a better clarity, higher impact strength, better low temperature flexibility and lower heat-seal temperatures. The impact strength, the puncture resistance and other properties increase significantly with the content of vinyl acetate up to the point where the material reaches a rubbery form, over 15-18% VA content. Other properties of EVA include good barrier properties, resistance to UV radiation and no odour so this polymer (when VA content is over a certain limit) competes with rubber and other vinyl products in many applications [34].

EVA has many practical uses, especially in sport equipment in its foamed version as padding (for example in ski boots) but one of its main applications is to absorb shocks, for example in sport shoes: this is the purpose of the materials studied in this thesis.
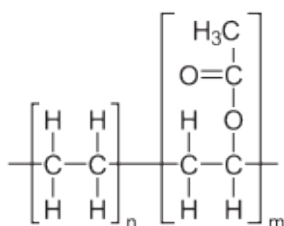
Figure III.1: chemical structure of ethylene vinyl acetate.

Considering the chemical structure in Figure III.1, n represents fraction of ethylene monomer content and m the one of vinyl acetate. The Vinyl Acetate monomer contains two

oxygen atoms and it is therefore polar, diversely from the ethylene monomer. This means that the higher is the vinyl acetate content in the blend, the greater is the polarity of the polymer. While considering adhesion the polarity degree of a material is important because it greatly affects the surface energy.

Three versions of EVA have been studied in this work:

- Unfilled EVA
- Filled EVA
- Foamed filled EVA

Due to non-disclosure agreement, neither copolymer blend ratio nor the additives of the mixture are known. The main direct difference between the two unfoamed versions is the transparency: while the unfilled version is somewhat clear (although not transparent) the filled EVA is completely opaque. Both these materials have been provided in 300x150x2mm sheets.

The third version of EVA is foamed and is the one practically used in real product; the density of the polymer has not been evaluated, since there was no need for the purpose of the thesis. The foamed EVA has been provided in 300x200x10 mm sheets and all these polymers have been supplied by Nike.

III.1.2   Polyamide 12 (PA 12)

Aliphatic polyamides are generally known for their original trade name as "Nylons". There are two types of polyamides: those produced from $\alpha + \omega$ amino acids and those obtained from condensation reactions between a diacid and a diamine. The technological nomenclature for polyamides is to add to the term "Nylon" the digit corresponding to the number of carbon atoms between the nitrogen atoms of the repeating unit. For $\alpha + \omega$ amino acid polyamides, such as the one used for this thesis, the repeating unit is the one in Figure III.2:
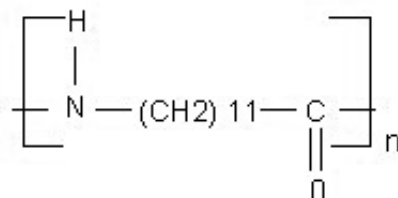
Figure III.2: structure of polyamide 12.

The polymer will be known as Nylon x+1, where *x* is the number of ethyl groups: in this case is 11, therefore its name is polyamide 12. In the linear and regular structure, strong molecular interactions are developed through H bonds acting between the NH group of one molecule and the C-O group of the adjacent chain. Unlike EVA, polyamide 12 is not a copolymer and its melting point does not depend on the blend formulation: it is equal to 175

°C [35].

Even if not as widely diffused as other polyamides, Nylon 12 possesses particular properties which make it a good material for many applications for instance in the automotive sector (especially fuel contact part), or in other applications such as pneumatic brake lines, industrial hose and tube, wire, cables and other medical (*e.g.* catheters) and sport applications (*e.g.* ski boots). Most of PA 12 peculiarities come form the fact that it has lower concentration of amides than any other available polyamide; some of its characteristics include [36]:

- The absorption of very little moisture, which confers it a very high degree of dimensional stability even in environment with fluctuating humidity levels, such as the one of shoes (since PA12 absorbs low moisture it has not been necessary to monitor the water content during the mechanical experiments);
- Conservation of very high impact resistance at low temperatures;
- Low coefficient of friction and excellent resistance to abrasion;
- High processability and high fatigue resistance;
- Excellent resistance to chemicals including hydraulic fluids, oils, fuels, grease, salt water and solvents;
- Exceptionally strong resistance to cracking under stress, including instances when encapsulates metal components.

The presence of nitrogen and oxygen in the polymer chain confers also to this polymer some degree of polarity, thus increasing the untreated surface energy. This polymer appears pale white opaque and Nike supplied it in 150x100x2 mm sheets.

III.1.3 *Polyurethane adhesive*

The name polyurethane (PU) describes any polymer made of a chain of organic units linked by urethane (carbamate) joints. In this thesis PU has been used as the adhesive to joint the EVA and the PA.

Polyurethanes are leading performers in many adhesive applications. PU adhesive systems can be classified as one- or two-component reactive adhesives, elastomeric solution adhesives, and water-dispersed adhesive. The one-component reactive adhesives are isocyanate-terminated prepolymers that cure by reaction with ambient moisture and are used, for example, for the manufacture of laminated films for packaging. The two-component reactive adhesives are formulated from polyisocianates and polyols. They are generally used as structural adhesives, especially for the bonding of plastic automotive parts; both types permit solvent-free applications and exhibit excellent properties which surpass those of adhesives based on other synthetic rubbers in resistance to fats, oil, and

plasticizers [37].

Polyurethane solution adhesives are elastomers soluble in solvent such as methyl ethyl ketone, toluene, ethyl acetate and cycloexanone. Depending on their molecular weight, the solution adhesives are either one- or two- component systems. Low molecular weight two-component systems require cross-linking via the addition of polyisocianates in order to achieve optimum properties. The properties of the higher molecular weight one-component systems can also be enhanced by the addition of polyisocianates.

A polyurethane adhesive has been selected as the best choice for this application because of its peculiarities in relation with bonding the shoe sole with the rest of the shoe. This purpose required in particular a good toughness and flexibility together with resistance to high deformations and fatigue. The technical polyurethane adhesive chosen is commercialized with the name Shoegoo™ (produced by Eclectic™). It is a one-component, 40-years proven adhesive very diffused in North America and Britain used especially to repair damage heels and shoe soles because it dries to waterproof and retains flexible and resistant to breaking or cracking.

Although the producer does not specify it, this adhesive seemed to be a toluene based one-component solution: toluene is cited in the safety information reported on the product.

III.2 *Contact angle measurements*

Contact angles have been measured on many different samples both plasma treated and untreated, polished and unpolished, clean and unclean. As explained in Chapter II, the main purpose of contact angle measurements is the calculation of surface energy although they have been used also for many other scopes, most noteworthy the optimization of the plasma treatment, which has been used secondarily also:

- to ascertain that a given polymer sheet had the properties of the others;
- to ascertain that the treatment was homogeneous on whole treated surface;
- to evaluate the effect of the plasma treatment after different time from the process;

All of these contact angle measurements have been obtained with the sessile drop method.

III.2.1 *Sessile drop apparatus*

The sessile drop apparatus used to measure drop shapes is similar to the one in Figure III.3:
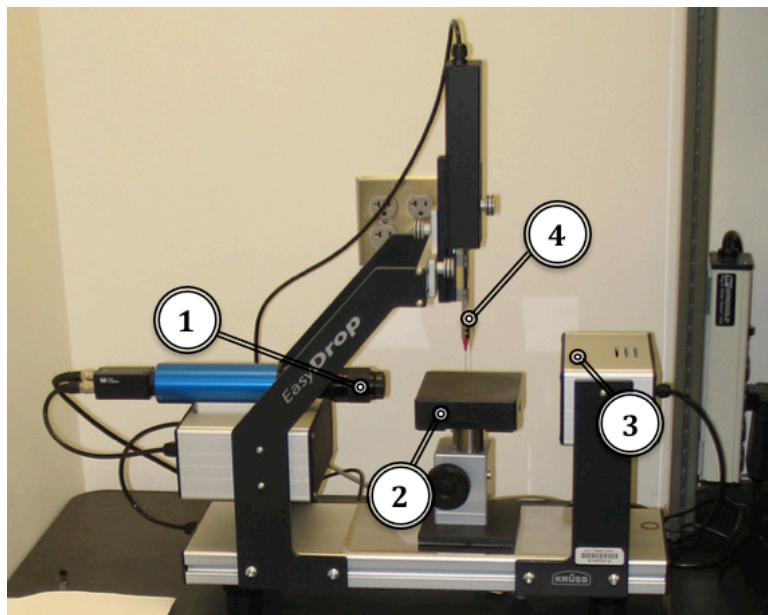
Figure III.3: sessile drop measurement apparatus.

Where:

1- Is a camera recording the image of the drop deposited and sending the information to a processor;
2- Is an adjustable plate where the material to be analysed is deposited: it can be moved up and down and turned in both directions. This is necessary when analysing something which is not macroscopically flat: by adjusting the plate it is possible to deposit the drop on a flat segment of a material even if the two surfaces (the one

deposited on the plate, and the one where the drop is placed) are not parallel;

3- Is a backlight which has to be regulated in order to create the best contrast possible between the drop and the background. It is important to set the light intensity in the beginning of the analysis and not to modify it during the measurements because this can alter the contrast;

4- Is a syringe used to place the drop on the substrate to analyse. The syringe is fixed on a support which allows, at first, to prepare a certain quantity of the liquid on the point of the needle. Then, the whole syringe can be moved up and down with extreme precision in order to gently deposit the drop on the surface without letting it to fall.

This goniometer apparatus is also composed by a computer and related software. The processor receives the image recorded by the camera and the software -after having adjusted all the parameters- displays the drop image and subsequently calculates all the geometric parameters like a goniometer.

III.2.1.1   Surfaces preparations

All of the four materials described in III.1 (3 EVAs and 1 PA) have been somewhat investigated with a contact angle analysis. The first step was the preparation of the surfaces to be analysed: the first and most important condition is their homogeneity. This is particularly important because contact angle measure is commonly considered to be a highly scattered analysis and therefore many drops need to be placed on the substrate to obtain reliable data. Since the drops cannot be deposited all on the very same spot (as explained later) it is critical that drops of the same liquid establish similar contact angles in different spots of the same surface. In order to be measured, the polymer sheets have first been cut in small pieces (approximately 60x15x2mm) with a simple cutter (there is no need in this case to debur the edges). For untreated surface analysis three cleaning conditions have been investigated for the four materials:

- **Polished surfaces**. Polished surfaces have been investigated to determine the properties of the pure polymer surface, without any influence due to normally present roughness or uncleanliness. The results of this analysis have been studied only for scientific and comparative purpose because the producer did not consider the polishing as one of the possible pre-operations to increase adhesion. The polishing machine used consists of a rotating plate where abrasive discs of different roughness are positioned. Starting from the rougher disc the adherend surface is pressed against the rotating plate that abrades it. By using increasingly smoother

discs it is possible to progressively reduce the roughness of the polymer abraded. When the surface becomes smooth enough it is possible to use a very fine diamond powder placed on a special support to polish the surface further on. The final step used for this process was a diamond powder with particles of nominal dimension of 0.25 μm which is assumed to be the roughness of the polished surface after the treatment. After the polishing, the surfaces are cleaned only with distilled water and let naturally dry.

- **Dry tissue-cleaned surfaces**. In this case the samples are simply wiped with a dry tissue to remove dust. With this cleaning it is not possible to remove deep contaminations which therefore rest on the surface. This process has been chosen for being very simple yet plausible for the producer. It is important not to rub the surfaces too much in order to avoid the creation of electrostatic forces that may affect the contact angle measures.

- **Detergent-cleaned surfaces**. In this case the specimens are deeply cleaned with a common dish detergent (in this case Fairy™ from P&G). It has been chosen to be deeper than a simple dry tissue wipe but still quick to perform in any condition. The samples are covered with the detergent and rubbed under the water. Subsequently they are abundantly rinsed with normal water until all the detergent has been removed from the surface. In the end, tap water is rinsed with distilled water and the samples are let to dry in the atmosphere for some hours.

The peel and the Double Lap Joint specimens have been realized only with detergent-cleaned polymers, as explained later.

III.2.1.2   Measurements procedure

After preparing the samples as outlined above, one of them is placed on the adjustable plate and all the image-related parameters are adjusted: these include the light intensity and the contrast of the image. Once the measurements apparatus is set up the syringe is placed in its position and a small amount of liquid is pressed out of the point of the needle. When the amount of liquid at the head of needle is enough the piston of the syringe should not be moved anymore. Using a small wheel on the apparatus it is possible to slowly move down the whole syringe until the edge of the drop touches the surface of the adherend and the liquid is deposited as gently as possible. It is important to be careful in this operation because the addition of a small pressure will completely ruin the experiment: this pressure would act as an additional spreading contribution, as indicated by equations II.2, 8.

If the light and the contrast are correctly adjusted, once the drop is properly placed onto the surface, its shape is something like Figure III.4.
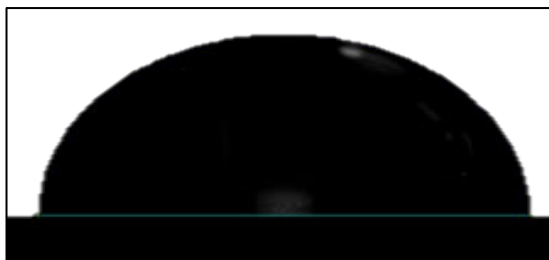
Figure III.4: example of sessile drop shape, as recognized by the software.

At this stage the software calculates the drop shape (height and width), both contact angles and their average. Once the drop is placed it is possible to take multiple measurements on the same drop. In order to reduce the error, in this work 4 different measurements at a temporal distance of one second have been taken for every drop.

Once the data are recorded the substrate is moved and a new drop is placed next to the previous, repeating the measurements. For each different surface and liquid a number of 5 to 10 drops (depending on the variability of the data) has been recorded. This procedure is in accordance with contact angle measurements standard [38], which requires a minimum of three drops.

III.2.2   *Test liquids*

Initially five liquids have been selected for surface energy analysis. Since a test liquid has to possess higher surface energy than the substrate not to spread freely (at least in one component) the choice of the liquids is narrowed to a very limited group of liquids with high surface tension. The most common liquids for contact angle analyses have been chosen, namely:

- Water, H_2O;
- Glycerol, $C_3H_8O_3$;
- Diiodomethane, CH_2I_2;
- Formamide, CH_3NO;
- Ethylene Glycol, $C_2H_6O_2$;

The glycerol has not been considered in the analysis due to problems explained later.

It is necessary, in order to calculate surface energies from contact angle with these liquids, to know their pure surface tensions. In literature many -different- values are available but it is not easy task to distinguish which ones are the most valuable, because theoretically they have been all calculated for pure substances. To overcome this problem a reasonable approach is to average several values found in literature. A website collecting several data is http://www.accudynetest.com [39]: the values found in this website have been averaged to obtain the final data to use in the fitting (as explained in II.2.3.3). Table III.1 shows the raw

data collected from the website (for each case only the data similar to the ones reported by others have been included) and the reference.

	γ_L^{tot} [mJ/m²]	γ_L^D [mJ/m²]	γ_L^P [mJ/m²]	Reference
Water	72.8	22.1	50.7	*Interfacial Forces in Aqueous Media, 2nd Edition*, Carel J. van Oss, CRC Press, Boca Raton, FL, 2006
	72.8	21.8	51.0	*Polymer Interface and Adhesion*, Souheng Yu, Marcel Dekker, New York, NY, 1982, p. 151; harmonic mean, derived from interfacial tension data
	72.8	22.6	50.2	*Polymer Interface and Adhesion*, Souheng Yu, Marcel Dekker, New York, NY, 1982, p. 151; harmonic mean, derived from contact angle data
Glycerol	63.4	37.0	26.4	A.F. Toussaint and P. Luner, in *Contact Angle, Wettability and Adhesion*, K.L. Mittal, editor, VSP, Utrecht, The Netherlands, 1993, p. 385
	63.4	40.6	22.8	*Polymer Interface and Adhesion*, Souheng Yu, Marcel Dekker, New York, NY, 1982, p. 151; harmonic mean, derived from contact angle data
Diiodomethane	50.8	44.1	06.7	*Polymer Interface and Adhesion*, Souheng Yu, Marcel Dekker, New York, NY, 1982, p. 151; harmonic mean, derived from interfacial tension data.
	50.8	48.5	02.3	J.R. Dann, *J. Adhsn. Sci. Tech.*, **21**, 961 (2007)
	50.8	49.0	01.8	*Polymer Interface and Adhesion*, Souheng Yu, Marcel Dekker, New York, NY, 1982, p. 151; harmonic mean, derived from contact angle data.
Formamide	57.9	34.3	23.5	A.F. Toussaint and P. Luner, in *Contact Angle, Wettability and Adhesion*, K.L. Mittal, editor, VSP, Utrecht, The Netherlands, 1993, p. 385
	58.2	36.0	22.2	*Polymer Interface and Adhesion*, Souheng Yu, Marcel Dekker, New York, NY, 1982, p. 151; harmonic mean, derived from contact angle data.
	58.0	39.0	19.0	*Interfacial Forces in Aqueous Media, 2nd Edition*, Carel J. van Oss, CRC Press, Boca Raton, FL, 2006
	58.2	39.5	18.7	J.R. Dann, *J. Adhsn. Sci. Tech.*, **21**, 961 (2007)
Ethylene Glycol	48.0	29.0	19.0	*Interfacial Forces in Aqueous Media, 2nd Edition*, Carel J. Van Oss, CRC

Table III.1: different surface tension data.

The mean values of Table III.1 data are reported in Table III.2:

Substance	γ_L^{tot} [mJ/m²]	γ_L^D [mJ/m²]	γ_L^P [mJ/m²]
Water	72.80	22.16	50.63
Glycerol	63.40	38.80	24.60
Diiodomethane	50.80	47.20	03.60
Formamide	58.07	37.20	20.85
Ethylene	48.00	29.00	19.00

Table III.2: averaged surface tensions data for pure liquids.

III.2.3 *Experimental expedients and problems*

There are a considerable number of errors to avoid while performing contact angle tests in order to reduce the scatter, and most of them are not reported on the ASTM standard. According to the experimental procedure described by Singh [2] it is important:

- Not to reuse the part of the surface used by one test liquid for any other liquid

because it can be contaminated;

- Not to reuse the same surface even after wiping-off the test liquids because the wiping action induces electrostatic charges one the surface which alter the results;

- The intensity of the light used in the goniometer apparatus should not be changed for the whole analysis but it must not be changed for at least the same specimen.

- Any treatment, (chemical, physical or mechanical) done to the surface, in essence, changes the surface chemistry and physiology, which again results in variation of results.

- As explained above, if the drop falls form the syringe through a certain height and lands on the test surface, the contact angle made is smaller than the equilibrium one. This happens because the drops acquires a momentum during its fall through the air which is lost and transformed in spreading pressure when the drop hits the sample, flattening out.

More than these, other important issues while measuring contact angle are:

- <u>The focus</u>. Since the contact angle establishes between the drop and the surface it is crucial that both are focused during the measure. The camera records the image from the side therefore shows the edge of the surface more than the actual spot where there is the drop. For this reason it is important to place all the drops near an edge and record the image from that side. It is possible only to use two liquids with each sample, placing the drops as indicated in Figure III.5 where firstly one liquid is placed and measured (each drop is deposited just before the recording), then it is removed being careful not to wipe also the other side of the sample, which can still be used once flipped to place the other test liquid.
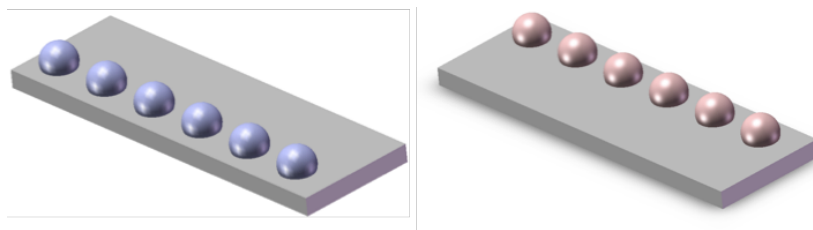
Figure III.5: no more than two test liquids can be used on a single specimen.

- <u>The time between the deposition and the measurement.</u> Once the drop is positioned on the surface and the camera is recording is not easy task to determine which one is the best moment to start the geometric measurement. This is because on one hand the drops take some instants to establish equilibrium but on the other hand the liquid starts evaporating or penetrating in the surface capillaries (this would result in a lower contact angle than the equilibrium one). One more point is that the time necessary to go to equilibrium depends on the viscosity of the liquid (for example

some problems arose with the use of glycerol, explained later on). To overcome this problem the best solution is to try to allow the same time to all liquids which have the same viscosity. All the test liquids but the glycerol posses the same viscosity therefore this approach seemed to mitigate the problem.

- <u>The time between the plasma treatment and the deposition.</u> Once the surface is treated with the plasma it is "activated". It can however be contaminated by the particles normally present in the atmosphere and if too much time is left between the plasma treatment and the measure some of its effect will be lost. This issue is better discussed later.

- <u>The temperature.</u> The plasma treatment causes the temperature of the polymer surface to rise significantly. Since not all the plasma treatments have the same intensity, and don't cause the same temperature increment, the temperatures of the substrates are different after dissimilar treatments. This increment in temperature may affect the behaviour of the liquids deposited. At the same time leaving all the surfaces to cool down to the same temperature may alter the effect of the plasma because of different cooling time. To understand the degree of this problem one material has been tested just after the treatment and after the cooling and the temperatures have been recorded: the results are outlined in Chapter IV.

- <u>Substrate deformation.</u> As explained the plasma treatment heats the samples causing their temperature to rise significantly. This causes a deformation of the samples which makes it difficult to assess the true contact angle.

In Figure III.6 the black arrow shows the direction of the recording of the image and the distortion of the surface:

Figure III.6: the distortion of the substrate causes the camera to record a wrong contact angle.

The left image shows the distortion of the samples where the drop is placed while the right ones display the contact angle as it is, and as the camera instead records it.

The solution adopted to solve this problem is explained in Figure III.7. The warped specimen is placed on a metal bar and pressed on the sides with other two metal bars; these operations have to be carried out without touching the specimen surface. At the end, the two edges of the samples are cut off, obtaining a smaller but flatter sample that allows the measurements also for heavily treated polymers.
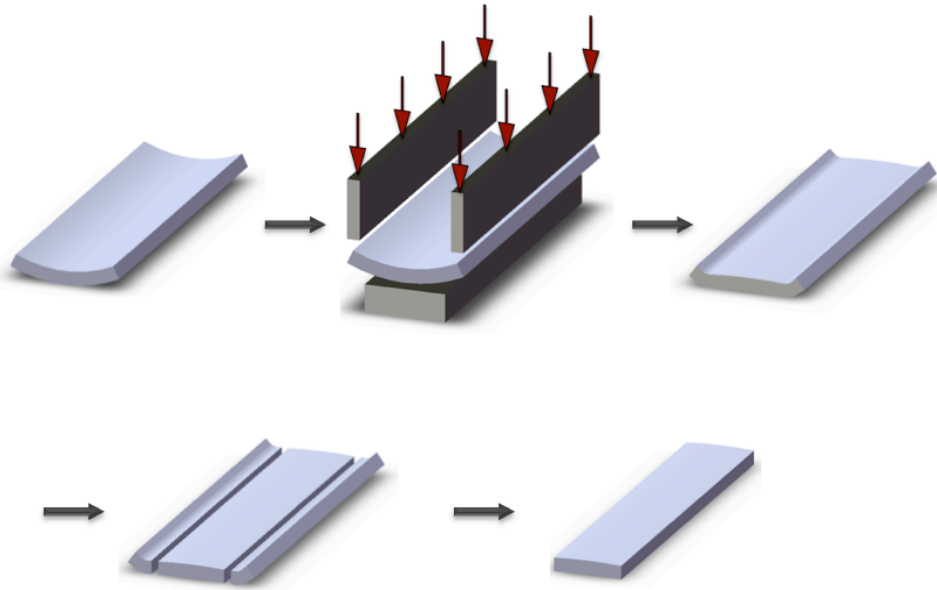
Figure III.7: graphic representation of the solution to the problem of specimens distortion.

III.2.4 *Glycerol problem*

As explained, glycerol was at first selected to be one of the test liquids and it is generally used for this purpose because it is harmless, easily commercially available and it possesses a good surface energy. In this analysis however some problems raised from its first use.

As explained in Chapter II.2.3 OWRK linear interpolation allows determining whether a data fits well with the straight fitting line or not. What has been observed in the first analysis on polished untreated surfaces was that the point corresponding to glycerol was always far from the fitting line, as shown in Graph III.1:

Adj. R-Square	0.68372	
	Value	Standard Error
Intercept	5.19157	0.88668
Slope	3.00113	0.96625
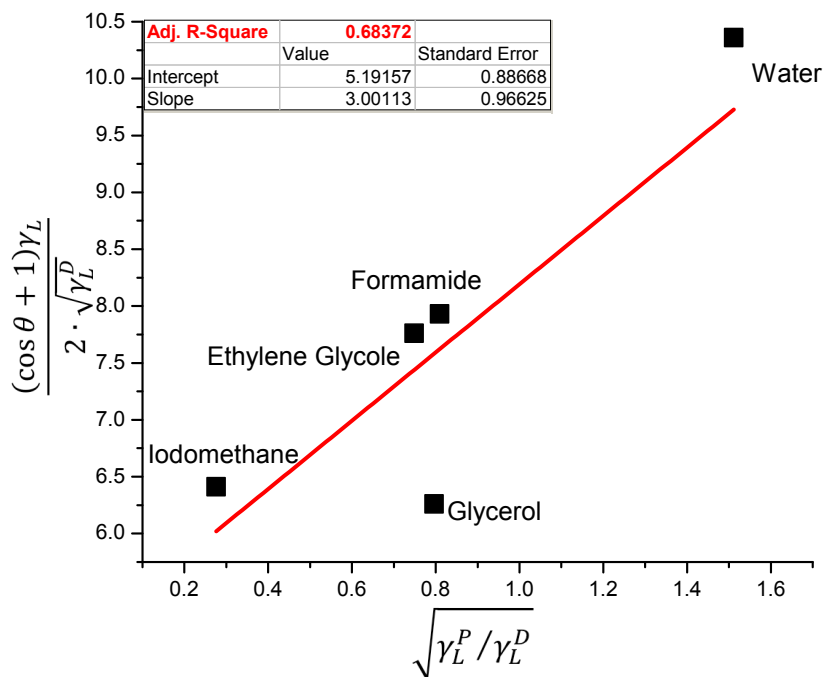
Graph III.1: graphic representation of OWRK fitting: glycerol is clearly far from the fitting line.

In Graph III.1, showing a real analysis, it can be seen that the coefficient of determination R^2 is low and the reason is clearly the distance of the Glycerol point from the points related to the other test liquids. This trend was confirmed also with the other polymers. A brief literature research confirmed this issue. According to *Van Oss* et al [40], "A drawback of glycerol is its high viscosity*, i.e.* 1490 times of that of water, at 20°, which complicates standardization of the timing of contact angle measurements, an important consideration, particularly when there is any degree of solubility between the solid and the liquid". This may be a justification for what obtained during the measurements. Since there were already other two liquids with a similar $\sqrt{\gamma_L^P / \gamma_L^D}$ ratio, glycerol has been discarded.

III.2.5 *Data analysis*

An important issue raised with first data evaluations was about deciding the best way to analyse the high amount of data collected. Together with a statistician at Imperial College different approaches have been evaluated.

The program used to fit the straight line (Origin Pro 8.5) already allows automatic calculation of both the slope and the intercept and their relative errors. In the first stage the errors have been evaluated manually to ascertain if the data proposed by the program were the same but during the evaluation of the error a new and more important issue raised: the choice was about deciding the best way to consider the precision of the single data in the complete fitting.

A first approach, which has been lately discarded, was to average the data for each test liquid and then to fit this four data (due to the four liquids) in a straight line. According to the Imperial College statistician this approach was not accurate enough. It was instead better to exploit all the data recorded, even if for some liquids there were more data than others: the fact that all the data for the same liquid were on the same abscissa while different liquids had diverse x-values weighted automatically the difference in the number of data.

Once established that best approach was to use all data available, there was still different ways to analyse them. The single values could be left unweighted or a different influence could be attributed to the points during the fitting. Different choices have been evaluated:

- Linear fit with unweighted data;
- Linear fit with inverse weight of the standard deviation, where at each single point has been assigned the standard deviation of the series of points related to the same liquid; (in this case the points with less error count more in the fitting);

- Linear fit with direct weight of the inverse of the squared variance, i.e. the points with more variance count less for the fitting.

Preliminary graphs and linear fittings have been assessed for the three approaches but the last one has been discarded due to the similarity with second, where the latter seemed to fit better the data.

The comparison between the unweighted case and the one where the weight is correlated to the inverse of the standard deviation is shown in the next six Graphs III.2-7. For three different surfaces both fitting ways have been calculated, and the residuals are shown in the side.
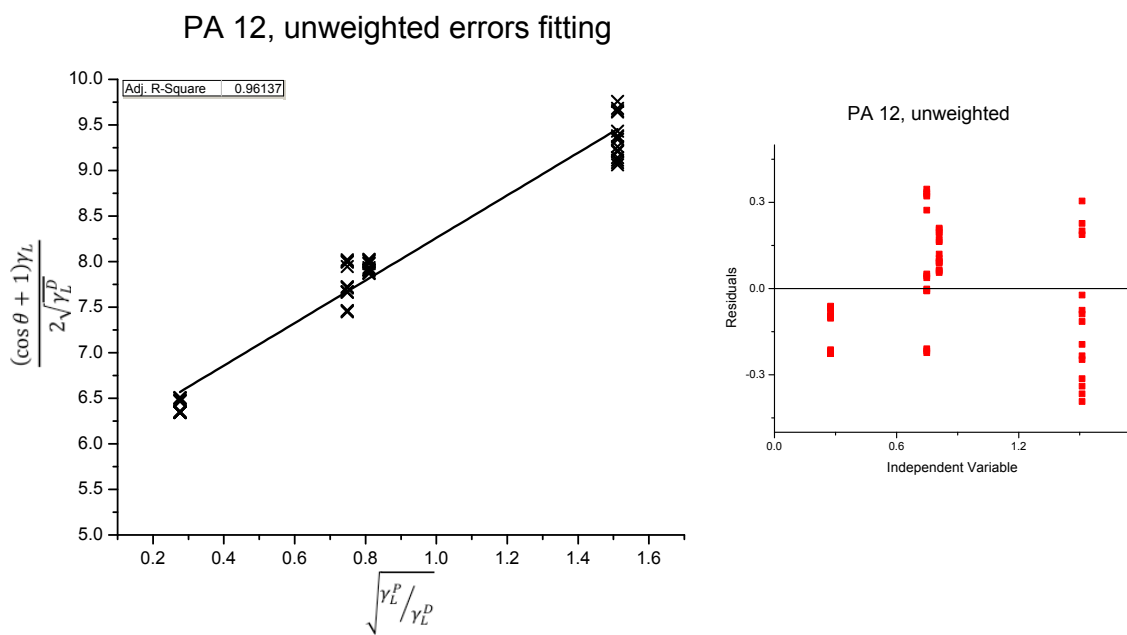
Graph III.2: polished PA 12 (OWRK unweighted error fitting).

PA 12, weighted errors fitting

| Adj. R-Square | 0.97544 |

$$\frac{(\cos\theta + 1)\gamma_L}{2\sqrt{\gamma_L^D}}$$

$$\sqrt{\gamma_L^P / \gamma_L^D}$$

PA 12, weighted

Residuals

Independent Variable
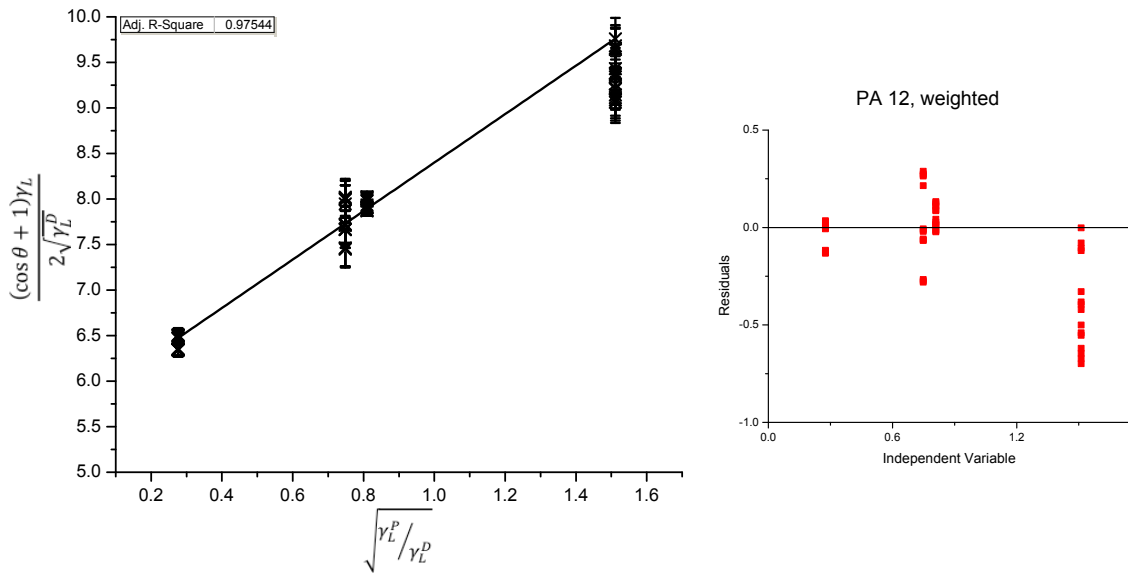
Graph III.3: polished PA 12 (OWRK weighted error fitting).

Filled EVA, unweighted errors fitting

| Adj. R-Square | 0.94727 |

$$\frac{(\cos\theta + 1)\gamma_L}{2\sqrt{\gamma_L^D}}$$

$$\sqrt{\gamma_L^P / \gamma_L^D}$$

Filled EVA, unweighted

Residuals

Independent Variable
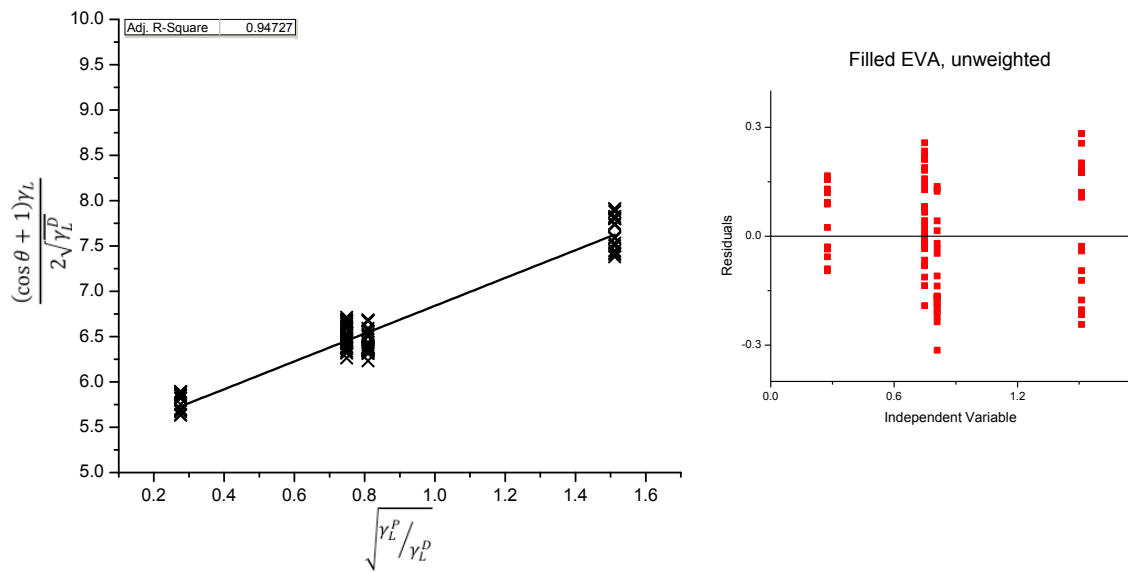
Graph III.4: polished filled EVA (OWRK unweighted error fitting).

Filled EVA, weighted errors fitting
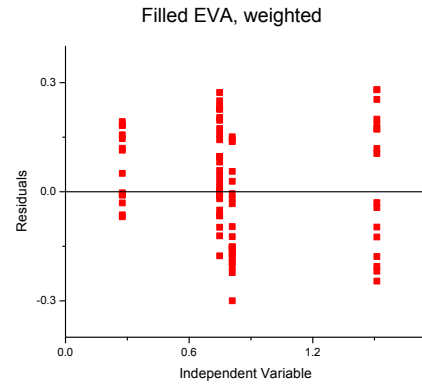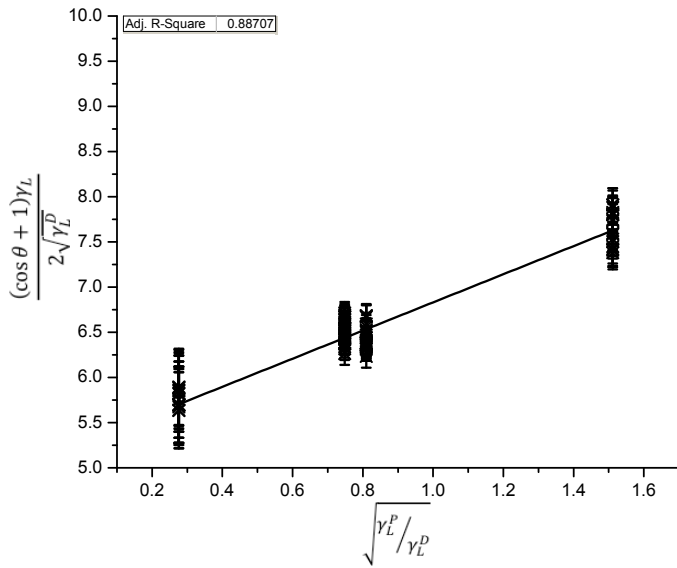
Graph III.5: polished filled EVA (OWRK weighted error fitting).

Unfilled EVA, unweighted errors fitting
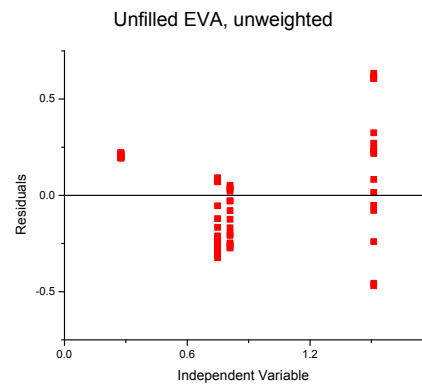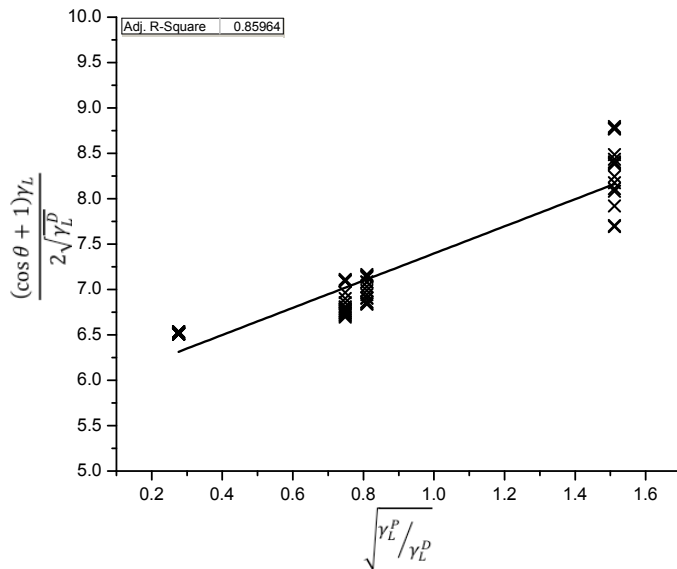
Graph III.6: polished unfilled EVA (OWRK unweighted error fitting).
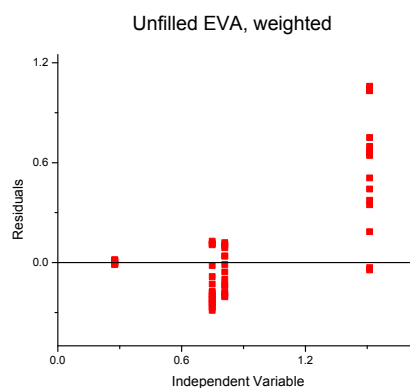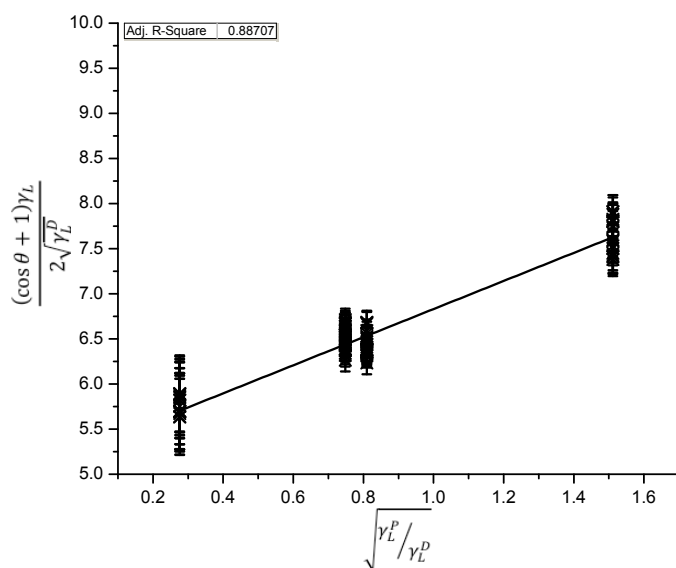
Graph III.7: polished unfilled EVA (OWRK weighted error fitting).

In the first and the third couple of data the residuals distribution show, in both cases, a parabolic trend but the fact that the curvature of the parabola is different implies that there is no evidence of systematic errors.

The error is always higher in the points with the higher ordinate because the contact angle scatter is multiplied by the value of the surface energy, which is proportional to the ordinate. This causes the points related to the liquids with the higher energy to have a greater distribution and it has not to be considered as a systematic error.

Graphs III.2-7 show that both approaches can be used to obtain reliable fittings in this case, but the choice has been to use the unweighted approach, not to introduce a new complication without improving the data analysis.

III.3 _Air plasma treatment_

III.3.1 _Air plasma apparatus_

The apparatus used for the plasma treatment is shown in Figure III.8:
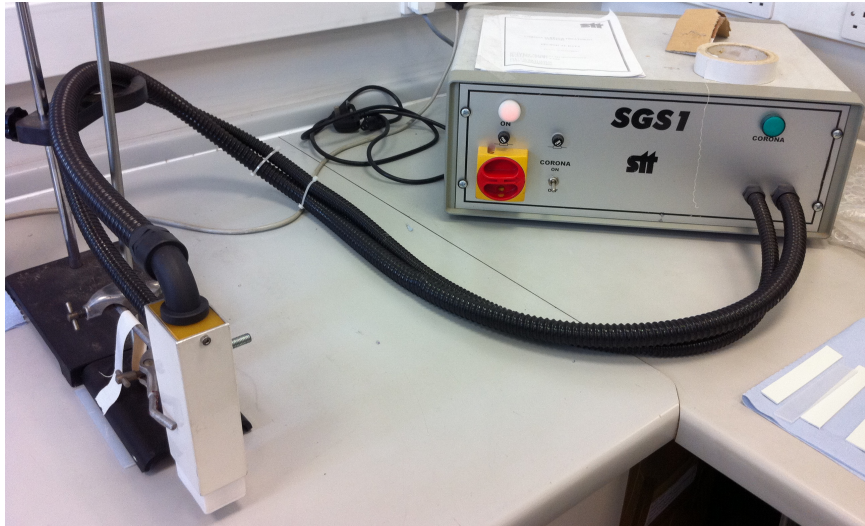
Figure III.8: forced air plasma treatment apparatus.

This apparatus is able to generate an arc with a tension of about 5 kV between the two electrodes on the head, of Type CJ.45 (the white device on the left on figure III.8). The S2 Type generator from STT, France (on the right in figure III.8), supplies the power, using a transformer able to provide a nominal secondary tension up to 7KV, starting from a primary with nominal voltage and amperage of 240V and 2A. The head is able to treat an area of 5.7 x 7.0 cm, and is shown in Figure III.9, where sparks are visible.

Figure III.9: plasma sparks coming out of the head of the treatment apparatus.

III.3.2 *Air plasma treatment*

In the absence of a conveyer belt, the treatment time was varied by physically moving the sample under the plasma torch, because the working area of the gun is not wide enough to treat the entire surface for the peel tests specimens. Since by manually moving the sample it is impossible to reach an adequate level of precision, the sample was placed on a flat rubber sheet, which was marked with a graded scale. This sheet was moved by hand using a reference to keep the speed always constant and as precise as possible. Despite this, some scatters in contact angle results are most certainly due to inhomogeneous plasma treatment: this problem has been mitigated by collecting more data, as explained previously. In this work many different treatment duration have been considered but this has been accomplished only increasing the number of the passes under the plasma spark, not increasing or decreasing the speed of the movement under the torch: this velocity has been set to 10 mm/s, in agreement with previous work [2].

The distance between the plasma and the surface has been set by mounting the head of the plasma on a support (Figure III.8) and fixing its height with the help of a calibre. Singh [2] found, for a polymer similar to PA 12, that the most effective distance to treat the surface was 10 mm, therefore this gap has been adopted for this material. For the EVAs however, there were no indications from previous works therefore an analysis to determine which one would have been best distance to improve surface energy has been carried out, varying the value from 5 to 20 mm.

As already explained, by varying the distance of the plasma arc from the surface and the number of passes the temperature of the surface change considerably. To measure the temperatures, a RS Infrared Thermometer (model 1327) with accuracy of ± 0.1°C was used: an infrared device has been chosen because it is important not to touch the surface once treated not to compromise the plasma effects.

III.4 Peel tests

As explained in Chapter II the use of peel tests to assess adhesive joints performances represents a natural extension of how these bonds are used so there is no surprise that such tests are so commonly performed. ASTM has formalized several peel tests, including: D1876, *Peel resistance of adhesives (T-peel tests);* D3176, *Floating roller peel resistance of adhesive;* D1781, *Climbing drum peel tests for adhesives;* D903, *Peel or stripping strength of adhesive bonds;*

These tests differ in the flexibility required of one or both of the adherends and the peel angle maintained during debonding the most used confiurations are surely the cited T-peel test (where both the adherends are required to be very flexible) and the fixed arm peel test, which allows one of the two adherend to be stiff (a scheme in Figure III.10).
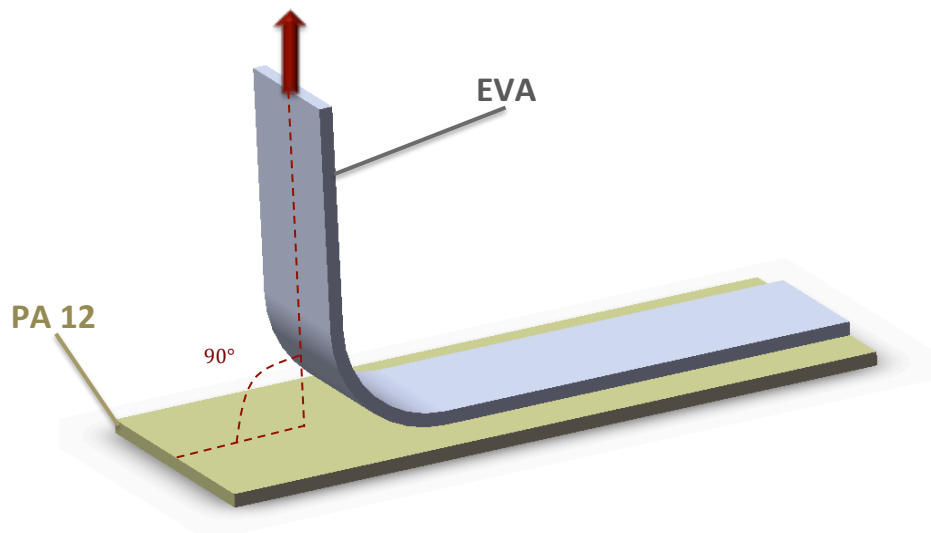
Figure III.10: operative scheme of a fixed-arm peel test.

Since PA 12 has been provided in 2mm thick sheets it is quite stiff, and T-peel tests cannot be performed. The actual junction designed for the shoes couples the PA with the foamed version of EVA. In this case both materials would be too stiff, therefore no peel tests could be executed; to overcome this problem, as explained, Nike supplied also two unfoamed versions of EVA, which have been used for the tests. The adhesion properties of a bond realized with the foamed and one with the unfoamed version should not differ considerably, since most of the resistance is due to surface interactions and the bulk properties should not affect adhesion.

To ascertain if this supposition was true however, shear-adhesive tests with Double Lap Joint specimens were performed to complete the analysis.

III.4.1 *Peel tests standard and protocol*

A number of tests for evaluating adhesives have been formalized and standardized. The International Standard Organization (ISO) and the American Society for Testing and Materials (ASTM) have compiled the most complete descriptions of these tests internationally and in the United States, respectively. Indeed, ISO committee developed a standard also for peel tests; these procedures however (such as [41]) indicate only how to measure peel strength (force per unit width for peeling) but do not include additional test information and analysis for converting peel strength into adhesive fracture toughness. Since there are important distinctions between these two properties, ESIS (European Structural Integrity Society) has developed a protocol for its determination [32], which has been explained in Chapter II. The protocol has been used to evaluate the fracture energy of the junctions.

III.4.2 *Peel tests apparatus*

Fixed-arm peel test has been relatively recently developed compared to other peel tests. This is because the configuration of the test is quite complicate, in general. It becomes easier when the peeling angle is fixed at 90°, as it was in this work. Since there has always to be a fixed angle between the strip and the substrate, while the front of the crack is advancing, it is necessary that the force pulling and the substrate moves relatively. A scheme of the specimen, supported by a horizontally mounted, translating carriage that is attached to the lower crosshead of the testing machine, is shown in figure III.11. "A tab on the end of the flexible material is attached to the upper grip of the testing machine. As the crosshead move apart during the testing, the flexible member is peeled from the panel. The movable carriage maintains a peel angle of approximately 90° [18]".
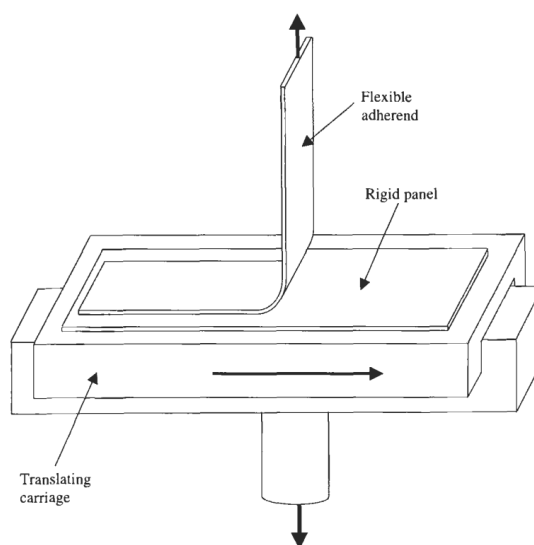
Figure III.11: fixed arm peel test apparatus.

The PA panel is fixed to the translating carriage with the help of six screws: such number has been considered enough to completely fix the PA to the trolley. The exact same configuration of Figure III.11 has been set up with the trolley shown in Figure III.12, as it can be seen in Figure III.13, where a peel angle of 90° is clearly visible.

Figure III.12: trolley used for the peel tests; the screws hold the fixed arm in position.
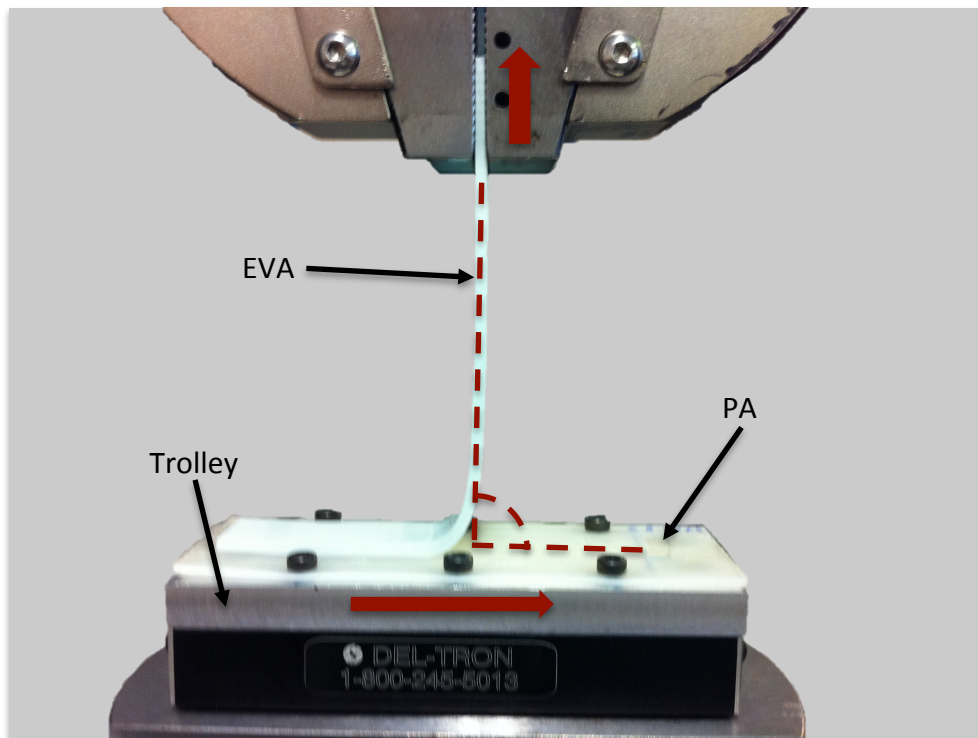
Figure III.13: peel test: 90° angle is clearly detectable.

III.4.3 Peel tests specimen

Peel tests specimens have been prepared in accordance with ESIS protocol [32]: "Specimens for conducting peel strength should be in the form of rectangular specimens where the two parts of the laminate have already been adhered but where there is a region of unadhered material (of nominal length 35mm). The overall dimensions of a peel specimen need not to be rigidly defined but for many test we have found that a length of 100mm and width 20mm proves to be quite satisfactory. Three specimens should be tested for each set of condition."

Most of the specimens have been prepared with the adhesive and two adherends; other samples have been made with no adhesive, as better explained later.

The adherends have different geometry:

- The EVA peeling strip, as schematically indicated in Figure III.10, is simply a 100 x 20 x 2 mm strip: its length has been subsequently enlarged to 135 mm because in this way a longer surface could be exploited to obtain data. A length higher than 135 mm would not be testable with the available trolley.
- The PA 12 sheet is a 36 x 100 x 2 mm sheet with 6 holes necessary to hold it to the trolley. The geometric dimensions are reported in Figure III.14.
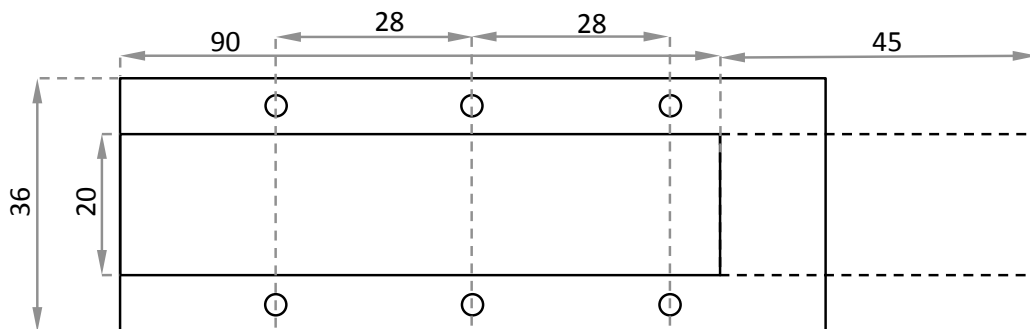
Figure III.14: geometric dimension of the peel specimens.

The holes accommodate the screws necessary to hold the PA sheet to the carriage shown in Figure III.12.

III.4.4 Peel specimens preparation

Preparing one of this peel test specimen required many operations:

- Laminates of both materials are obtained with a simple cutter from the sheets provided with dimension 135 x 20 x 2 mm for the EVA and 100 x 36 x 2 mm for the PA 12; the PA is marked out for the subsequent operations (on the opposite side);
- The laminates obtained are completely covered with Fairy™ detergent and wiped deeply, rinsed thoroughly with normal water for many minutes and then rinsed again with distilled water. They are let to dry in atmosphere for 12 hours;

70

- The surfaces of both materials are plasma treated, each one at the distance designed by the experiment; there should be as little time as possible between one operation and the subsequent;
- The surfaces are let to cool for 10 minutes, and their temperature is measured with the thermometer; a small strip of PTFE is prepared, its function is to serve as crack initiation;
- The polyurethane adhesive is placed abundantly all over the surfaces, on both materials, as shown in Figure III.15;
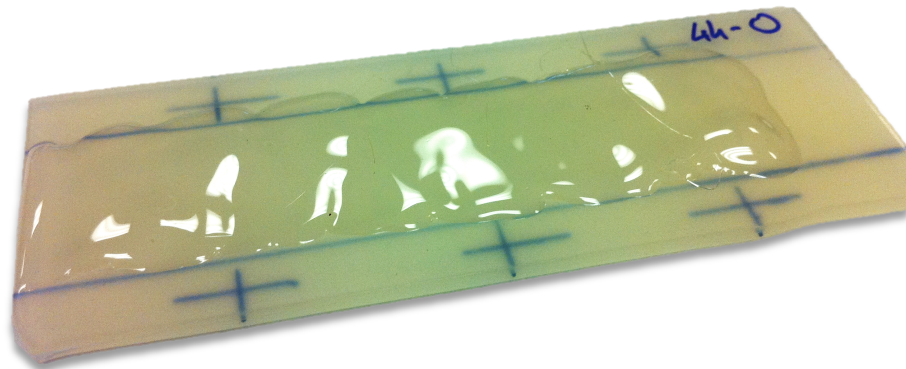
Figure III.15: peel test specimen in preparation: the glue is placed abundantly all over the surface.

- The adhesive is let to dry for exactly 4 minutes, in agreement with the glue manufacturer's specification.
- After 4 minutes the small PTFE is placed in position, in the case of Figure III.15 it would be placed on the right, covering all the area without glue and a small part of the one with the glue, in agreement with the specimens design.
- The two materials are put in contact (in figure III.11 the blue lines, which are on the opposite side of the glue, are used to place the strip in the correct position);
- The glue in excess is pulled out applying a small pressure on a metal bar of the same dimension of the EVA strip, in order to avoid inhomogeneity in the first distribution of the glue;
- After the first pressure a major pressure is applied by placing a 10 Kg weight on the junction: this pressure (about 5 kPa on the bonded area) is distributed homogeneously by a rigid metal bar (with the same area of the EVA strip, which is placed between the weight and the sample. The weight is kept in position for 72 hours, until the glue completely dries (in agreement with the glue manufacturer's specifications);
- After 72 hours the weight is removed and the edges of the EVA strip are cut with a razorblade to eliminate from the specimen any part that could lead to problems due to boundary conditions. The reasoning behind this extremely important operation is

later explained thoroughly;

- The holes needed to fix the PA to the trolley subsequently used for the test are created using a "die cutter";

III.4.5 *Excess of adhesive*

Once the glue is dried for 72 hours the specimen looks like the representation in Figure III.16, where the back view is highlighted, to better explain the problem. As it can be seen, the EVA, after the plasma, is generally warped, in a way that it is no more a perfect strip, but it has the edges bent as shown in Figure III.16 (the distortion is exaggerated in this view). Moreover, in all samples there is an excess of glue at the edges, due to the fact that the thickness of the adhesive is determined completely by positioning the weight, and therefore an excess of glue is placed in the first stage.
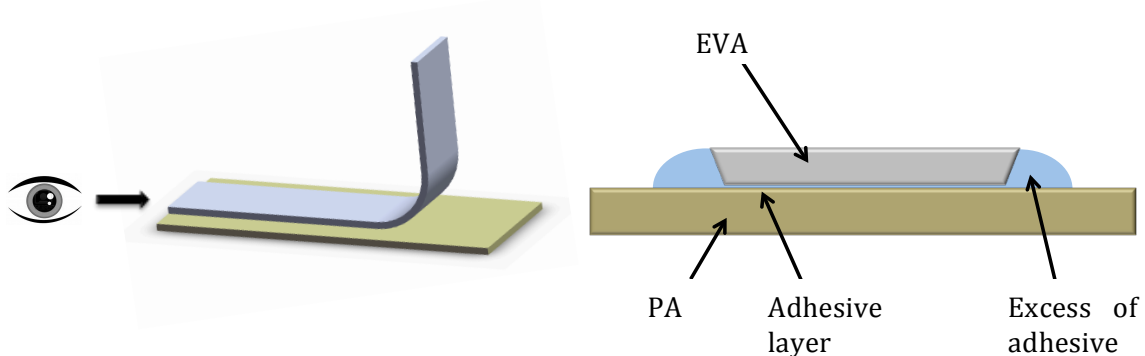
Figure III.16: back view of the peel test specimen before the elimination of excess of glue.

At this stage, in the first samples, the excess of adhesive was cut off with a razorblade, as shown in Figure III.17, perpendicularly to the edges of the EVA strip.

Figure III.17: the excess of adhesive in the first samples was cut perpendicularly to the edges.

The entire first set of samples was prepared this way. Once these first specimens were tested, it has been noticed that the adhesive left on the sides affected the results: it promoted the propagation of the defects present on the sides (because the cut with the razorblade in those section was imperfect, due to the high cutting resistance of the adhesive). After the first set of tests the problem was identified and the edges were cut deeper (as shown in Figure III.18), to the point that it was impossible for the adhesive to be accumulated on the sides. Even if this reduced the total width of the junction the

reproducibility of the tests greatly increased.

Figure III.18: new samples have minor width but the homogeneity is greatly improved.

The problem described and a lack of precise control over the many parameters which can affect the preparation of the specimens, caused the first samples not to be reproducible. With time and temperature control implemented along the entire process of sample preparation, a far by higher level of reproducibility has been reached.

III.4.6   Tests

The specimens have been tested with an Instron™ electromechanical dynamometer. The test is controlled keeping constant the speed of the crosshead at 10 mm/min (the protocol suggests to "select a common peel crack speed") and the machine automatically records the loads along the test with intervals of 1000 values/min. The fracture starts propagating from the PTFE film and shows different possible behaviours, as better explained in Chapter V. To better analyse the dynamometer data, with the awareness of how the crack was propagating, notes have been taken along the entire set of tests describing the behaviour of the peel.

III.5   Tensile tests for peel protocol

In order to assess the interfacial work of fracture (or adhesive toughness) with peel tests it is necessary, as explained in chapter II, to determine the stress-strain behaviour of the flexible arm peeled. Even if an approximate peel analysis is possible considering bilinear o power law stress-strain behaviour, a complete digitization of the curve allows a more precise assessment.

The tensile properties of flexible arm have been assessed with ASTM D638-10 standard, [42]. This standard test covers the determination of the tensile properties of unreinforced and reinforced plastics in the form of standard dumbbell-shaped test specimens when tested under defined condition of pretreatment, temperature, humidity and testing machine speed. This test method can be used for testing materials of any thickness up to 14mm, and since the specimens used have a 2mm thickness, it is appropriate.

III.5.1 Tensile tests specimens

As for all other kind of specimens, these specimens should be tested with the greatest care to ensure that all samples are prepared the same way. However, for time constrains, it was not possible to obtain the tensile specimens from virgin sheets but instead part of the polymers used for the peel tests specimens have been adapted, after the adhesive test. This was possible because those specimens were not glued nor excessively plasma treated and therefore no mechanical properties had been modified by the previous pretreatment.

The geometry of the dumbbell sample is indicated by the standard and reported in Figure III.19:
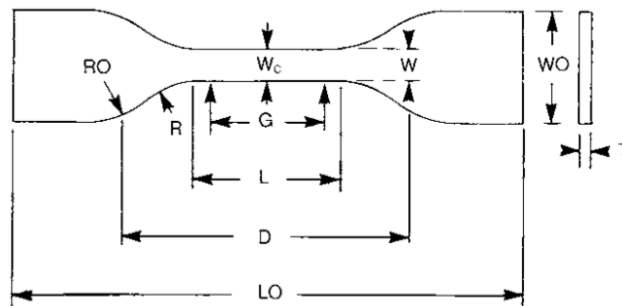
Figure III.19: geometry of the dumbbell tensile specimens.

Dimension (see figure	[mm]
W - width of narrow section	3
L - length of narrow section	20
WO - width overall	15
LO - length overall	85
G - gage length	15
D - distance between grips	45

Table III.3: dumbbell tensile specimen dimensions.

The test speed has to be the same of the peel tests, therefore 10 mm/s was used.

III.6 _Adhesive shear tests_

These tests have been set up after the evidence that with the materials provided it would have been impossible to perform 90° fixed arm peel tests in junctions joining PA 12 and foamed EVA: none had the required flexibility to be used as the peeling arm. Since adhesion is a surface phenomenon and mechanical testing of adhesion involves mainly surface mechanisms, one of the solution exploited to compare adhesion between the foamed and the unfoamed version has been to use another type of mechanical test. A simple geometry, suiting the characteristics of both materials, is the one of Double Lap Joints (DLJ); a scheme of DLJ tests is represented in Figure III.20:
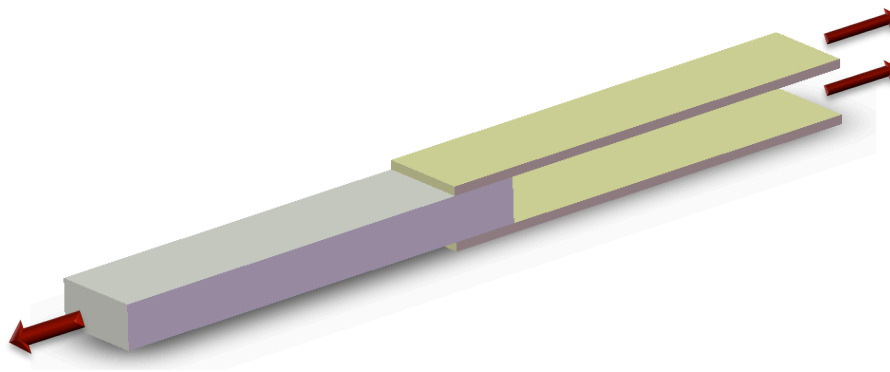
Figure III.20: double lap joint specimen.

In this type of tests the junction are stimulated by shear stresses (mode II) instead of opening forces acting in fixed arm peel tests (mode I). Nonetheless it has been hypothesized that DLJ tests results obtained from -PA/unfoamed EVA- and -PA/foamed EVA- junctions could be used to compare the adhesive properties of these different types of EVAs. These specimens have been prepared with the geometry outlined in Figure III.21, indicated by BS EN 1465:2009 [43].
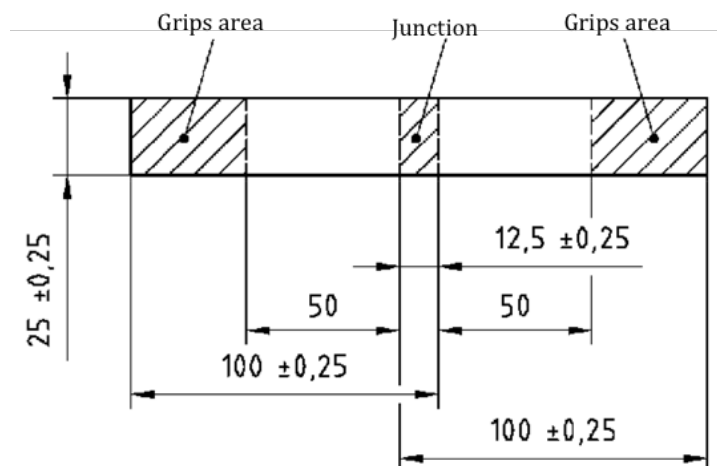
Figure III.21: top side of DLJ geometry.

The thickness of the central bar changes with the adherend, as shown in Figure III.22. The samples prepared with the unfoamed EVA have been prepared with the filled version of the polymer; the filled unfoamed EVA has been chosen because it possesses the same chemical composition of the foamed version.
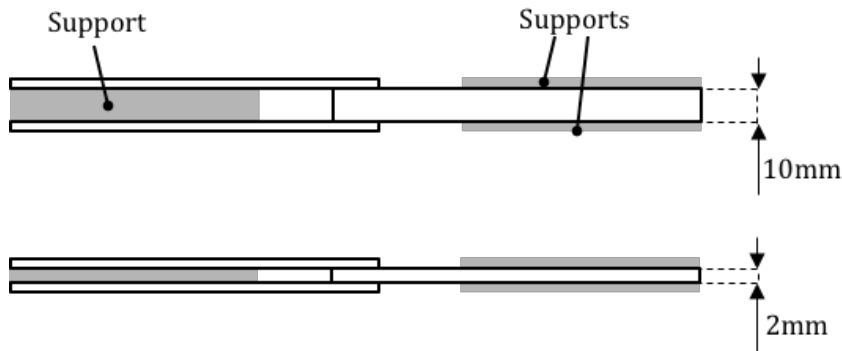
Figure III.22: front view of DLJ samples.

III.6.1 *Double Lap Joint specimens preparation*

DLJ samples preparation is less complicated than peel specimens, and has been done following the subsequent procedure:

- The polymer strips are firstly prepared, simply cutting them off the polymer sheets with the due geometry;
- PTFE strips are placed to separate the bonding area by the nonbonding one: since the application of the glue is not precise, the presence of PTFE allows an accurate delimitation of the jointed area;
- PTFE strips are covered with paper, in order to conserve their antiadhesive properties after the plasma (and in order to protect them from melting under the heat generated by the treatment);
- The surfaces are treated with the plasma.
- The adherends are let to cool for 10 minutes, their surface temperature is measured and the paper protecting the PTFE is removed.
- An excessive quantity of Polyurethane adhesive is applied and let to dry for 4 minutes.
- The surfaces are placed in position to joint and are let to dry for 72 hours with a pressure of about 40 kPa holding them in position.

After the complete procedure samples such as the one in Figure III.23 are obtained.
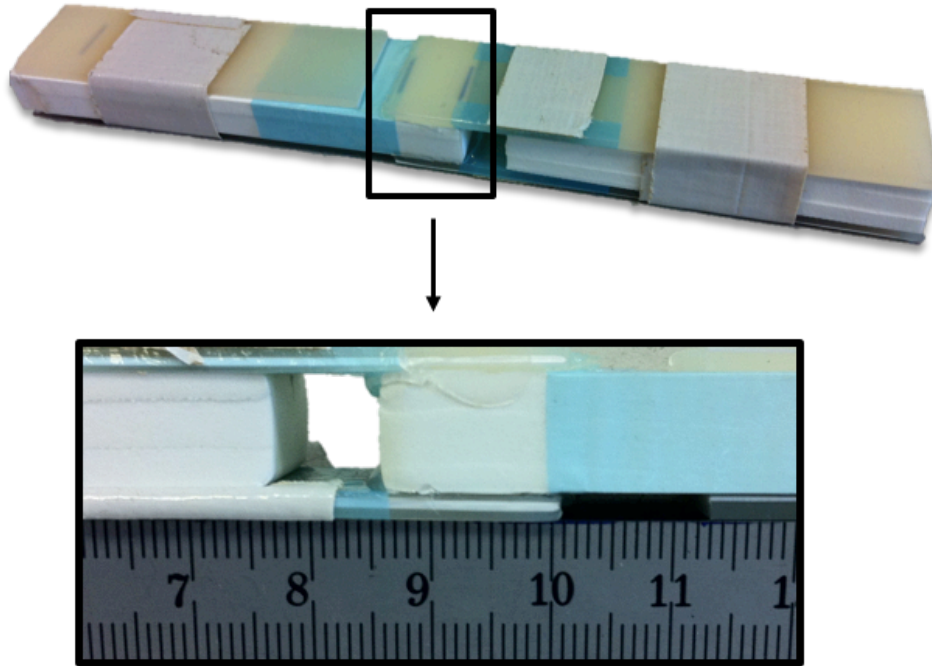
Figure III.23: PA 12 / Foamed EVA DLJ specimen; in the lower figure the small junction is highlighted, together with a ruler to show the real dimensions.

Four samples have been successfully tested for each joint, with a constant crosshead speed of 10mm/min. Although some problems arose in the gripping of the junctions in the first stage, they have been solved using pneumatic grips and biadhesives strips to fix the arms with the supports, in order not to slick: all experimental procedures adopted to fix the supports indicated in Figure III.22 to the joint arm do not influence the result of the test.

IV. CHAPTER: SURFACE ENERGY RESULTS

The first tests carried out investigated the effect of different cleaning methods on surface energy.

IV.1 *Polished surfaces*

When investigating a material property, it is necessary to eliminate any external contamination: dirt and roughness are the most common in surface energy analysis, and can both influence the results obtained. Polishing eliminates both, and allows assessment of pure polymer surface. The polishing technique adopted in the work has been explained in Chapter III.

- Polyamide 12

The polishing of polyamide is quite straightforward and it is not difficult to obtain the desired smoothness. In Graph IV.1 the OWRK fitting for the polymer.

Adj. R-Square	0.97544	
	Value	Standard Error
Intercept	5.73846	0.03647
Slope	2.66149	0.05011
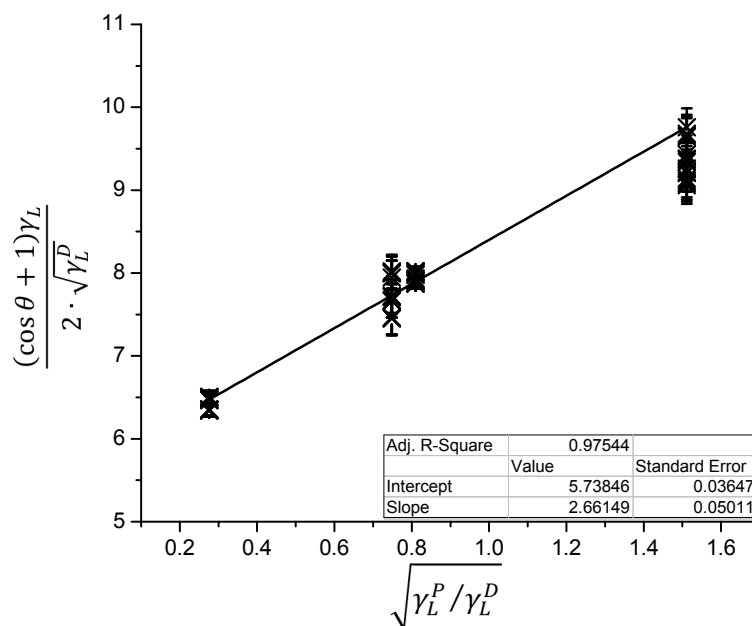
Graph IV.1: PA 12 surface energy analysis (OWRK method, polished, no plasma).

In Chapter II the OWRK method has been explained thoroughly and in Chapter III it has been explained how data are analysed. Once these means are established the evaluation of the surface energy components is straightforward and the assessment of their error comes from practical physics.

In this case, from the fitting in graph IV.1:

$\gamma_S{}^P$: $(2.66)^2$ $= 7.07 \text{ mJ/m}^2$

$\gamma_S{}^D$: $(5.73)^2$ $= 32.83 \text{ mJ/m}^2$

$\gamma_S{}^{tot}$: $7.07 + 32.83$ $= 39.90 \text{ mJ/m}^2$

For the evaluation of an error, in a linear regression such as

$$y = b_0 + b_1 x \qquad (IV.1.1)$$

where, as shown in chapter III:

$$y = \frac{(\cos\theta + 1)\gamma_L}{2\sqrt{\gamma_L^D}} \qquad\qquad x = \sqrt{\frac{\gamma_L^P}{\gamma_L^D}}$$

$$b_0 = \sqrt{\gamma_S^D} \qquad \text{(intercept)}$$

$$b_1 = \sqrt{\gamma_S^P} \qquad \text{(slope)}$$

combined standard errors are:

- If $Z = A \cdot B$

$$\left(\frac{\Delta Z}{Z}\right)^2 = \left(\frac{\Delta A}{A}\right)^2 + \left(\frac{\Delta B}{B}\right)^2 \qquad (IV.1.2)$$

- If $Z = A + B$

$$(\Delta Z)^2 = (\Delta A)^2 + (\Delta B)^2 \qquad (IV.1.3)$$

- If $Z = A \cdot A$

$$\left(\frac{\Delta Z}{Z}\right)^2 = 2\left(\frac{\Delta A}{A}\right)^2 = \left(\frac{4 \cdot \Delta A}{A}\right)^2 \qquad (IV.1.4)$$

$$\frac{\Delta Z}{A \cdot A} = \frac{4 \cdot \Delta A}{A} \qquad \Delta Z = 4 \cdot \Delta A \cdot A \qquad (IV.1.5,6)$$

Therefore the surface energy is, for polished PA 12:

$\gamma_S{}^P$: $7.07 \pm 0.53 \text{ mJ/m}^2$

$\gamma_S{}^D$: $32.83 \pm 0.83 \text{ mJ/m}^2$

$\gamma_S{}^{tot}$: $39.90 \pm 0.99 \text{ mJ/m}^2$

- <u>Unfilled EVA</u>

The unfilled EVA OWRK fit is shown in Graph IV.2:
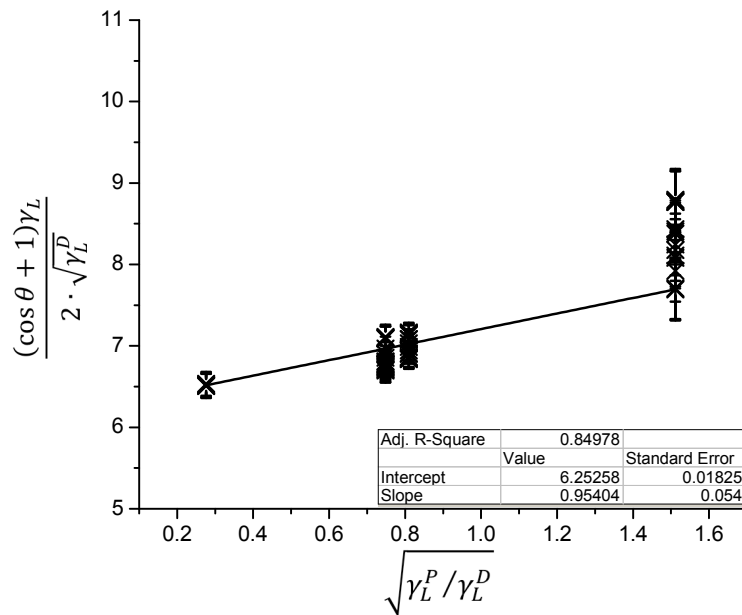
Graph IV.2: unfilled EVA surface energy analysis (OWRK method, polished, no plasma).

From the data in Graph IV.2 is possible to obtain the values for the surface energy components, as for the previous material:

γ_S^P: 0.91 ± 0.20 mJ/m^2

γ_S^D: 39.06 ± 0.45 mJ/m^2

γ_S^{tot}: 39.97 ± 0.49 mJ/m^2

- Filled EVA

The surface energy assessment for a polished surface of the filled EVA is reported in Graph IV.3.
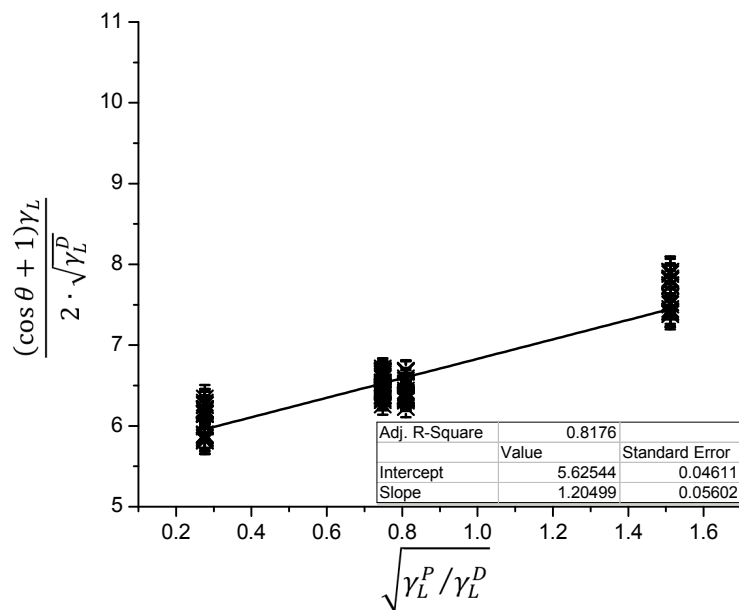
Graph IV.3: filled EVA surface energy analysis (OWRK method, polished, no plasma).

The surface energy components are:

$\gamma_S{}^P$: 1.45 ± 0.22 mJ/m²

$\gamma_S{}^D$: 31.64 ± 1.04 mJ/m²

$\gamma_S{}^{tot}$: 33.09 ± 1.06 mJ/m²

- Foamed Filled EVA

As mentioned, the surface energy evaluation for the foamed EVA was not possible. This material is made by a thick foamed bulk and a thin unfoamed surface layer (probably due to its production technology). It is not possible to evaluate the foamed bulk, because of its intrinsic inhomogeneity, but neither to assess the surface layer because of its micro-roughness. Since it cannot be polished (the external layer is very thin) a clean smooth surface is not obtainable.

An attempt to measure the contact angles on the simply cleaned surface layer gave an high a scatter and either a polish attempt did not provide results: the diamond particles used to polish stuck in the tiny cavities of the material, thus sophisticating the surface energy of the pure material.

The surface energy assessment of this material has been abandoned, but another mean has been used to assess its ability to bond: double lap joints, as explained in Chapter III, V.

- Polished surfaces results comparison

In Table IV.2 the summarized results of the polished analysis:

	$\gamma_S{}^P$ [mJ/m²]	$\gamma_S{}^D$ [mJ/m²]	$\gamma_S{}^{tot}$ [mJ/m²]
PA 12	7.07 ± 0.53	32.83 ± 0.83	39.90 ± 0.99
Unfilled EVA	0.91 ± 0.20	39.06 ± 0.45	39.97 ± 0.49
Filled EVA	1.45 ± 0.22	31.64 ± 1.04	33.09 ± 1.06

Table IV.1: polished surface energy assessment.

As shown the total surface energy is basically the same for the PA 12 and the Unfilled EVA, with the exception that the polar component of the polyamide is higher. Since both polymers contain polar groups the only difference might be their concentration. In this case the fraction of vinyl acetate in the EVA is unknown (Chapter III.1.1), but it is possible to hypothesize that it is quite low, because both the EVAs carry a small fraction of polar surface energy.

IV.2 *Cleaned surfaces*

The presence of dirt or any kind of organic contamination affects the wettability of a surface. As explained previously, it is important from a technological point of view to understand the effects of surfaces cleaning with respect to their ability to be adhesively bonded. For this reason two different types of cleaning were assessed and compared, a dry tissue wiping and a common dishwashing detergent (whose peculiarities are described in Chapter III). In Graph IV.4 and Graph IV.5 the surface energy assessment for detergent cleaned and dry tissue cleaned PA 12.

	Value	Standard Error
Intercept	5.46189	0.0201
Slope	0.7963	0.05146
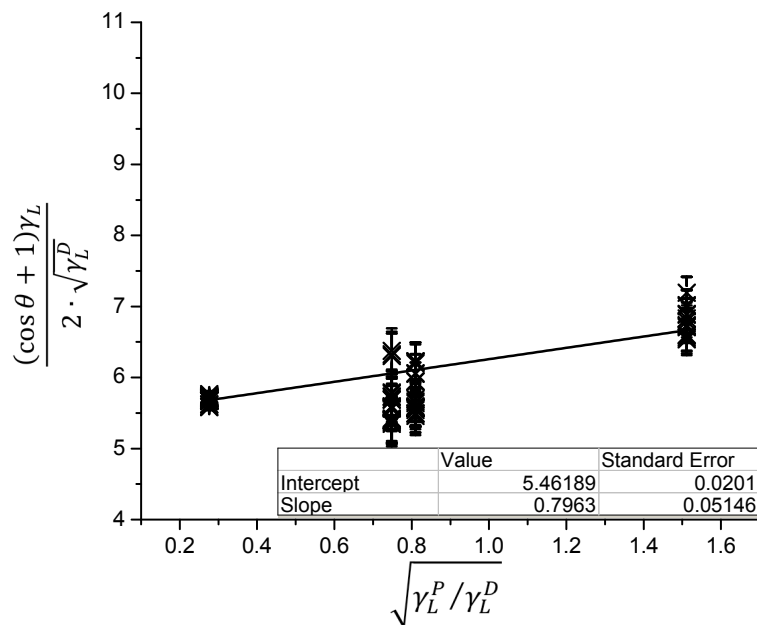
Graph IV.4: PA 12 surface energy analysis (OWRK method dry tissue cleaned, no plasma).

	Value	Standard Error
Intercept	6.11714	0.03537
Slope	0.58953	0.04882
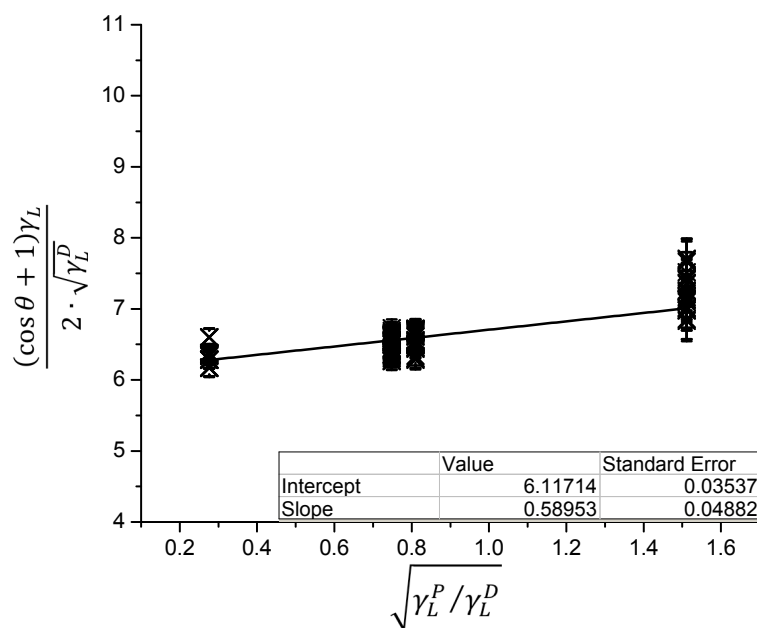
Graph IV.5: PA 12 surface energy analysis (OWRK method detergent cleaned, no plasma).

In Graph IV.6 a graphic comparison between the three different cleaning procedures, and in Table IV.2 the results summarized.
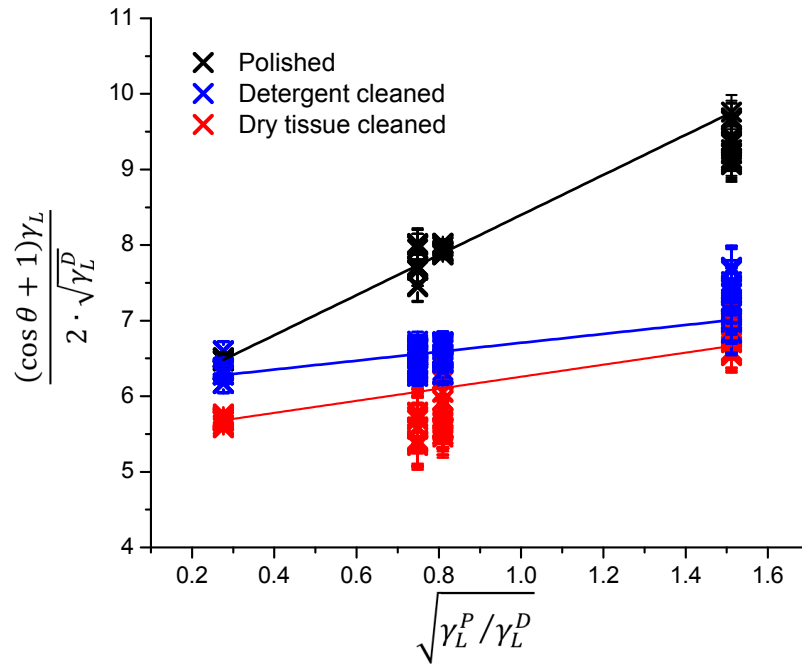
Graph IV.6: PA 12 surface analysis (OWRK method, different cleaning method comparison).

	γ_S^P	γ_S^D	γ_S^{tot}
	$[mJ/m^2]$	$[mJ/m^2]$	$[mJ/m^2]$
Polished	7.07 ± 0.53	32.83 ± 0.83	39.90 ± 0.99
Detergent	0.35 ± 0.11	37.33 ± 0.86	37.68 ± 0.87
Dry tissue	0.62 ± 0.16	33.71 ± 0.44	33.71 ± 0.47

Table IV.2: surface energy analysis results for PA 12 with different cleaning method.

In Graph IV.7 a histogram displaying the results:
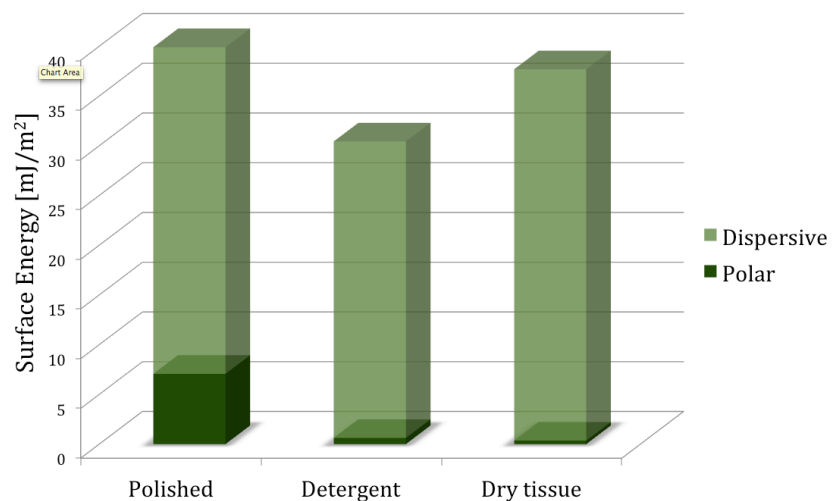
Graph IV.7: surface energy fractions for differently cleaned PA 12.

As displayed by the graphs and Table IV.1 there is a little difference of total surface energies although the polar component is appreciable only on the polished surface. This might be due (since the chemical composition of the PA 12 indicates the presence of polar groups) to the fact that when the surface is not polished organic contaminations "shield" the polar groups.

IV.3 _Air plasma treatment optimization_

Main objective of this thesis is the optimization of the plasma treatment to improve adhesion therefore a large part of the work has been devoted to this task.

IV.3.1 _Plasma treatment parameters_

To modulate the intensity of the treatment with this forced air plasma mainly three parameters could be modified:

- Speed;
- Distance;
- Number of passes;

Since the dimension of the plasma torch is smaller than the one of the surfaces to be treated it is straightforward that the substrates have to be moved under the arc. The **speed** at which the samples were moved under the plasma torch was a first parameter to modulate the intensity of the plasma, as indicated in Figure IV.1.
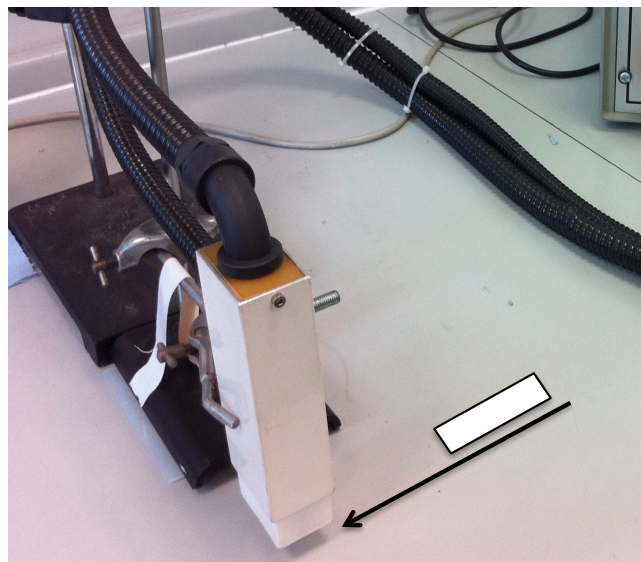
Figure IV.1: the sample is moved under the plasma torch.

This parameter however has been already optimized [2], therefore it has been kept constant at 10 mm/s.

One of the parameter that mostly influenced the intensity of the treatment was the **distance**

of the substrate from the plasma gun, as indicated in Figure IV.2:
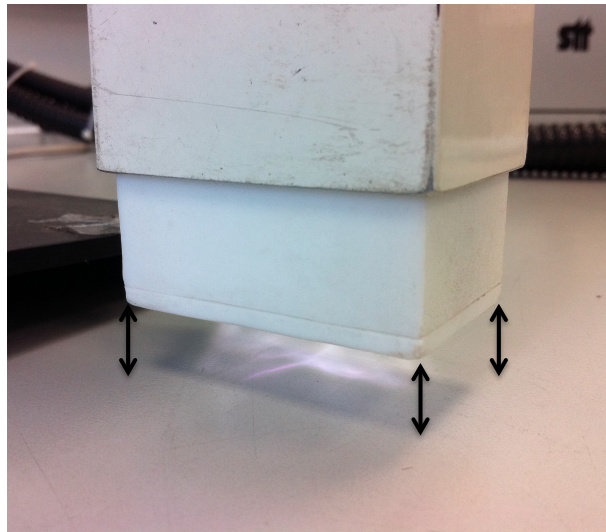
Figure IV.2: distance of the substrate form the plasma torch.

Singh [2] already optimized the treating distance for a polymer similar to polyamide 12 used in this study and found that 10mm was the best value, therefore such distance has also been used for the PA 12. For what regards the EVA, however, the distance has been varied between 5 and 20 mm, since there was no evidence that any distance would be the best.

Last parameter to modulate the intenstiy of the plasma treatment was the **number of passes** under the electric arc. These have been varied between 0 and 4 for all the materials, since after four passes a certain degree of degradation was visible on the surface in the form of brown spots.

In Table IV.3 the various conditions are listed:

Plasma parameters

	Speed [mm/s]	Distance [mm]	N° of passes [-]
PA 12		0 - 1 - 2 - 3 - 4	10
Filled EVA	10	0 - 1 - 2 - 3 - 4	5 - 10 - 15 - 20
Unfilled EVA		0 - 1 - 2 - 3 - 4	5 - 10 - 15 - 20

Table IV.3: variation of parameters to modulate the intensity of plasma treatment.

IV.3.2 _Plasma treatment optimization_

To optimize a forced air plasma treatment means to adjust all the variable parameters to obtain the highest surface energy possible. To ascertain the surface energy and its components in each condition an Owen-Wendt-Rabel-Kaelble would be necessary and would require a contact angle analysis for each liquid. Since it is necessary to deposit 5 to 10 drops for each substrate, in every treatment conditions, the operation would be extremely time consuming therefore the optimization has been based on the water contact angle.

Water is the liquid with the highest surface energy among the ones used therefore it has been used as an indicator, in each treatment, to investigate the intensity of the plasma. Once the lowest water contact angle was reached, however, a complete OWRK investigation was necessary to assess correctly the value of the surface energy and to distinguish its components.

Other OWRK complete analyses have been carried out in other significant conditions.

IV.3.3 _PA 12 plasma optimization_

The optimization of PA involves only the number of passes since speed and distance are fixed. A problem arose with this optimization, which required the test to be repeated many times using up to 3 single specimens (each with up to 10 water drops) for each condition; this problem was the appearance of chicken scratches.

IV.3.3.1 PA 12 Chicken scratches

One of the phenomena happened during the polyamide plasma treatment was the distinct formation of "chicken scratches" (Figure IV.3), a sort of inhomogeneous sign on the surface of the treated material visible on particular observation angles which did not appear on EVAs surfaces. Their occurrence was not a single one-off event caused by material properties of a single specimen but their formation was indeed repeatable.

Their manifestation has been a problem to the extent that being not homogeneously distributed on the surface they can affect the surface energy analysis, since a drop placed on a chicken scratch might behave differently compared to one in another position. As deeply studied by _Singh_ [2], the formation and the veracity of such scratches is directly correlated to the intensity of the plasma treatment.

First appearance of chicken scratches as individuals

Uniformly treated surface
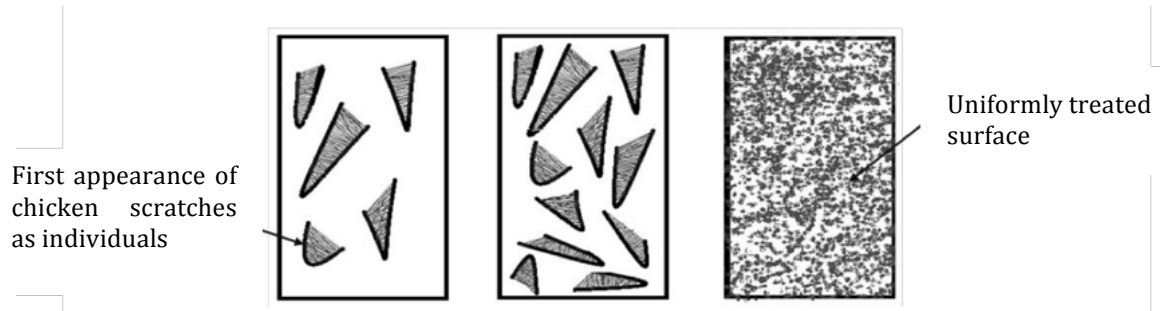
Figure IV.3: formation of chicken scratches, firstly as individuals then uniformly [2].

"They appear firstly as individual, distinct entities and finally merging together to form a uniform treatment over the surface", as described in Figure IV.3 and shown in Figure IV.4 (on similar surfaces by *Singh*, [2]).
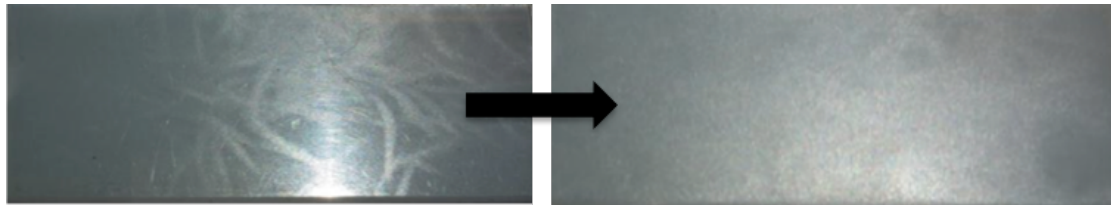
Figure IV.4: formation of chicken scratches from a milder plasma treatment to a stronger one [2].

IV.3.3.2 Causes for chicken scratches

Singh [2] deeply studied the causes of chicken scratches formation, using the same exact apparatus as the one of this work. Although to a naked eye the plasma flame seems to be impinging onto the surface at a uniform rate and with planar leading-edge, he found, with the help of a high speed camera, that only some portion of the surface were treated, as shown in Figure IV.5 [2].
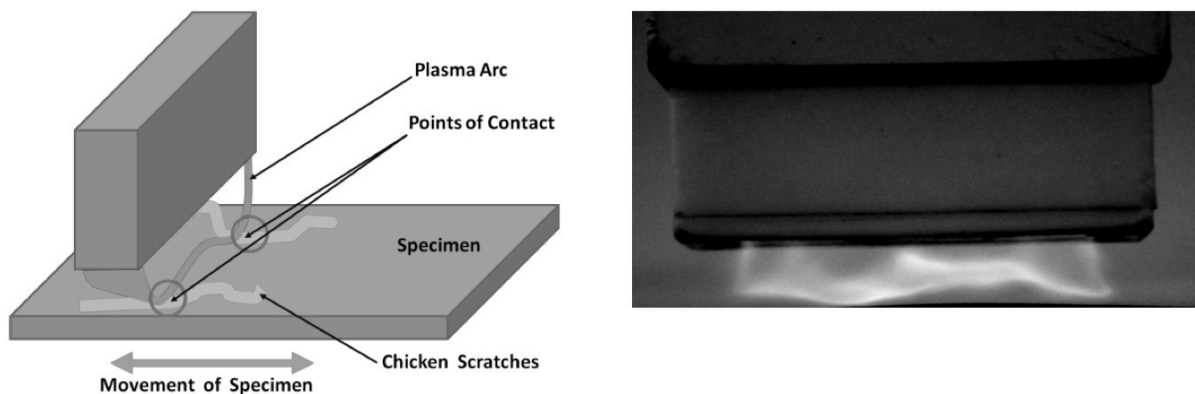
Figure IV.5: the arc treats only a randomly determined small portion of the PA 12.

Videos and images showed that the plume did not fall uniformly onto the surface but instead flickered randomly and only the portion of the substrate in touch with the flame was getting treated, leaving the rest untreated. The plasma apparatus is designed to produce 50-60 arcs per second and the pressurized air causes it to assume random shape. The movement of the specimen under the torch causes some regions of the surface to be randomly treated thus resulting in random formation of the scratches.

"The random flickering of the flame implies that as the specimen moves, the same region may or not may get treated more than once. As the treatment continues, eventually the whole surface is filled with the scratches and the surface treatment assumes uniformity with respect to amount and distribution" [2].

Once the reasons for the scratches was ascertained, *Singh* investigated the reason which caused them to be visible only in certain conditions and found that it was simply due to light reflection.

The presence of such chicken scratches and the fact that they caused an inhomogeneous treatment is clear also analysing Graph IV.8 and Graph IV.9, which show water contact angle on treated PA 12 versus number of plasma passes, for both samples cleaned with detergent and with dry tissue (the point for 0 passes refers to the polished surface).
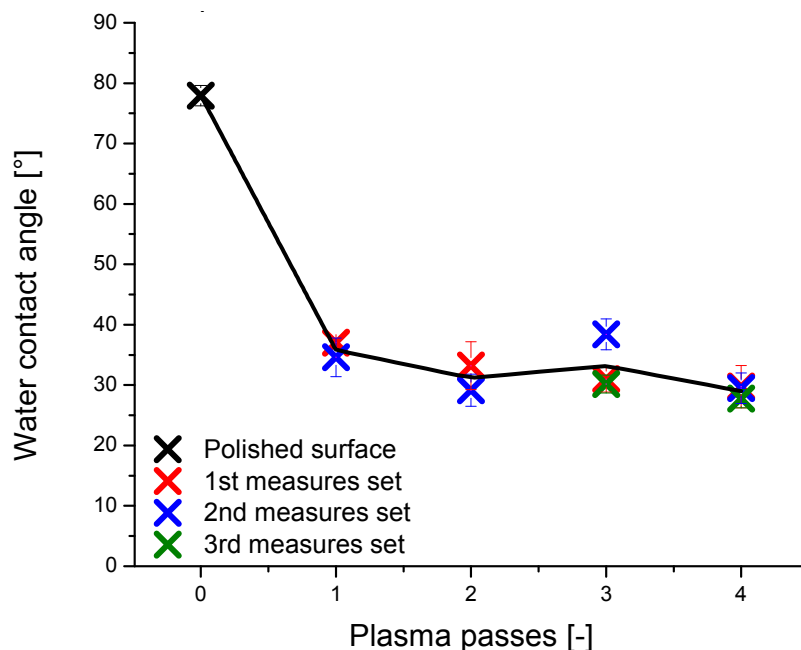
Graph IV.8: water contact angle on dry tissue cleaned PA 12 versus number of plasma passes.
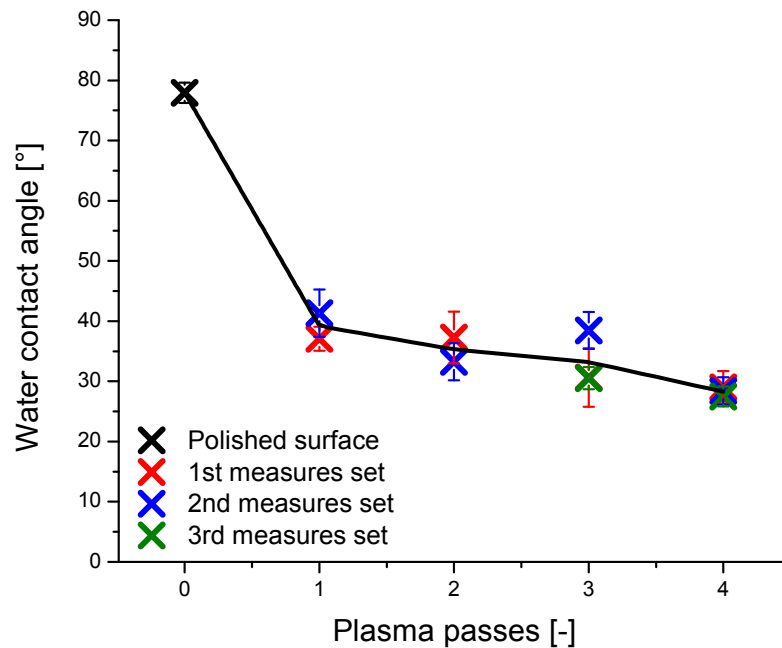
Graph IV.9: water contact angle on detergent cleaned PA 12 versus number of plasma passes.

Before evaluating the trends a first evidence in Graph IV.8 and Graph IV.9 is the different result in different measures sets i.e. different samples: this is due to differences in treatment among the samples and it is probably caused by the fact that the surface is manually moved under the plasma torch. Even if best effort has been used to keep the speed constant a certain error is most surely embedded with the manual movement.

Another data shown is the error bar for each point. In general these errors decrease with the augment of the number of passes, thus confirming what was expected by the presence of the chicken scratches: the homogeneity of the treatment is correlated to the intensity of the treatment simply because to obtain homogeneity the chicken scratches have to cover all the surface.

For what concerns the water contact angle it diminishes strongly from the first pass in both cases and then continues to somehow decrease but being less affected by the number of passes. In both cases the best conditions, the ones with the lower contact angle, have been reached with four passes. The material has been subjected also to five treatments, to investigate if the trend was confirmed for higher number of passes, but the surface started showing signs of deterioration probably due to the high temperature induced by the plasma: this effect was clear on the surface with the appearance of brown spots.

One last consideration about Graphs IV.8 and IV.9 is that there seems to be little difference between the two cleaning type, especially after the first passes.

Once best conditions of plasma treatment were ascertained for both cleaning type, OWRK analyses have been carried out, to investigate to what extent the plasma increased the

surface energy of the polymer.

The surface energy analysis with OWRK method for dry tissue cleaned and detergent cleaned PA 12 are reported in Graph IV.10 and Graph IV.11 (10 mm 4 passes):

Adj. R-Square	0.97961	
	Value	Standard Error
Intercept	4.1989	0.10012
Slope	6.68987	0.10117
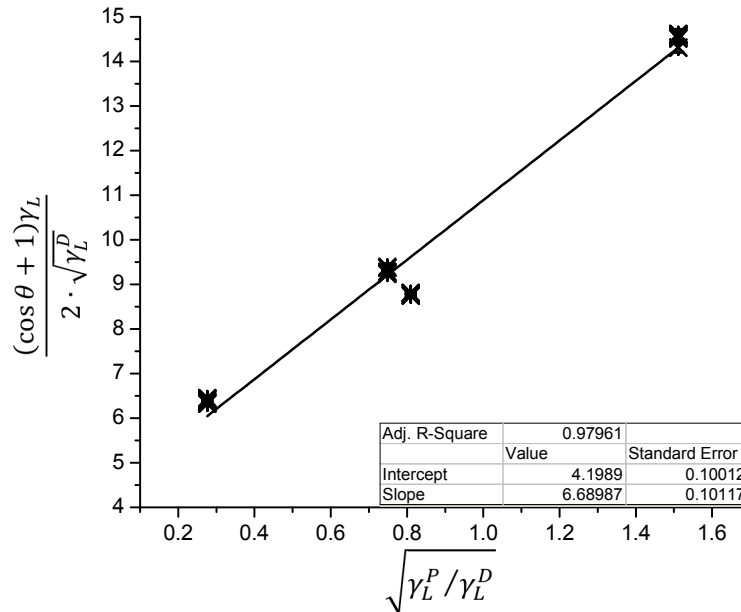
Graph IV.10: PA 12 surface energy analysis (OWRK method, dry tissue cleaned, plasma 10 mm 4 passes).

The surface energy components are:

γ_S^P: 44.74 ± 2.70 mJ/m^2

γ_S^D: 17.62 ± 1.68 mJ/m^2

γ_S^{tot}: 62.36 ± 3.18 mJ/m^2

Adj. R-Square	0.97381	
	Value	Standard Error
Intercept	4.16304	0.10913
Slope	6.78372	0.11413
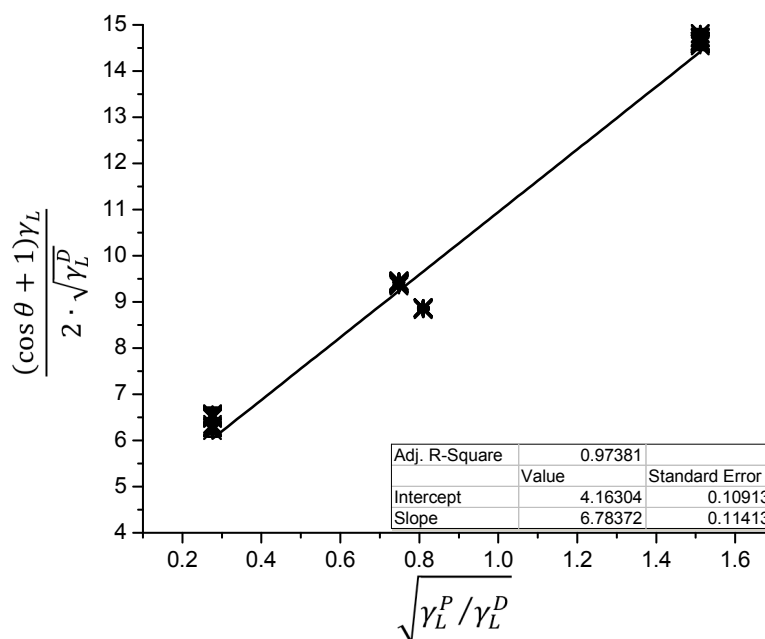
Graph IV.11: PA 12 surface energy analysis (OWRK method, detergent cleaned, plasma 10 mm 4 passes).

For dry tissue cleaned treated PA 21, the surface energy components are:

γ_S^P: 45.96 ± 3.09 mJ/m²

γ_S^D: 17.30 ± 1.82 mJ/m²

γ_S^{tot}: 63.26 ± 3.59 mJ/m²

At first, the results obtained for 10 mm - 4 passes treatment seems to indicate that -for the PA12- there is no difference between a quick dust removal with a dry tissue and a deep surface cleaning with a detergent. More importantly, the OWRK fit indicates a strong increase in surface energy, due to an important increment of the polar component, which compensates a little decrease in the dispersive component. The reduction in the dispersive component might be due to the fact that the engraftation of polar group on the surface has reduced the fraction of the surface with non-polar groups (therefore reducing the extent of surface intermolecular forces on the surface).

IV.3.4 *Filled EVA plasma treatment optimization*

The optimization carried out for PA12 has been performed also for both the unfoamed EVAs. In these cases however the distance of the plasma torch from the substrate has been one of the parameters to optimize.

To ascertain which one were best conditions, contact angle analyses have been carried out varying the distance, the number of passes, and the cleaning method.

IV.3.4.1 *Dry tissue filled EVA*

The first analyses carried out investigated the water contact angle for dry tissue cleaned EVA. Results are shown in Graphs IV.12-15.

5 mm distance plasma treatment, tissue cleaned
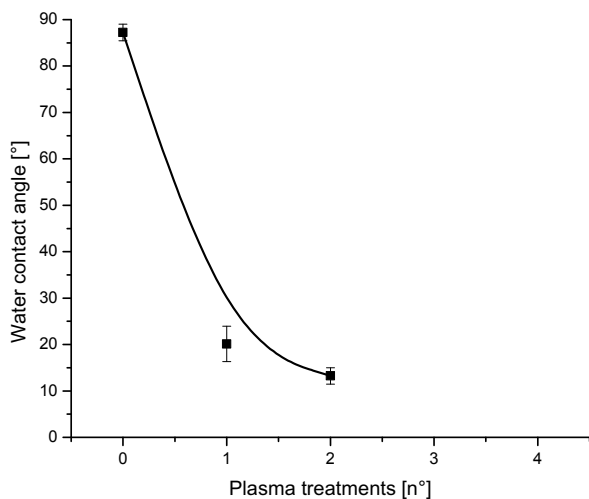
Graph IV.12: dry tissue cleaned filled EVA water contact angle versus n° of passes, 5 mm plasma.

10 mm distance plasma treatment, tissue cleaned
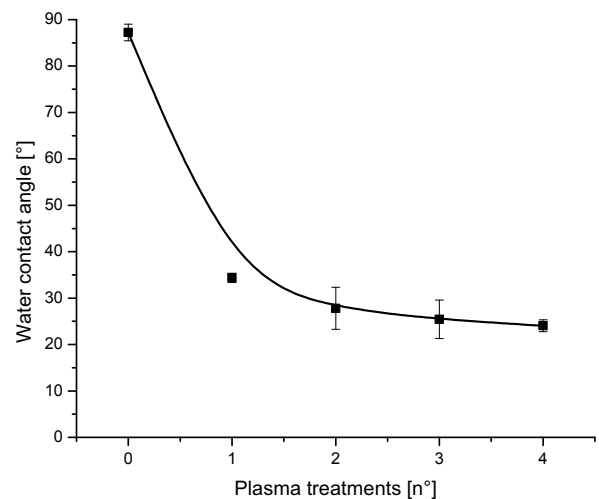
Graph IV.13: dry tissue cleaned filled EVA water contact angle versus n° of passes, 10 mm plasma.

15 mm distance plasma treatment, tissue cleaned
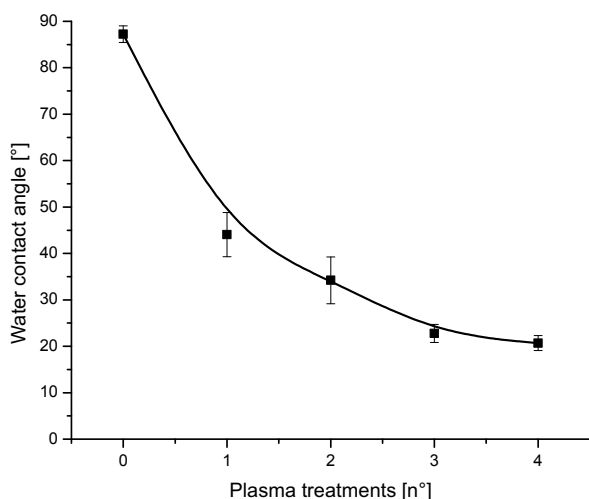
Graph IV.14: dry tissue cleaned filled EVA water contact angle versus n° of passes, 15 mm plasma.

20 mm distance plasma treatment, tissue cleaned
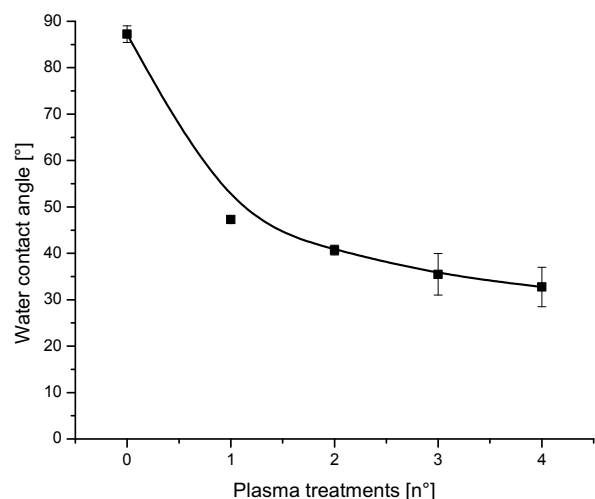
Graph IV.15: dry tissue cleaned filled EVA water contact angle versus n° of passes, 20 mm plasma.

In the case of 5 mm distance it has not been possible to proceed with the third and the fourth treatments because the intensity of the plasma at this gap generated enough heat to soften considerably the EVA and more important it started degrading the surface. Even if the water contact angle would have been lower, the surface must not degrade under the plasma otherwise their mechanical characteristics would be compromised.

The results of the four analyses are summarized in Graph IV.16.
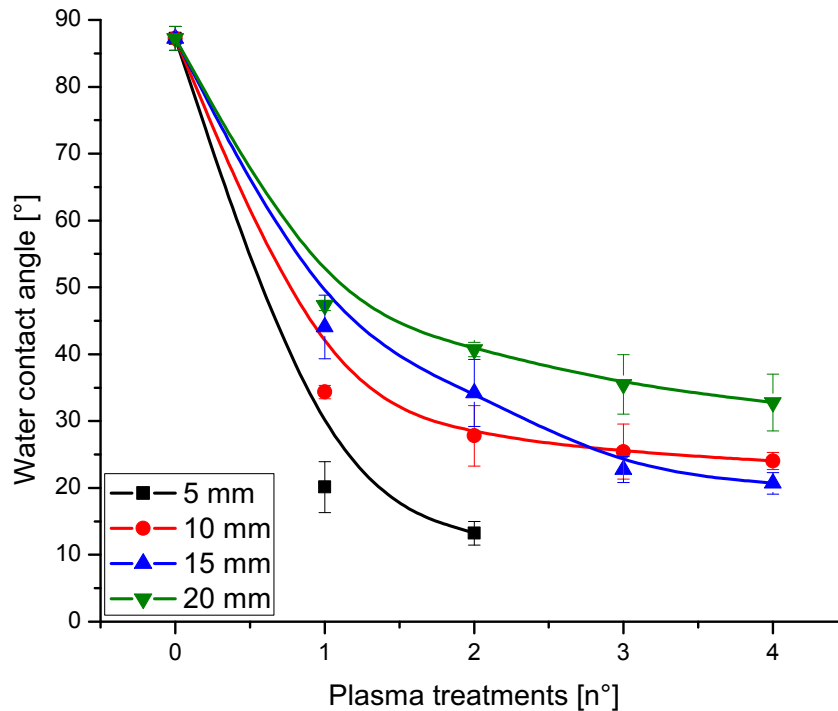
Graph IV.16: dry tissue cleaned filled EVA, water contact angle versus different distances plasma treatment.

Graph IV.16 shows that the distance of the plasma torch is the most important parameter in determining the water contact angle. The trend seems to be similar at different distances with a strong decrease at the first pass and a lower influence of the subsequent passes. The intersection of the lines related to 10 and 15 mm seems to be caused only by experimental errors probably due to the manual movement of the samples under the plasma source. The lowest water contact angle has been reached for 5mm and two passes therefore a complete OWRK analysis has been carried out with these parameters. As it has been said, after the third treatment at 5 mm it was clear that surface degradation started occurring (little light brown spots appeared on the surface). OWRK analysis has been carried out also for 5mm - pass, to ascertain the influence of the second passes on both surface energy components.

IV.3.4.2   0° contact angle test liquids

With these analyses a new problem arose: liquids showing 0° contact angle. As explained in chapter II, if a liquid possesses a lower surface energy than the substrate where it is deposited, it spreads freely on the surface. Since the scope of the plasma treatment is to enhance the surface energies of the adherends, in happened that their energy reached a point when it was higher than the ones of some liquids, causing them to spread freely, not showing any contact angle (if a contact angle is lower than 10° it becomes difficult to

measure it, since there is little contrast and the software confuses the angle with the surface). In this case ethylene glycol and formamide showed little or 0° contact angle. When a 0° contact angle established it has been possible to state that the energy of the substrate was higher than the one of liquid: however, it has been impossible to evaluate how greater it was. Since negative contact angles do not have any experimental manifestation, it is impossible to calculate the spreading coefficient S (explained in chapter II.2.1). For this reason in the OWRK fitting the points have been plotted in the position where they would have been if the equilibrium contact angle would be exactly 0°, with spreading coefficient equal to 0. Since from experimental contact analyses it was only clear that the point on the plot was not below that position, (but might absolutely be above) the data is represented with a square and an arrow pointing above. This shows that the real position is uncertain and since for contact angles between 0° and ≈ 10° it is difficult to assess a value, the real point might even be slightly below the position indicated by the square. Obviously these points cannot be used to calculate surface energies, therefore in these cases only two liquids were used for the fitting, the ones displayed with crosses.

In Graph IV.17 and Graph IV.18 analysis for 5mm and both one and two passes.
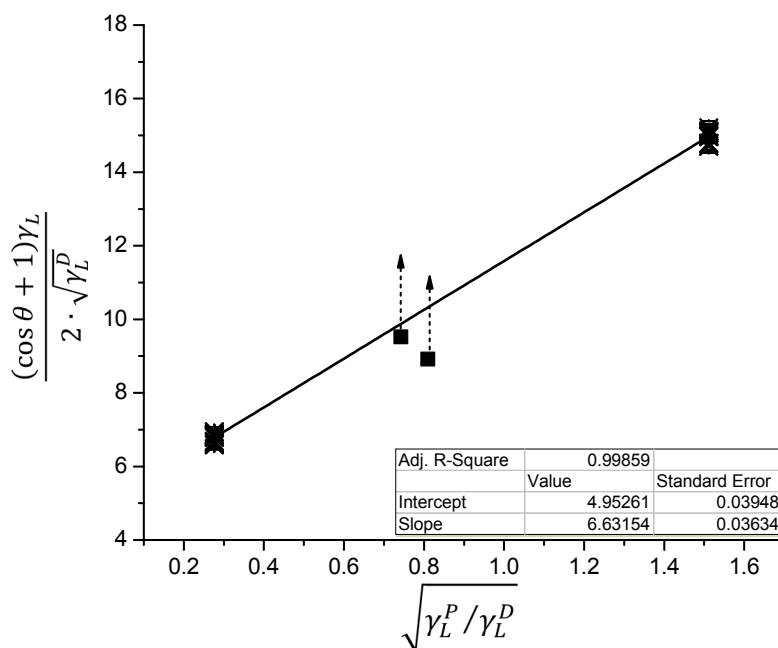
Graph IV.17: filled EVA surface energy analysis (OWRK method, dry tissue cleaned, 5 mm 1 pass).
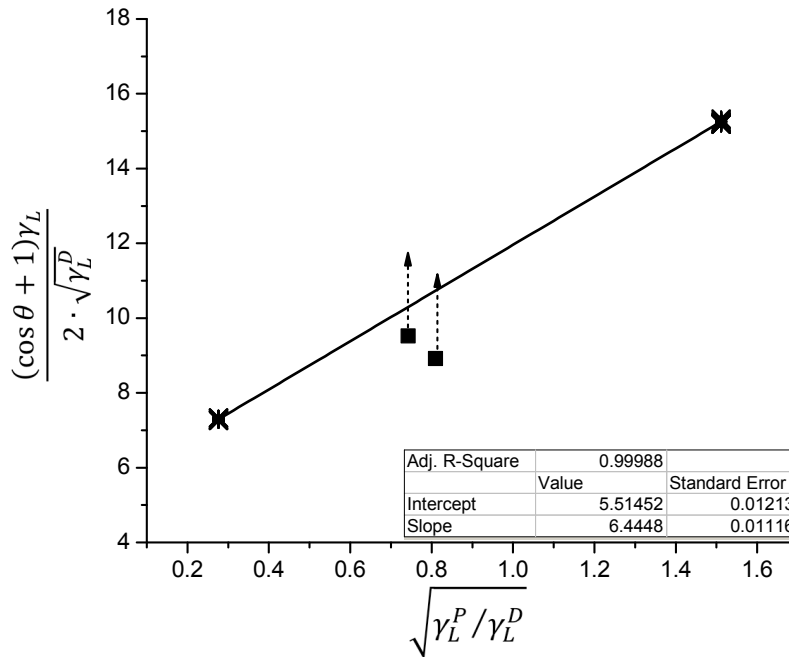
Graph IV.18: filled EVA surface energy analysis (OWRK method, dry tissue cleaned, plasma 5 mm 2 passes).

The surface energies obtained from the graphs are, for the 5 mm 1 pass:

γ_S^P: 43.80 ± 0.95 mJ/m²

γ_S^D: 24.50 ± 0.77 mJ/m²

γ_S^{tot}:   68.39 ± 1.22 mJ/m²

and for 5mm - 2 passes treatment:

γ_S^P: 41.47 ± 0.25 mJ/m²

γ_S^D: 30.36 ± 0.26 mJ/m²

γ_S^{tot}:   71.83 ± 0.36 mJ/m²

The difference in surface energy between one and two passes is in this case minimal, and two liquids are unfortunately not enough to investigate thoroughly the balance between the two fractions.

IV.3.4.3   Detergent cleaned filled EVA

The same polymer has been tested with detergent cleaned substrates, firstly investigating the effect of the distance with different number of passes. In Graphs IV.19-22 the water contact angle in function of these two variables.

5 mm distance plasma treatment, detergent cleaned
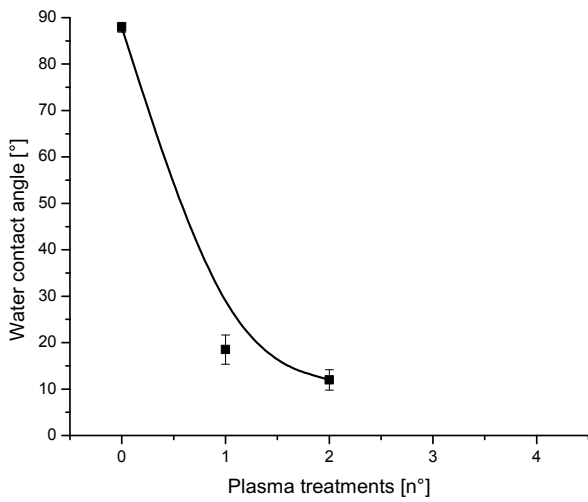
Graph IV.19: detergent cleaned filled EVA water contact angle versus n° of passes, 5 mm plasma.

10 mm distance plasma treatment, detergent cleaned
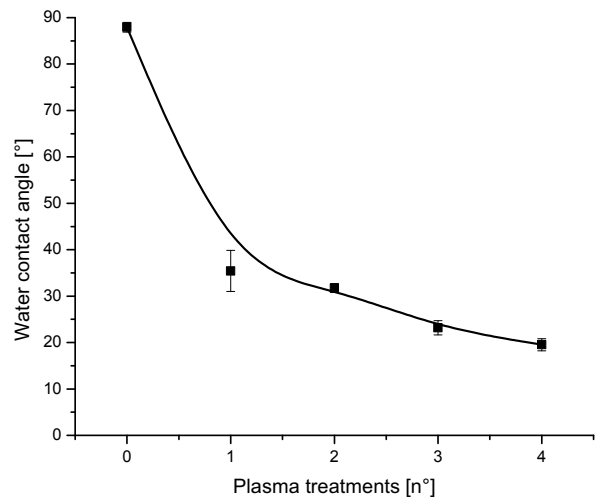
Graph IV.20: detergent cleaned filled EVA water contact angle versus n° of passes, 10 mm plasma.

15 mm distance plasma treatment, detergent cleaned
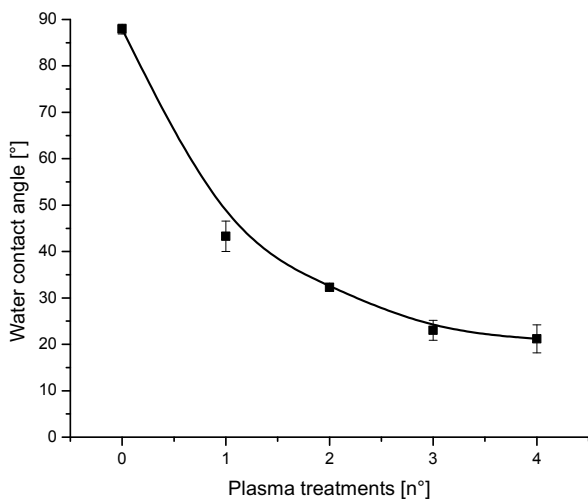
Graph IV.21: detergent cleaned filled EVA water contact angle versus n° of passes, 15 mm plasma.

20 mm distance plasma treatment, detergent cleaned
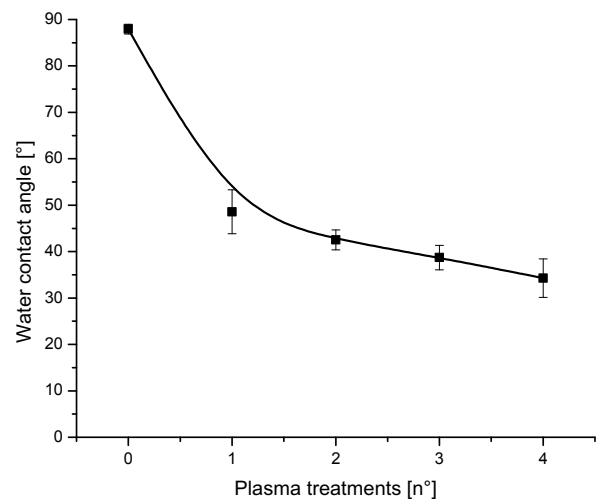
Graph IV.22: detergent cleaned filled EVA water contact angle versus n° of passes, 20 mm plasmas.

Clearly the degradation occurring after three passes at 5mm for the dry tissue cleaned surface happens also for the detergent cleaned EVA. The results of the analysis are resumed in Graph IV.23.
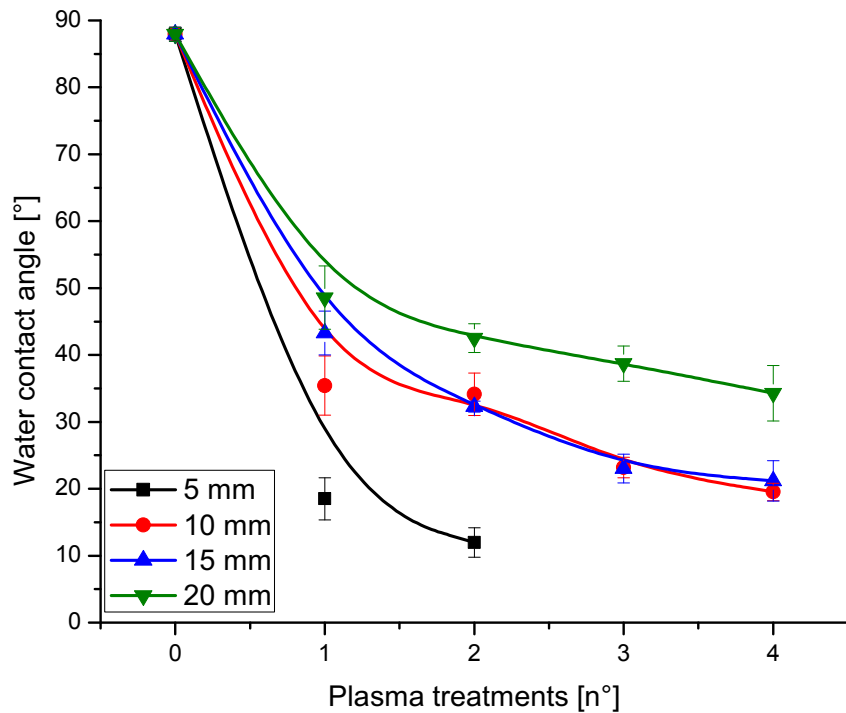
Graph IV.23: detergent cleaned filled EVA, water contact angle versus different distances plasma treatment.

As for the dry tissue cleaned surface analysis, shown in graph IV.16, the lowest contact angle is reached for 5mm passes. Also in this case the curves related to 10mm and 15mm treatments intersect, thus maybe indicating that the intensity of the plasma treatment was similar at this distances for high number of passes.

Complete OWRK analyses have been carried out also in these cases, at 5mm, for one and two passes: results are displayed in Graph IV.24 and Graph IV.25.

Adj. R-Square	0.99948		
		Value	Standard Error
	Intercept	4.88921	0.0146
	Slope	6.72463	0.02452
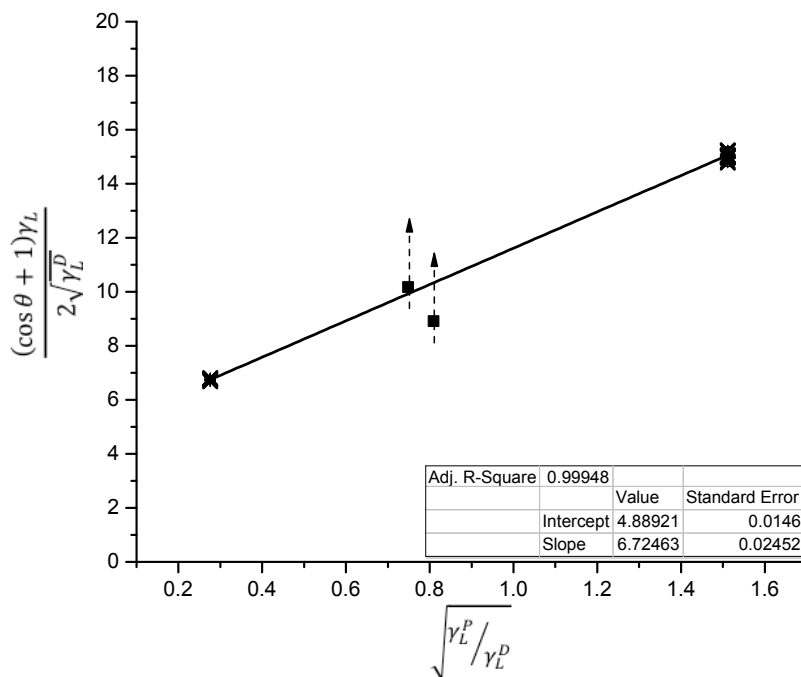
Graph IV.24: filled EVA surface energy analysis (OWRK method, detergent cleaned, plasma 5 mm 1 pass).

Where:

$\gamma_S{}^P$: 45.15 ± 0.65 mJ/m²

$\gamma_S{}^D$: 23.81 ± 0.28 mJ/m²

$\gamma_S{}^{tot}$: 68.96 ± 0.71 mJ/m²
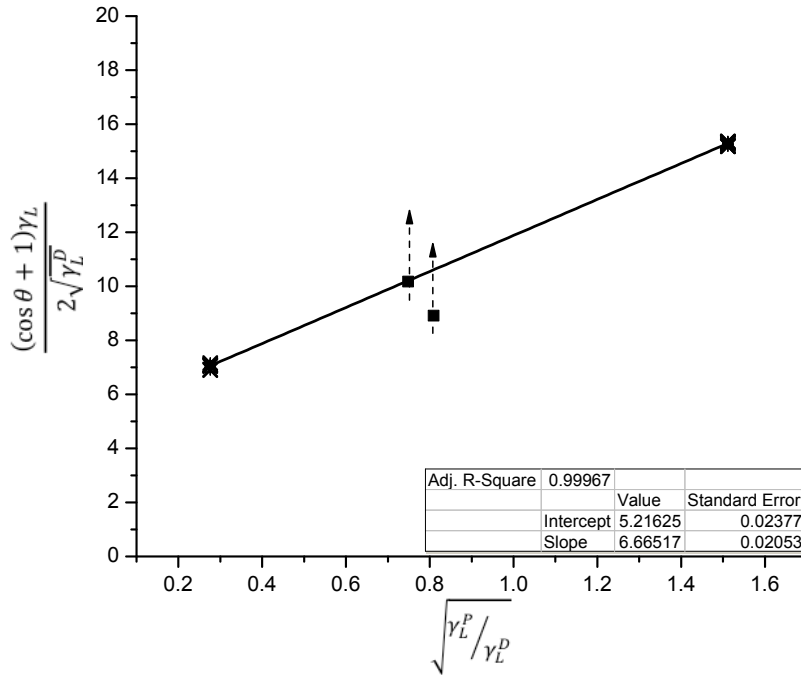
Graph IV.25: filled EVA surface energy analysis (OWRK method, detergent cleaned, plasma 5 mm 2 passes).

Where:

$\gamma_S{}^P$: 44.35 ± 0.53 mJ/m²

$\gamma_S{}^D$: 27.14 ± 0.50 mJ/m²

$\gamma_S{}^{tot}$: 71.49 ± 0.73 mJ/m²

In Table IV.4 summarized results for all the 5mm treatments on filled EVA.

Filled EVA

	5 mm x 1 pass			*5 mm x 2 passes*		
	$\gamma_S{}^P$	$\gamma_S{}^D$	$\gamma_S{}^{tot}$	$\gamma_S{}^P$	$\gamma_S{}^D$	$\gamma_S{}^{tot}$
	[mJ/m²]	*[mJ/m²]*	*[mJ/m²]*	*[mJ/m²]*	*[mJ/m²]*	*[mJ/m²]*
Dry tissue	43.80 ± 0.95	24.50 ± 0.77	68.39 ± 1.22	41.47 ± 0.25	30.36 ± 0.26	71.83 ± 0.36
Detergent	45.15 ± 0.65	23.81 ± 0.28	68.96 ± 0.71	44.35 ± 0.53	27.14 ± 0.50	71.49 ± 0.73

Table IV.4: surface energy results for filled EVA 5mm treatments.

As displayed by Table IV.4 there are no significant differences between the two cleaning methods, as happened for the polyamide. Although it was not expected that the second pass at 5 mm would have increased the dispersive component, a more precise analysis should be carried out to confirm this trend, since two liquids are not sufficient to obtain complete results.

It has been said that the third pass at 5mm might have been enhanced the surface energy of this material even further: unfortunately the third pass caused an unacceptable softening of the substrate. Analysing Graphs IV.12-25 there is the impression that at all distances the marginal effect of the third pass is much lower than the first and the second. Graphs IV.26-29 show the effect of plasma at different distances: graphs have been plotted here for different number of passes, in order to display the trend and to understand the incremental effect of the third and the four plasma treatment, based on the data for the distances higher than 5 mm.
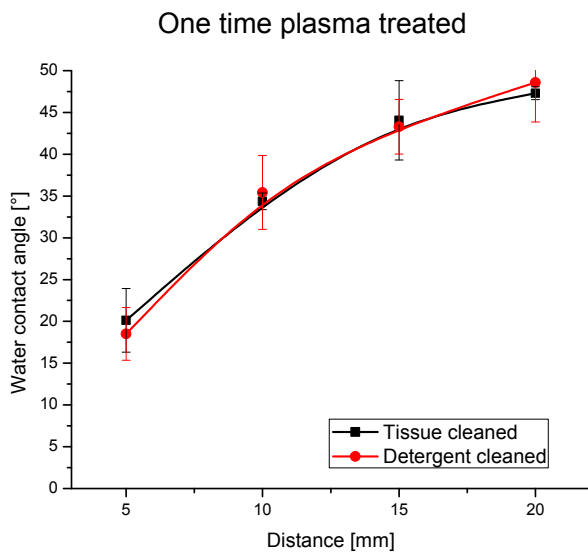
Graph IV.26: effect of distance on the water contact angle for the first plasma pass, filled EVA.
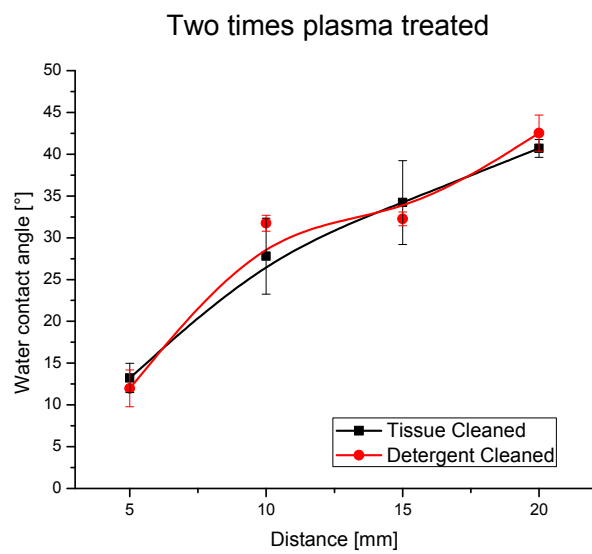
Graph IV.27: effect of distance on the water contact angle for the second plasma pass, filled EVA.

Three times plasma treated	Four times plasma treated
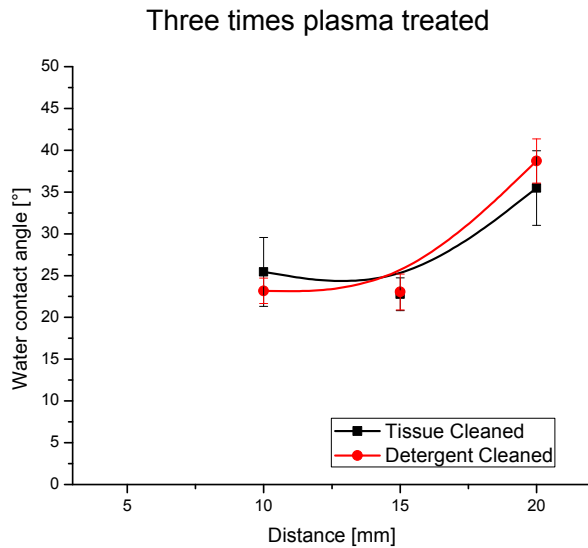
Graph IV.28: effect of distance on the water contact angle for the third plasma pass, filled EVA.
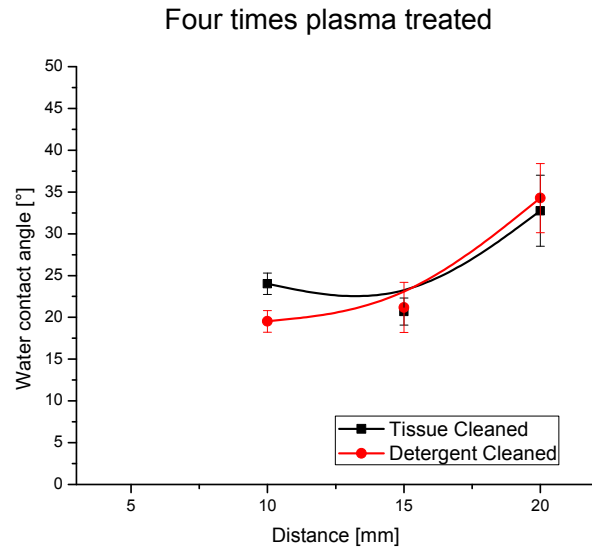
Graph IV.29: effect of distance on the water contact angle for the fourth plasma pass, filled EVA.

As displayed on Graphs IV.26-29 the first two passes had a different effect on the surface. It seemed that the first two treatments had a large marginal effect on the change in surface energy while the third and the fourth seemed to be reaching a plateau for 10 and 15 mm gap.

According to these trends it might be possible that an eventual third treatment at 5mm, if possible, would have not additionally increased the surface energy significantly.

Summarizing, the analysis shows that for filled EVA, with both cleaning methods, the highest surface energy has been obtained treating the surface with 2 passes of plasma at 5mm. The study shows moreover that there was no significant difference in the two cleaning method, as suggested by the PA 12 analysis; being the unfilled version of the EVA similar to the filled one, the optimization of this last polymer has been carried out for only one cleaning method.

IV.3.4.4 Temperature effect

As explained in Chapter III the plasma, especially for most intense treatments, strongly increases the temperature of the sample. Leaving the substrate to cool after the treatment affects its surface energy for two reasons: first, the liquids used to measure the contact angle may be influenced by the temperature of the substrate and second, dust or water vapour in the atmosphere may deposit on the surface, thus reducing the activation effect due to the plasma.

A quick evaluation has been carried out to evaluate to what extent this expected reduction would have influenced the results. In this case the evaluation has been performed on the most intense process, the one at 5 mm and two passes. Plenty of time (at least half an hour) between each pass and before the contact angle measurement has been left for the substrate to cool down.

Tissue cleaned EVA water contact angle:

Immediately after the treatment	13.23 ± 1.76 [°]
Completely cooling down between and after the treatment	17.76 ± 4.19 [°]

Detergent cleaned EVA water contact angle:

Immediately after the treatment	11.98 ± 2.19 [°]
Completely cooling down between and after the treatment	16.13 ± 1.22 [°]

As expected the contact angle rises, even if slightly, as symptom of beginning of surface deactivation. Since the decrease is little, and a continuous deactivation after the plasma is expected and reported by many study, (*e.g.* [44]), the effect of the temperature on tests liquids should be little and negligible.

The deactivation of the surface with time has been studied for similar plasma treatment also on the PA 12. *Borcia et al.* [44] investiged this polymer in different conditions with different plasmas but they always found that the "ageing survey data showed the degree of post-treatment recovery for all polymer types (including PA 12). As expected, most of this recovery took place in the first 2-3 days after the treatment, all further evolution being less important". Among other polymers however, *Borcia et al.* [44] found that the polyamides investigated were the ones retaining the highest wettability after ageing.

IV.3.5 _Unfilled EVA plasma treatment optimization_

The plasma optimization for the unfilled version of the EVA was the same as for the filled one. Graphs IV.30-33 show the water contact angle for different distances.

Unfilled EVA, 5 mm distance plasma treatment
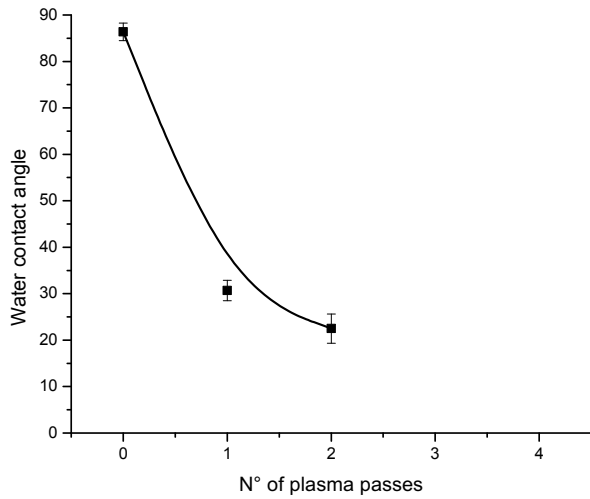
Graph IV.30: unfilled EVA water contact angle versus n° of passes, 5 mm plasma.

Unfilled EVA, 10 mm distance plasma treatment
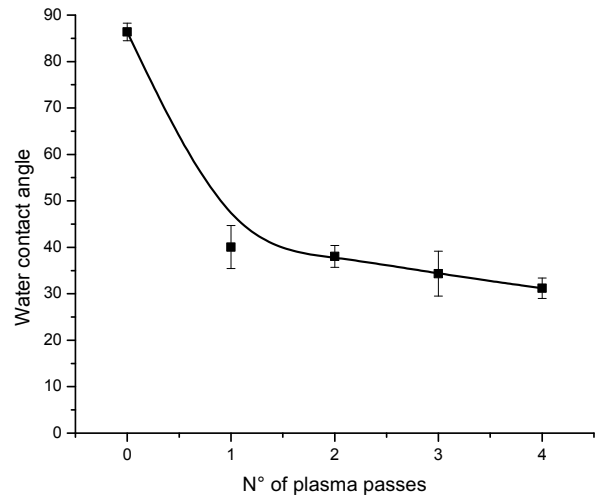
Graph IV.31: unfilled EVA water contact angle versus n° of passes, 10 mm plasma.

Unfilled EVA, 15 mm distance plasma treatment
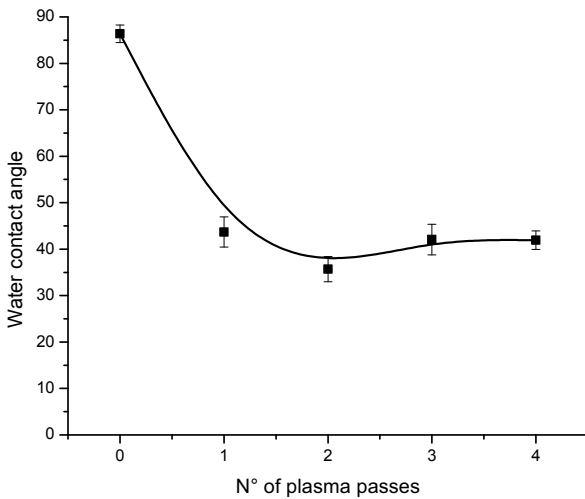
Graph IV.32: unfilled EVA water contact angle versus n° of passes, 15 mm plasma.

Unfilled EVA, 20 mm distance plasma treatment
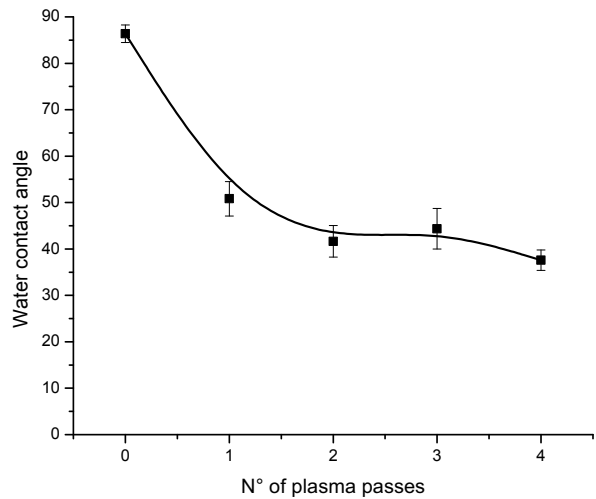
Graph IV.33: unfilled EVA water contact angle versus n° of passes, 20 mm plasma.

Graphs IV.30-33 are collected in Graph IV.34, which shows the trends for all distances.
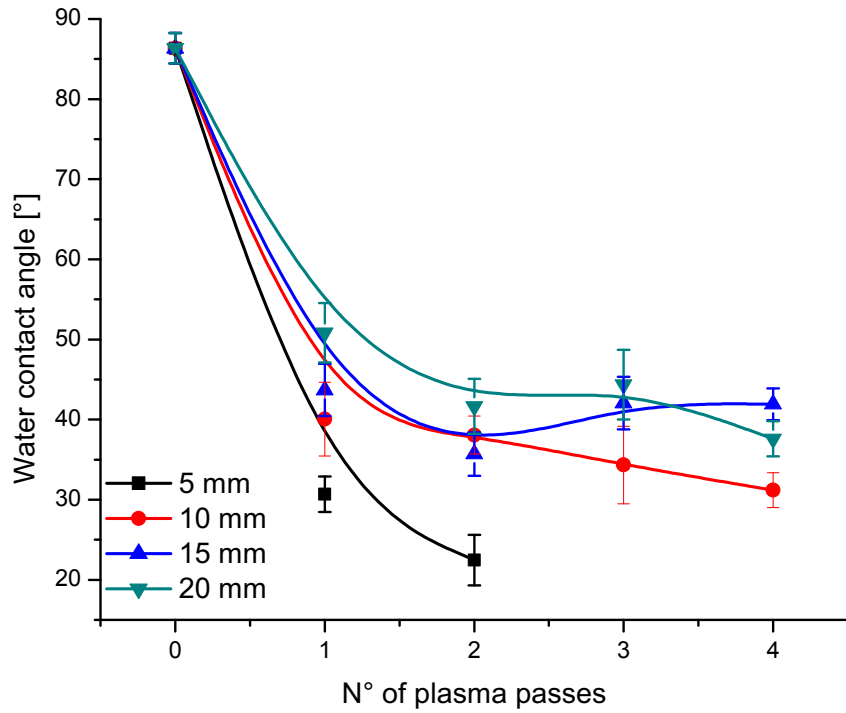
Graph IV.34: unfilled EVA, water contact angle versus different distances plasma treatment.

As found for the filled EVA, 5 mm was the best distance to treat also the unfilled polymer. In Graph IV.35 and Graph IV.36 a complete OWRK analysis at 5mm for one and two passes.

Adj. R-Square	0.96091	
	Value	Standard Error
Intercept	4.39957	0.13612
Slope	6.3984	0.13832
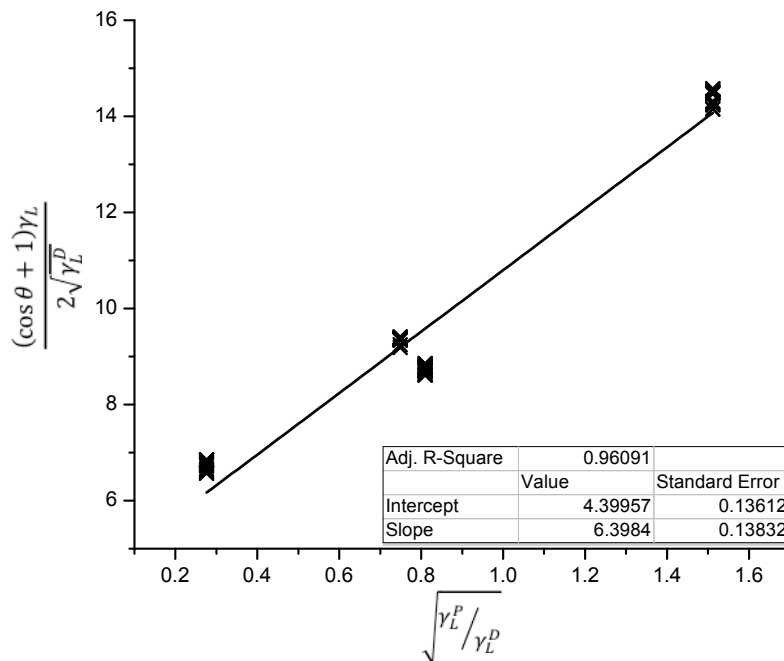
Graph IV.35: unfilled EVA surface energy (OWRK method, plasma 5 mm 1 pass).

Where:

$\gamma_S{}^P$:   40.83 ± 3.52 mJ/m²

$\gamma_S{}^D$:   19.27 ± 2.38 mJ/m²

$\gamma_S{}^{tot}$:   60.10 ± 4.25 mJ/m²
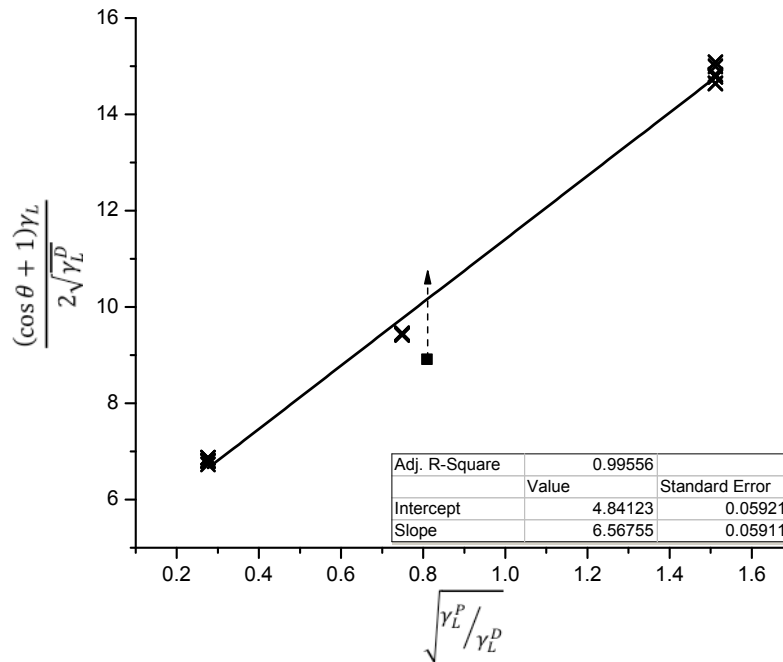
Graph IV.36: unfilled EVA surface energy (OWRK method, plasma 5 mm 2 passes).

$\gamma_S{}^P$:   43.03 ± 1.59 mJ/m²

$\gamma_S{}^D$:   23.42 ± 1.14 mJ/m²

$\gamma_S{}^{tot}$:   66.45 ± 1.96 mJ/m²

In Table IV.5 the results of surface analysis summarized for unfilled EVA.

Unfilled EVA

	$\gamma_S{}^P$	$\gamma_S{}^D$	$\gamma_S{}^{tot}$
	[mJ/m²]	[mJ/m²]	[mJ/m²]
5 mm x 1	40.83 ± 3.52	19.27 ± 2.38	60.10 ± 4.25
5 mm x 2	43.03 ± 1.59	23.42 ± 1.14	66.45 ± 1.96

Table IV.5: surface energy results for unfilled EVA 5 mm distance.

In this case both fractions of surface energy slightly increased with the second pass.

IV.4 *Conclusions*

In this chapter the effect of many parameters has been investigated with the goal of maximizing the surface energy modification induced by a plasma treatment. These included:

- Cleaning method   (dry tissue wiping / detergent wiping / polishing up to 0.25 μm)
- Distance of the plasma torch   (5 - 10 - 15 - 20 mm)
- N° of passes under the plasma gun   (0 - 1 - 2 - 3 - 4)

This study has been carried out on three polymers and the effect of the temperature has also been quickly considered.

This analysis allowed establishing, within the range of parameters investigated, which one were best conditions to treat the surfaces to obtain the highest possible surface energy increment. It has been established that in most effective plasma treatments the cleaning method prior to the plasma did not affect the final surface activation. The optimized parameters for the polymers are reported in Tables IV.6 - 8, where the initial and the final value of the surface energy are reported, together with the percentage increment.

Polyamide 12

Initial (polished)				10 mm x 4 passes			Δ Percentage		
γ_S^P	γ_S^D	γ_S^{tot}		γ_S^P	γ_S^D	γ_S^{tot}	γ_S^P	γ_S^D	γ_S^{tot}
$[mJ/m^2]$	$[mJ/m^2]$	$[mJ/m^2]$		$[mJ/m^2]$	$[mJ/m^2]$	$[mJ/m^2]$	[%]	[%]	[%]
7.07	32.83	39.90	*Dry tissue*	44.74	17.62	62.36	**+532 %**	**-46.3 %**	**+56.3 %**
			Detergent	45.96	17.30	63.62	**+550 %**	**-47.3 %**	**+59.4 %**

Table IV.6: PA 12 surface energy enhancement.

Filled EVA

Initial (polished)				5 mm x 2 passes			Δ Percentage		
γ_S^P	γ_S^D	γ_S^{tot}		γ_S^P	γ_S^D	γ_S^{tot}	γ_S^P	γ_S^D	γ_S^{tot}
$[mJ/m^2]$	$[mJ/m^2]$	$[mJ/m^2]$		$[mJ/m^2]$	$[mJ/m^2]$	$[mJ/m^2]$	[%]	[%]	[%]
1.45	31.64	33.09	*Dry tissue*	41.47	30.36	71.83	**+2760 %**	**-4.0 %**	**+117.1 %**
			Detergent	44.35	27.14	71.49	**+2958 %**	**-14.2 %**	**+116.0 %**

Table IV.7: filled EVA surface energy enhancement.

Unfilled EVA

Initial (polished)				5 mm x 2 passes			Δ Percentage		
γ_S^P	γ_S^D	γ_S^{tot}		γ_S^P	γ_S^D	γ_S^{tot}	γ_S^P	γ_S^D	γ_S^{tot}
$[mJ/m^2]$	$[mJ/m^2]$	$[mJ/m^2]$		$[mJ/m^2]$	$[mJ/m^2]$	$[mJ/m^2]$	[%]	[%]	[%]
0.91	39.06	39.97	*Dry tissue*	43.03	23.42	66.45	**+4628%**	**-40.0 %**	**+66.2 %**

Table IV.8: unfilled EVA surface energy enhancement.

In the entirety of cases the polar components rises significantly, while the dispersive ones always slightly decreases. The balance, however, is always positive, even if the Owen-Wendt-Rabel-Kaelble interpolations in the case of 5mm and 2 passes treatments are only an estimations of real values, since obtained on linear fits based on only with two points.

In Graph IV.37 a graphic representation of what indicated in table IV.6-8.
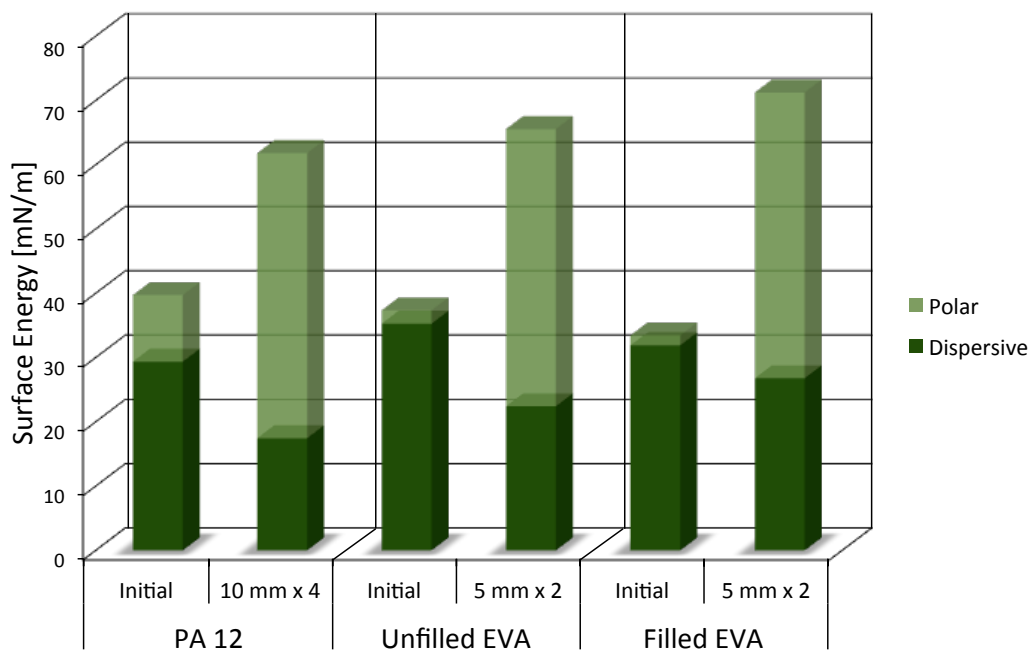
Graph IV.37: surface energy enhancement in the plasma treated polymers.

It is fundamental to acknowledge that in this study the concept of "plasma treatment optimization" is centred on the scope of obtaining the highest surface energy possible. This does not necessarily mean (and Chapter V proves it) that this represents best condition for adhesion.

V. CHAPTER: MECHANICAL TESTS RESULTS

The plasma treatment optimization outlined in Chapters III and IV reached its objective indicating the best conditions to enhance surfaces energies of all adherends. To ascertain that these treatments improved joints resistance and to verify if selected parameters were the best for this scope, mechanical tests were required. As explained in Chapter III, for flexible adherends the fixed arm peel test is particularly indicated. Their results are outlined in this chapter, together with those of other mechanical tests carried out.

V.1   Tensile tests

In order to analyse fixed arm peel tests data it is necessary, as described in Chapter II, to perform uniaxial tensile tests on the flexible arm of the peel specimen. Three tensile samples for each of the polymers used as flexible arm were tested, as described in Chapter III.

V.1.1   Tensile tests results

The complete uniaxial tensile stress-strain curves obtained for both the unfoamed versions of EVA are similar and resemble the one in Graph V.1, where an unfilled EVA sample characteristic is represented.
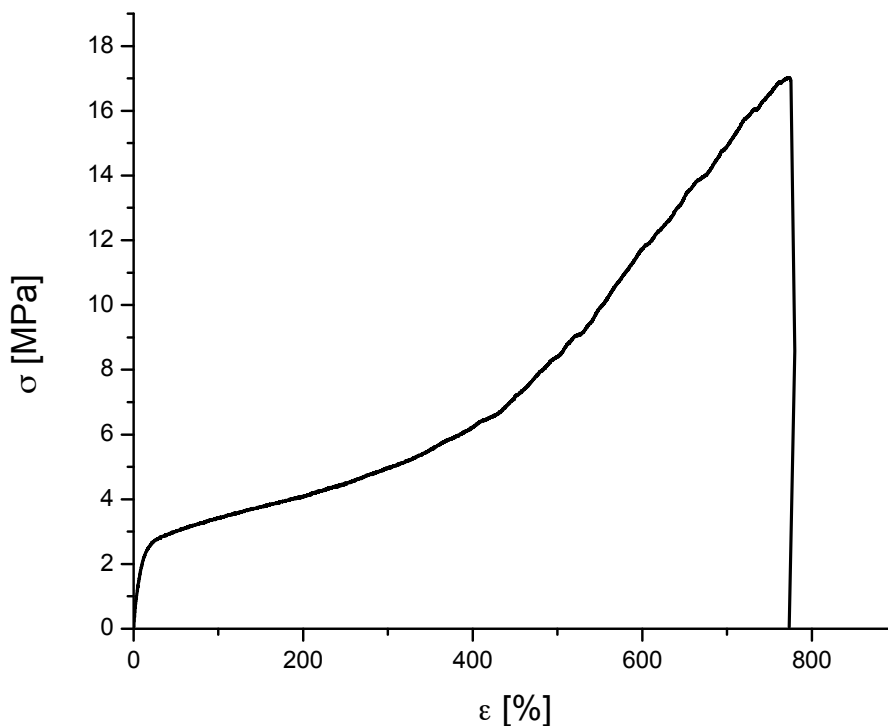
Graph V.1: uniaxial tensile stress-strain behaviour, unfilled EVA.

Graph V.1 shows that the polymer is able to withstand a noteworthy maximum deformation, up to 780%, and that significant strain hardening occurs. The causes for these phenomena

might be several, but their investigation lies out of the scope of this thesis.

The objective of the tensile tests was to obtain uniaxial tensile moduli and to provide stress-strain curves for the peel tests analyses. In such tests elongation is quite small, therefore only the initial parts of the tensile curve have been used. The data obtained from different samples have been averaged, as shown in **Error! Reference source not found.** and **Error! Reference source not found.** for both EVAs.
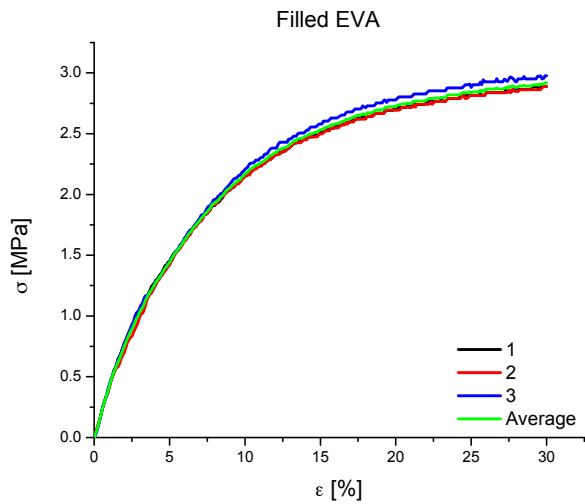
Graph V.2: uniaxial stress-strain behaviour data obtained from three filled EVA samples and relevant average curve.
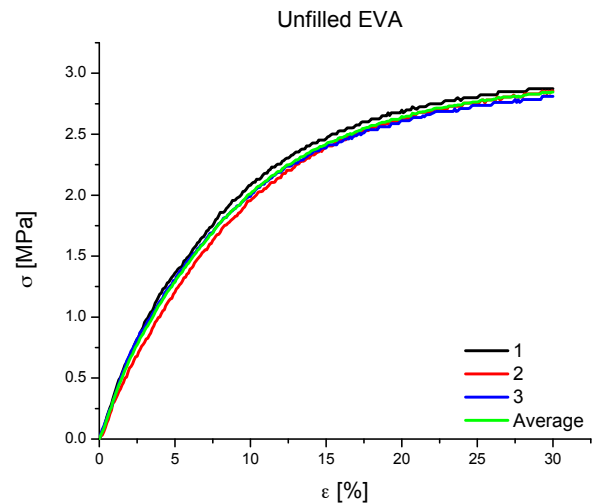
Graph V.3: uniaxial stress-strain behaviour data obtained from three unfilled EVA samples and relevant average curve.

Once average data are calculated it is possible to obtain the tensile moduli by linearly fitting the first portion of the curves. This has been done for both polymers, and the results are exhibited in **Error! Reference source not found.**.

Adj. R-Square	0.99748	
	Value	Standard Error
Intercept	0	--
Slope	32.44122	0.57674

Adj. R-Square	0.99722	
	Value	Standard Error
Intercept	0	--
Slope	42.31049	0.79014
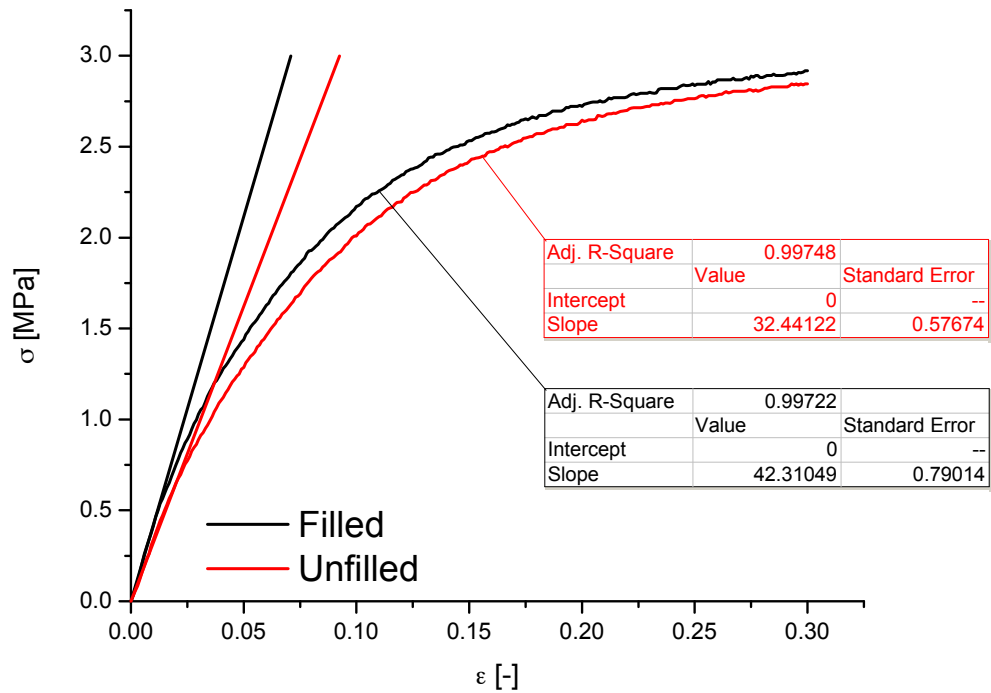
Graph V.4: uniaxial tensile stress-strain behaviours and linear fits of the first portion for filled and unfilled EVAs.

Graph V.2 and Graph V.3 indicate that the fillers did not strongly modify the tensile properties of the unfilled copolymer blend.

With these simple tests has not been possible to evaluate a precise yield point, required by the IC peel software. A value of 0.5 MPa adequate for the purpose, has been identified where significant deviation from linearity occurred.

The uniaxial tensile moduli are:

- Filled EVA: 42.31 ± 0.79 MPa;
- Unfilled EVA: 32.33 ± 0.57 MPa;

The IC Peel software related to the ESIS protocol also required the tensile modulus of the adhesive, which is 26.20 MPa according to the adhesive technical data sheet provided by the producer [45].

V.2   *Peel tests*

V.2.1   *Bonding parameters*

The results obtained from surface energy analysis demonstrated the conditions in which the highest surface energies were obtained. These parameters (and other sets of conditions) have been used to prepare peel test specimens, in order to assess adhesive resistance. In the first stage, four different categories of specimens have been analysed, whose specifications are summarized in Table V.1.

n°	Bond materials		Plasma distance	Plasma passes	Adhesive
1a	PA / Filled EVA	PA	10 mm	4 passes (speed 1 cm/s)	PU
		EVA	5 mm	2 passes (speed 1 cm/s)	
1b	PA / Unfilled EVA	PA	10 mm	4 passes (speed 1 cm/s)	PU
		EVA	5 mm	2 passes (speed 1 cm/s)	
2a	PA / Filled EVA	PA	5 mm	4 passes (speed 1 cm/s)	
		EVA	5 mm	2 passes (speed 1 cm/s)	
2b	PA / Unfilled EVA	PA	5 mm	4 passes (speed 1 cm/s)	
		EVA	5 mm	2 passes (speed 1 cm/s)	
3a	PA / Filled EVA	PA	5 mm	4 passes (speed 1 cm/s)	PU
		EVA	5 mm	2 passes (speed 1 cm/s)	
3b	PA / Unfilled EVA	PA	5 mm	4 passes (speed 1 cm/s)	PU
		EVA	5 mm	2 passes (speed 1 cm/s)	
4a	PA / Filled EVA	PA	-	-	PU
		EVA	-	-	
4b	PA / Unfilled EVA	PA	-	-	PU
		EVA	-	-	

Table V.1: parameters for specimens preparation, first set.

The reasons behind these choices were the following:

1 a/b: this combination of materials has been chosen because highlighted by the surface energy analysis to be the best in enhancing the plasma treatment effects.

2 a/b: these sets have been prepared to meet one of the producer's scopes: obtain an adhesive junction without using any adhesive but instead relying on the increase in surface temperature induced by the plasma on the surfaces. In order to obtain the highest temperature possible, both materials have been treated up to the point where degradation of the surface was detectable. Since the harshest treating conditions for the EVAs were already found to be 5mm and 2 passes, these settings

have been used. For the PA 12 however, a 5mm distance proved to be more effective in increasing the surface temperature and the peak of temperature increment without surface degradation has been reached with 4 passes.

3 a/b: this set has been chosen to test the adhesive strength in samples treated with the same intensity of 2a/b but improving the junction with the presence of adhesive. This allowed also investigating harsher plasma conditions.

4 a/b: these are the reference conditions for the untreated materials.

V.2.2   *Data analysis*

The analyses of peel tests results are not straightforward and an Excel worksheet (IC Peel software) has been used to evaluate adhesive fracture energy. The first step for adhesive fracture energy evaluation is a peel strength analysis. Load/crosshead displacement curves for each specimen were recorded and they were similar to the one provided in Graph V.5:
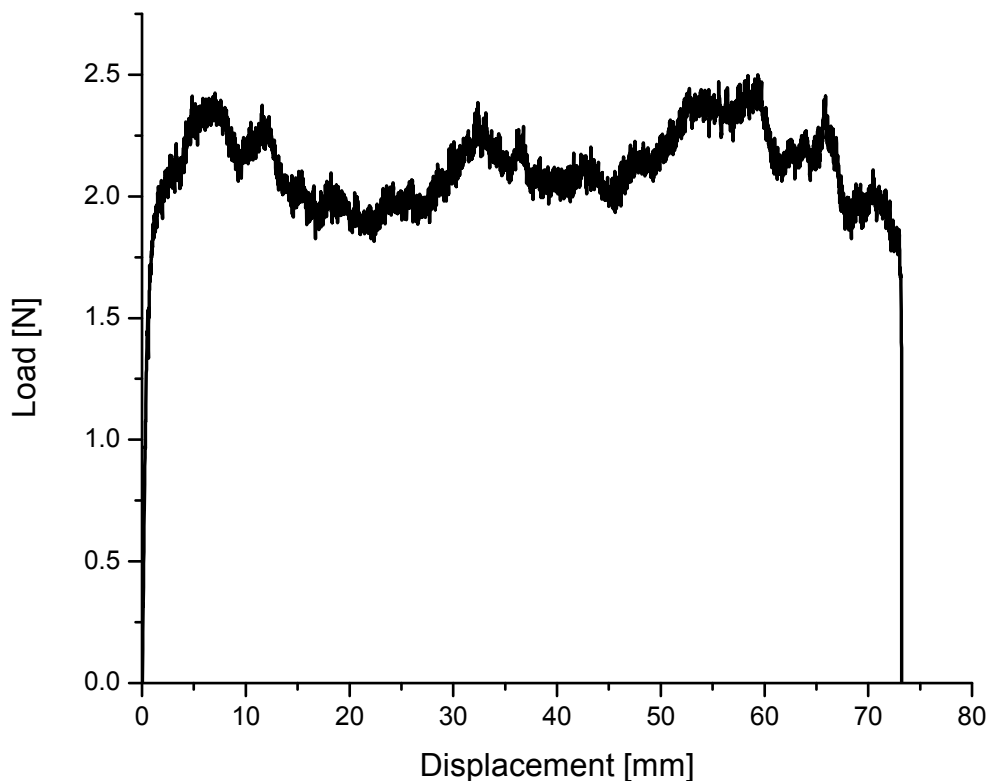
Graph V.5: peel load versus crosshead displacement in a 1b type sample fixed arm peel test.

Data in Graph V.5 show an almost constant value of load during the test, as expected. This indicates a stable propagation of the crack, which is one of main features of fixed arm peel tests. Although there is a certain degree of scatter this is absolutely normal in these tests:

actually the specimen displayed in Graph V.5 was one of the most regular records, where the whole range could be used to assess adhesive fracture energy. To calculate adhesive fracture energy (and peel strength) it is necessary to select the range of data to consider in the analysis. It is clear that the first portion of Graph V.5 represents the loading of the junction and therefore those values do not correspond to peel forces (moreover the first part may be influenced by the presence of the PTFE needed to initiate the crack); the same goes for the last portion, where before the unloading there is a region where the crack reaches the end of the specimen, the geometry being different, and must therefore be discarded. In this case useful data lie between crosshead displacements ranging from 5.17 to 66.37 mm. In Graph V.6 the calculated mean peel load of this case is highlighted.

		Value	Standard Error
Load [N]	Intercept	2.14254	0.00237
	Slope	0	--
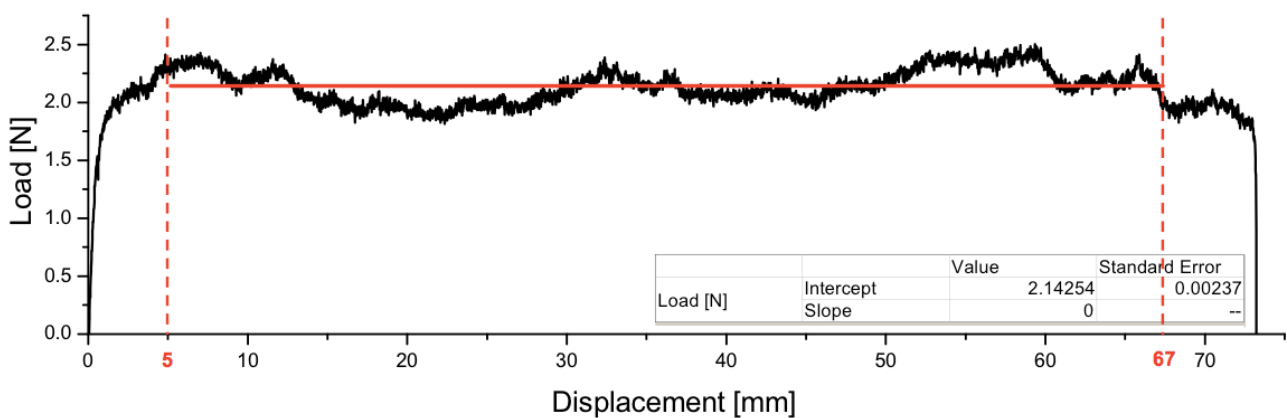
Graph V.6: peel load versus crosshead displacement, data selection and mean value
(unfilled EVA type 1b specimen).

In this case the mean peel load is 2.14 N and, since the width of the junction was 17.9 mm, the mean peel strength is 1.20 N/cm.

V.2.3   Fracture considerations

The peel tests performed showed three main cases of fracture:
- Adhesive fracture in the PA/PU interface.
- Adhesive fracture in the EVA/PU interface.
- Mixed fracture.

Some evidences explained later suggest that also cohesive fracture of a thin weak layer in any of the two adherends' surfaces might have happened.

V.2.3.1   Mixed fracture

Each sample displayed one or more of the previously described fracture cases; when the junction debonds in more than one interface during the test this may happen in two different ways:
- Longitudinally: the first part which is peeled off displays separation between two

given surfaces while at the end fracture proceeds propagating in another interface; for instance PA/PU interface in the beginning and EVA/PU in the end.

- Transversally: the propagation proceeds with one interface debonding on one side and another debonding on the other side, both propagating at the same time.

When the debonding happens in two different interface transversally is a case of mixed fracture. A clear example of mixed transversal propagation is represented in Figure V.1.
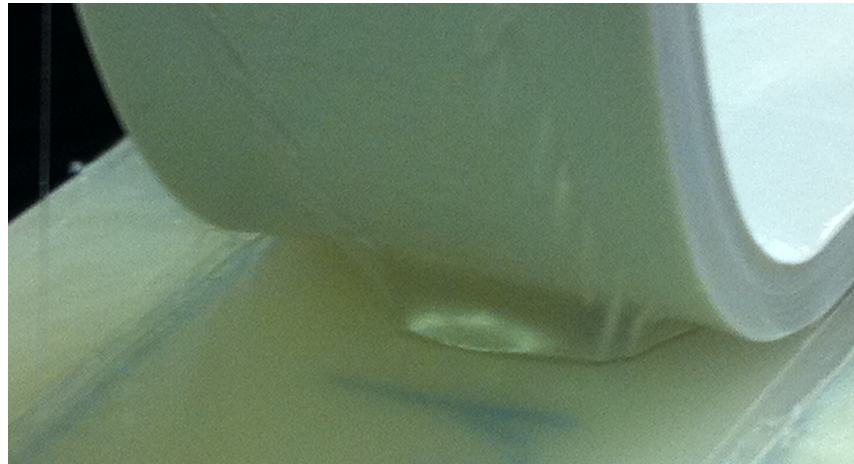
Figure V.1: transversally-mixed fracture propagation.

In Figure V.1 the junction debonds in the PA/PU interface on the sides and on the EVA/PU interface in the centre. This event influences the adhesive fracture energy calculation since a considerable higher amount of energy is used to break the junction: first, the PU adhesive stretches considerably and second, the subsequent propagation of the crack over the mixed spot eventually debonds also the second interface, thus accounting an extra energy which does not refer to the primary propagation. This contribution is not important for practical purposes, since the structural integrity of the joint is already compromised. In Figure V.2, two stages of the same propagation are shown:
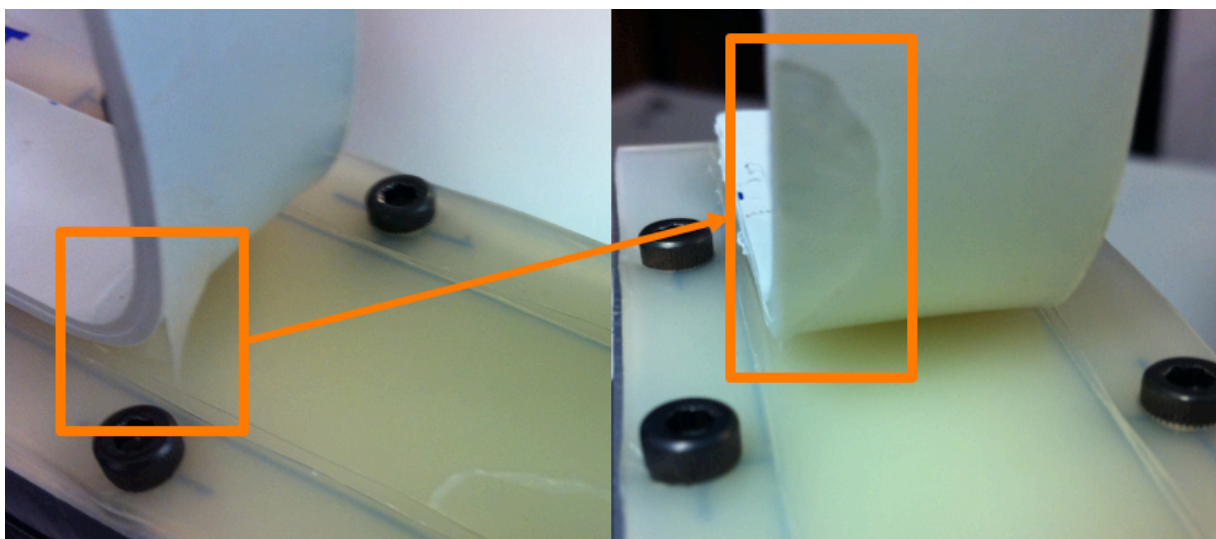
Figure V.2: fracture proceeds along two different interfaces, debonding the PU from both the adherends.

Sometimes the situation is not as clear as the case displayed on Figure V.2; in some cases the phenomenon interests small portions of the junctions and its presence is more easily detectable by analysing the peel load data, which in those cases shows a sudden increase in load. When mixed transversal separation occurred the portion of the surface interested by the phenomenon has been excluded from the analysis, since it is not possible to properly account for its strength for two reasons: first, it is not possible to evaluate the fraction of crack propagating in one interface and the one developing in another; second, it is not easy to account for the polyurethane stretching.

The range of data used to obtain the peel strength and subsequently the adhesive fracture energy is indicated in the peel results report and those intervals are the ones where cracks proceeded in a single interface along the entire transverse section.

V.2.3.2   Mixed fracture causes

Since the specimens displaying mixed fracture in a considerable range had to be discarded a quick investigation has been performed to understand why such phenomenon happened. In principle, since there are no differences in treatment and bonding procedures between one part of the surface and another, such events should not occur. Moreover, among different samples, it has been noticed that mixed fracture involved different parts of the joints thus not revealing a specific problem. What has been found after several tests was that this occurrence was simply ascribable to the specimens' preparation. The complex procedure described in Chapter III has been developed starting from the results obtained with the first tests. After these, a very rigid control has been introduced on all the parameters including:

- Surface temperature after the plasma treatment and before glue deposition;
- Temporal control over each phase of the bonding procedure, with chronometer;
- Increment of the curing time of the adhesive from 24 to 72 hours;
- Improvement in the locking system which held in position the adherends with the weight during the drying phase.

The control over the last variable in particular seemed to be very effective in reducing the occurrence of mixed fracture propagation. The new procedure adopted to prepare the samples resulted not only in an almost complete disappearance of mixed propagation but also in a greatly improved reproducibility of results among specimens prepared with the same treatment and bonding conditions.

V.2.3.3   Fracture initiation

Another problem occurred with the first specimens during fracture initiation. As explained in Chapter III, a thin strip of PTFE has been placed to start the crack propagation, as shown

in Figure V.3:
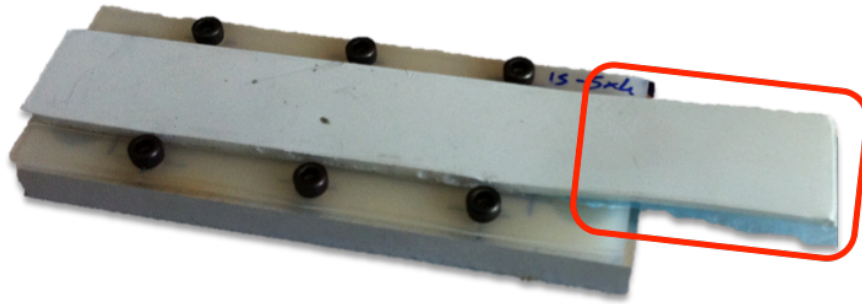
Figure V.3: a PTFE strip is placed during the preparation of the specimen to act as a fracture initiator.

In the first specimens prepared there has been no rigid control over the adhesive thickness in the part where the PTFE was placed. This led to an accumulation of adhesive both above and below PFTE, which bonded also with the frontal edge of the polyamide sheet. When the specimens have been tested this accumulation of PU jointed more strongly over a wider surface of the one being peeled resulted in the formation of a polyurethane "bridge" connecting the peel crack front and a region outside the test area. This phenomenon is shown in Figure V.4:
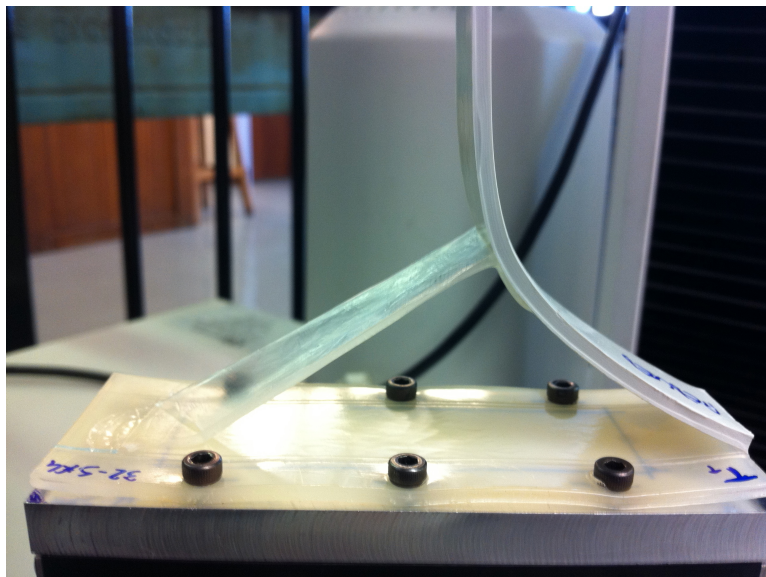
Figure V.4: a strip of Polyurethane is formed between a region out of the surface test and the crack front.

In most cases the bridge develops in the first part of the test and then debonds from the area outside the test surface naturally. This event is clearly shown by the peel load vs. crosshead displacement data of a specimen in Graph V.7:
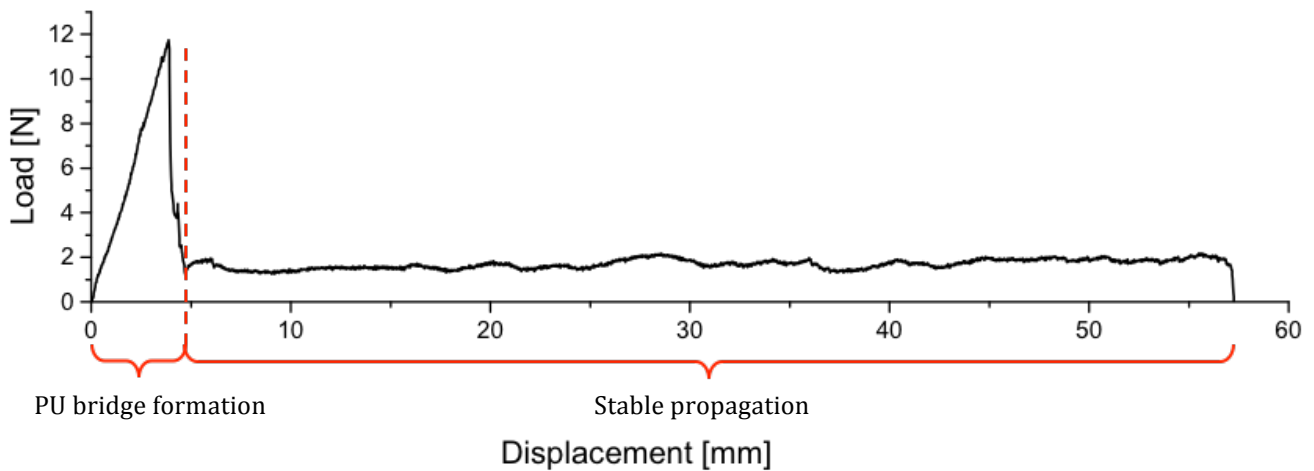
Graph V.7: peel load versus crosshead displacement curve shows the formation of a PU bridge as an increment in load.

If the link debonds naturally before the end of the test the data recorded after the break indicate a stable propagation, as it is for most of the specimen displayed in Graph V.7, and can be used to evaluate the adhesive fracture energy.

This problem has been solved with a simple procedure: each specimen is pre-tested to understand which one is the weak interface, the one where the crack propagates. Once the crack starts propagating (and the adherends opening), the specimen is held in position and a razorblade cuts the adhesive outside the test area, in order to avoid the PU "bridge" formation. After this operation the sample is unloaded and a crack resembling the true behaviour is created. This allowed exploiting a bigger area of the joint for the analysis since in some cases (such as the one in figure V.4) the bridge did not break until the end of the test, thus compromising the whole experiment.

V.2.4   *Peel tests results*

The most important parameters obtained from peel test analysis are peel strength and adhesive fracture energy but it is possible to calculate many other parameters, including the total input energy, the plastic work of bending and the radius of curvature of the peel arm at the root. In Table V.2 an exemplificative extract of some of the most important results obtained with the IC Peel worksheet is reported: a common set of input peel loads has been used and, once the other parameters are inserted, calculations are readily made.

The calculations are based on theory reported in Chapter II.4.3.2. Input energy is evaluated from the peel load, the peeling angle and the width of the flexible strip: in Table V.2 G has already been corrected for tensile and plastic deformation of the peel arm (the stress-strain curve is necessary for accounting these factors, even if they are often negligible).

Data		Results				
P	θ	G_c	G_d	G_{tot}	G	R
[N]	[°]	[J/m²]	[J/m²]	[J/m²]	[J/m²]	[mm]
...	...	...	...	...	...	...
2.34	90.00	86.33	64.07	150.40	150.26	10.39
2.30	90.00	85.30	63.00	148.30	148.17	10.45
2.33	90.00	86.09	63.83	149.93	149.79	10.40
2.29	90.00	84.99	62.68	147.67	147.54	10.47
2.27	90.00	84.12	61.82	145.94	145.81	10.53
2.24	90.00	83.21	60.92	144.14	144.01	10.59
2.24	90.00	83.30	61.01	144.31	144.18	10.59
2.25	90.00	83.49	61.20	144.70	144.57	10.57
2.31	90.00	85.64	63.36	149.00	148.86	10.43
2.28	90.00	84.54	62.23	146.77	146.64	10.50
2.27	90.00	84.29	61.99	146.28	146.15	10.52
...	...	...	...	...	...	...

Table V.2: extract of IC Peel protocol results with most important features.

The meaning of Table V.2 symbols are reported below, together with an indicative range of minimum and maximum for each variable among all the specimens analysed.

θ: peel angle (=90°);

P: peel force (0.8 - 4 N);

G_c: adhesive fracture energy (40 - 130 J/m²);

G_d: plastic work in bending; (15 - 110 J/m²);

G_{tot}:   input energy corrected for stored strain energy and tensile dissipation on the peel arm (50 - 240 J/m²);

G: total input energy (50 - 240 J/m²);

R: radius of curvature of the peel arm at the root (8 -15 mm);

Although it is useful to check that a major part of the total input energy is used for plastic bending purposes, the most important result to assess the quality of the joint is the adhesive fracture energy. Peel strength of the joint (peel load divided by the flexible arm width) is also reported as a main result because of its ease of determination and diffusion in analysing joints.

V.2.4.1   1a/1b

1a	PA / Filled EVA	PA	10 mm	4 passes (speed 1 cm/s)	PU
		EVA	5 mm	2 passes (speed 1 cm/s)	
1b	PA / Unfilled EVA	PA	10 mm	4 passes (speed 1 cm/s)	PU
		EVA	5 mm	2 passes (speed 1 cm/s)	

Table V.3: 1a/1b specimens parameters.

In Table V.3 a recall of the parameters used to prepare 1a/1b specimens, in Table V.4 their results. Specimens are numbered for identification purposes.

1a/1b

Specimen n°	Type	Analysed range [mm] (Crosshead displacement)		Fracture Interface	Peel Load [N/cm]	Fracture energy [J/m^2]
2	1a	5.32 - 24.42	29.76 - 44.50	PA / PU	1.73	98.23 ± 7.4
4	1a	7.30 - 13.62	35.55 - 49.08	PA / PU	1.71	96.71 ± 6.8
6	1a	4.25 - 35.05		PA / PU	1.94	108.4 ± 13.7
26	1a	40.96 - 77.70		PA / PU	1.35	76.52 ± 6.8
3	1b	21.15 - 59.05		PA / PU	1.23	81.77 ± 8.6
7	1b	19.77 - 59.62		PA / PU	1.66	106.1 ± 11.6
21	1b	9.02 - 51.97		PA / PU	1.90	119.7 ± 12.3
23	1b	5.17 - 66.37		PA / PU	1.20	79.90 ± 4.6
24	1b	3.43 - 39.38		PA / PU	1.43	76.52 ± 6.8

Table V.4: 1a/1b specimens results.

In this set a high number of test results has been dropped because of the problems described previously. In all these specimens the separation occurred in the PA/PU interface: the surface energy analysis showed that with this plasma treatment conditions the layer with lowest energy is the PA, thus in accordance, in this case, with the peel tests results. The results outlined in Table V.4 could be merged since there is no difference between 1a and 1b since in both cases occurred in the PA/PU interface, thus not involving the EVA.

2a	PA / Filled EVA	PA	5 mm	4 passes (speed 1 cm/s)	No PU
		EVA	5 mm	2 passes (speed 1 cm/s)	
2b	PA / Unfilled EVA	PA	5 mm	4 passes (speed 1 cm/s)	No PU
		EVA	5 mm	2 passes (speed 1 cm/s)	

Table V.5: 2a/2b specimens parameters.

One of the goals of the project was to develop an effective way to bond the adherends without using adhesives. To reach this objective without any other operation one of the possible solutions tried was to increase the temperature of the surfaces as much as possible with the heat generated by the plasma arcs. High temperature have been reached with both polymers, up to 80°C for the PA 12 (5mm 4passes) and up to 60°C for the EVA (5mm 2passes). As soon as possible after the treatment the surfaces have been put in contact (before starting cooling) and a pressure has been applied: about 10 kPa (20kg on the specimen surface) have been applied to the first specimens but no significant adhesion was established and the two adherends fell apart immediately once moved. Other specimens have been produced with this technique, trying to exploit more polymer diffusion and increasing pressure. The surfaces could not be heated more but it has been applied an almost instantaneous pressure corresponding to the one exercised by a 70kg man (there has been no time to set in position more than 20kg lead weights). A very weak adhesion resulted, but its degree was negligible and it was very inhomogeneous along the specimen length. In Graph V.8 an example of peel load for a 2a specimen without adhesive is reported: the peel load is very low and adhesion very inhomogeneous throughout the specimen length.
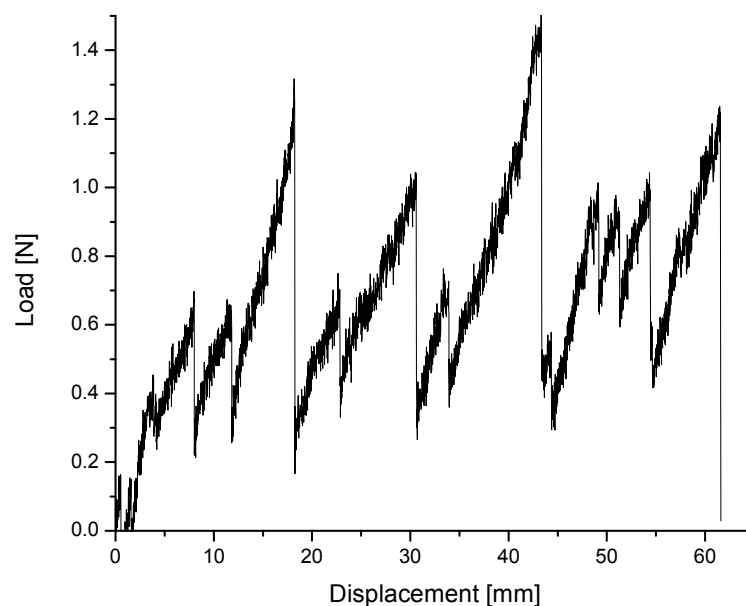
Graph V.8: peel load versus crosshead displacement in a specimen prepared without adhesive.

The attempt of obtaining joints without adhesive through heating was finally discarded after testing 2a/2b specimens.

V.2.4.3   3a/3b

3a	PA / Filled EVA	PA	5 mm	4 passes (speed 1 cm/s)	PU
		EVA	5 mm	2 passes (speed 1 cm/s)	
3b	PA / Unfilled EVA	PA	5 mm	4 passes (speed 1 cm/s)	PU
		EVA	5 mm	2 passes (speed 1 cm/s)	

Table V.6: 3a/3b specimens parameters.

In Table V.7 the results obtained from peel tests on 3a/3b samples (the ones tested in the harshest plasma conditions) are shown. As for type 1a/1b samples, these joints suffered the problems described previously in terms of reproducibility and scatter: many of the junctions prepared with these parameters have been discarded.

3a/3b

Specimen n°	Type	Analysed range [mm] (Crosshead displacement)	Fracture Interface	Peel Load [N/cm]	Fracture energy [J/m^2]
14	3a	38.49 - 58.78	PA / PU	1.93	110.5 ± 11.1
17	3a	34.96 - 45.03	PA / PU	1.87	102.6 ± 4.8
18	3a	28.15 - 51.42 59.28 - 69.72	PA / PU	1.41	81.28 ± 10.3
20	3a	2.23 - 70.63	PA / PU	1.66	94.16 ± 15.0
13	3b	3.22 - 68.18	PA / PU	1.27	84.36 ± 15.5
16	3b	6.37 - 20.57 27.38 - 75.35	PA / PU	1.48	96.24 ± 11.0
25	3b	1.38 - 57.93	PA / PU	1.22	80.99 ± 7.0

Table V.7: 3a/3b specimens results.

As displayed in Table V.7, also in this case the entirety of the junctions debonded at the interface between the polyamide and the adhesive, meaning that the polyurethane after the propagation is completely on the EVA surface.

V.2.4.4   4a/4b

4a	PA / Filled EVA	PA	No plasma	PU
		EVA	No plasma	
4b	PA / Unfilled EVA	PA	No plasma	PU
		EVA	No plasma	

Table V.8: 4a/4b specimens parameters.

These specimens have been tested to measure adhesion improvement due to plasma treatment and represent the reference case for every comparison. The results for untreated joints are displayed in Table V.9:

4a/4b

Specimen n°	Type	Analysed range [mm] (Crosshead displacement)	Fracture Interface	Peel Load [N/cm]	Fracture energy [J/m²]
42	6a	1.66 - 72.66	EVA / PU	1.24	72.92 ± 14.5
46	6a	6.58 - 71.85	EVA / PU	1.60	91.71 ± 6.4
47	6a	4.73 - 66.21	EVA / PU	1.41	81.79 ± 4.4
50	6a	6.32 - 65.79	EVA / PU	1.57	89.86 ± 14.9
64	6a	2.65 - 74.73	EVA / PU	1.34	78.03 ± 17.4
45	6b	14.18 - 63.25	EVA / PU	0.59	43.84 ± 5.4
48	6b	19.32 - 63.77	EVA / PU	0.67	48.69 ± 9.0
49	6b	4.36 - 68.84	EVA / PU	0.58	43.19 ± 8.2
65	6b	28.42 - 59.57	EVA / PU	0.75	53.75 ± 10.0

Table V.9: 4a/4b specimens results.

Table V.10 summarizes the firsts fixed arm peel tests results.

	Joint materials		Distance	Passes	Adhesive	Mean Peel Load [N/cm]	Adhesive fracture energy [J/m²]
1a	PA / Filled EVA	PA	10 mm	4 pas.	PU	1.68	94.95 ± 8.7
		EVA	5 mm	2 pas.			
1b	PA / Unfilled EVA	PA	10 mm	4 pas.	PU	1.48	92.79 ± 8.8
		EVA	5 mm	2 pas.			
2a	PA / Filled EVA	PA	5 mm	4 pas.	-	-	-
		EVA	5 mm	2 pas.			
2b	PA / Unfilled EVA	PA	5 mm	4 pas.	-	-	-
		EVA	5 mm	2 pas.			
3a	PA / Filled EVA	PA	5 mm	4 pas.	PU	1.72	97.14 ± 10.3
		EVA	5 mm	2 pas.			
3b	PA / Unfilled EVA	PA	5 mm	4 pas.	PU	1.32	87.20 ± 11.2
		EVA	5 mm	2 pas.			
4a	PA / Filled EVA	PA	-	-	PU	1.43	82.86 ± 11.5
		EVA	-	-			
4b	PA / Unfilled EVA	PA	-	-	PU	0.647	47.20 ± 8.2
		EVA	-	-			

Table V.10: 1-4 specimens type main results.

Results displayed in Table V.10 did not allow establishing which ones were best conditions to treat the surface, although there was a certain improvement in adhesion for both joints, with a considerable increment in joint resistance for the unfilled EVA.

Since only minor improvement was achieved for the filled EVA boosting the intensity of the plasma, two new sets of specimens have been realized reducing the intensity of treatment: these tests have been performed also to investigate the hypothesis that the severe adherends modification induced by the plasma could have started the surfaces degradation. For these reasons new samples have been prepared using a milder plasma treatment: 10

mm distance for only one pass. New samples preparation conditions are outlined in Table V.11.

n°	Bond materials		Plasma distance	Plasma passes	Adhesive
5a	PA / Filled EVA	PA	10 mm	1 pass (speed 1 cm/s)	PU
		EVA	10 mm	1 pass (speed 1 cm/s)	
5b	PA / Unfilled EVA	PA	10 mm	1 pass (speed 1 cm/s)	PU
		EVA	10 mm	1 pass (speed 1 cm/s)	
6a	PA / Filled EVA	PA	10 mm	1 pass (speed 1 cm/s)	-
		EVA	10 mm	1 pass (speed 1 cm/s)	
6b	PA / Unfilled EVA	PA	10 mm	1 pass (speed 1 cm/s)	-
		EVA	10 mm	1 pass (speed 1 cm/s)	

Table V.11: new specimens preparation parameters.

V.2.4.5   5a/5b

In Table V.12 the results obtained with 5a/5b specimens.

Specimen n°	Type	Analysed range [mm] (Crosshead displacement)	Fracture Interface	Peel Load [N/cm]	Fracture energy [J/m^2]
52	5a	16.52 - 60.32	PA / PU	1.70	96.23 ± 11.1
54	5a	2.03 - 17.52	PA / PU	2.28	125.1 ± 4.4
55	5a	5.77 - 74.8	PA / PU	2.08	114.9 ± 17.6
56	5a	2.85 - 27.18 43.09 - 67.52	PA / PU	2.07	114.7 ± 12.7
57	5a	3.82 - 73.03	PA / PU	2.00	110.9 ± 10.4
70	5a	27.82 - 74.68	PA / PU	1.64	93.24 ± 7.1
53	5b	2.08 - 69.38	PA / PU	1.78	113.0 ± 15.7
59	5b	9.07 - 58.47	PA / PU	1.99	124.0 ± 18.0
60	5b	4.57 - 45.29	PA / PU	1.96	122.7 ± 11.7
61	5b	11.76 - 44.72	PA / PU	1.92	120.8 ± 8.4
62	5b	10.74 - 75.53	PA / PU	1.85	117.1 ± 22.9

Table V.12: 5a/5b specimens results.

As for 4a/4b samples almost all the specimens prepared have been used and useful data have been obtained since few cases of mixed propagation occurred.

V.2.4.6   6a/6b

Since specimens 5a/5b revealed that a milder treatment had better effects on the junction strength, new samples have been prepared with mild plasma and no adhesive, to see if any

adhesion could be achieved without polyurethane glue. More than 10 of these samples have been prepared but none showed any degree of adhesion, simply falling apart when moved after 72 hours under pressure.

V.3   *Peel tests results and considerations*

In Table V.13 a complete list of the results obtained from fixed arm peel tests.

	Joint materials		Distance	Passes	Adhesive	Mean Peel Load [N/cm]	Adh. fracture energy [J/m²]
1a	PA / Filled EVA	PA	10 mm	4 pas.	PU	1.68	94.95 ± 8.7
		EVA	5 mm	2 pas.			
1b	PA / Unfilled EVA	PA	10 mm	4 pas.	PU	1.48	92.79 ± 8.8
		EVA	5 mm	2 pas.			
2a	PA / Filled EVA	PA	5 mm	4 pas.	-	-	-
		EVA	5 mm	2 pas.			
2b	PA / Unfilled EVA	PA	5 mm	4 pas.	-	-	-
		EVA	5 mm	2 pas.			
3a	PA / Filled EVA	PA	5 mm	4 pas.	PU	1.72	97.14 ± 10.3
		EVA	5 mm	2 pas.			
3b	PA / Unfilled EVA	PA	5 mm	4 pas.	PU	1.32	87.20 ± 11.2
		EVA	5 mm	2 pas.			
4a	PA / Filled EVA	PA	-	-	PU	1.43	82.86 ± 11.5
		EVA	-	-			
4b	PA / Unfilled EVA	PA	-	-	PU	0.647	47.20 ± 8.2
		EVA	-	-			
5a	PA / Filled EVA	PA	10 mm	1 pas.	PU	1.96	109.2 ± 10.5
		EVA	10 mm	1 pas.			
5b	PA / Unfilled EVA	PA	10 mm	1 pas.	PU	1.90	119.5 ± 15.3
		EVA	10 mm	1 pas.			
6a	PA / Filled EVA	PA	10 mm	1 pas.	-	≈ 0	≈ 0
		EVA	10 mm	1 pas.			
6b	PA / Unfilled EVA	PA	10 mm	1 pas.	-	≈ 0	≈ 0
		EVA	10 mm	1 pas.			

Table V.13: peel tests results.

Results outlined in Table V.13 indicate that a significantly high error is present in all results. This is not very surprising since in these tests a high scatter is always expected. Many considerations are carried out considering this fact and hence attributing a major importance to the mean values obtained.

In Table V.14 a comparison between the base case (no plasma) and the other combinations, where the adjective "severe" plasma refers to treatment 3a/b, "medium" refers to treatment 1a/b and "mild" to 5a/b:

	No plasma	Severe plasma		Medium plasma		Mild plasma	
	G_c [J/m^2]	G_c [J/m^2]	$\Delta\text{‰}_{0plasma}$	G_c [J/m^2]	$\Delta\text{‰}_{0plasma}$	G_c [J/m^2]	$\Delta\text{‰}_{0plasma}$
Filled EVA	82.86	97.14	**+17.23%**	94.95	**+14.59%**	109.2	**+31.78%**
Unfilled EVA	47.20	87.20	**+84.74%**	92.79	**+96.58%**	119.5	**+153.2%**

Table V.14: plasma treatments comparison.

Some conclusions can be drawn from results displayed in Table V.13 and Table V.14:

- All plasma treatment designed improved the adhesive resistance of the joint.
- For both EVAs the results obtained with "severe" and "medium" plasma treatment indicated comparable improvements in adhesion.
- With both EVAs the fracture energy obtained with samples prepared with "mild" plasma treatment was higher: this set of parameters (10mm 1pass for both materials) resulted to be the best to improve adhesive resistance.
- There was a noteworthy increment of adhesive resistance especially in the PA/Unfilled EVA joint, where adhesive fracture energy more than doubled with the mild plasma treatment.
- No technologically exploitable (nor precisely measurable) adhesion established in joints prepared with no glue and severe plasma treatment.
- No adhesion at all established in joints prepared without adhesive and mild plasma treatment.

In Graph V.9 peel test results are summarized. Graph V.10 shows instead the mean peel loads for all sets of tests: although peel load does not properly characterize the resistance of the joints (other parameters also influence it), it is easy and still commonly used.
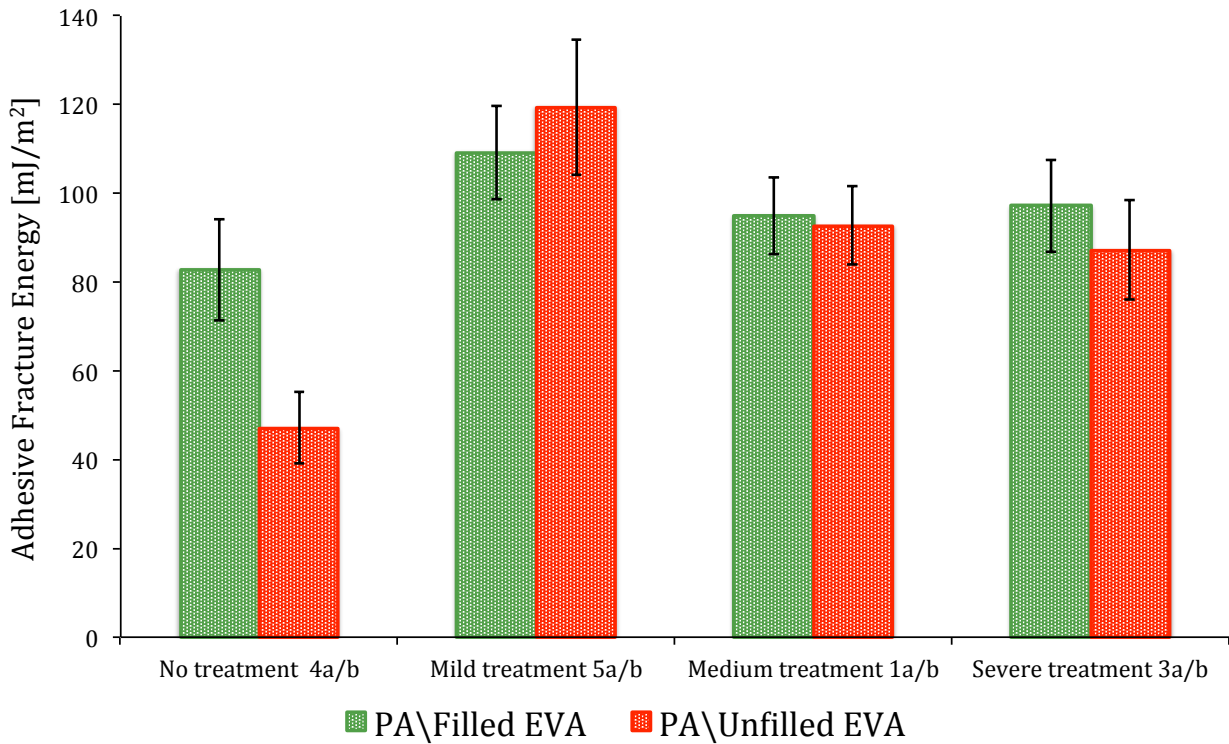
Graph V.9: histogram comparing adhesive fracture energies of different joints.
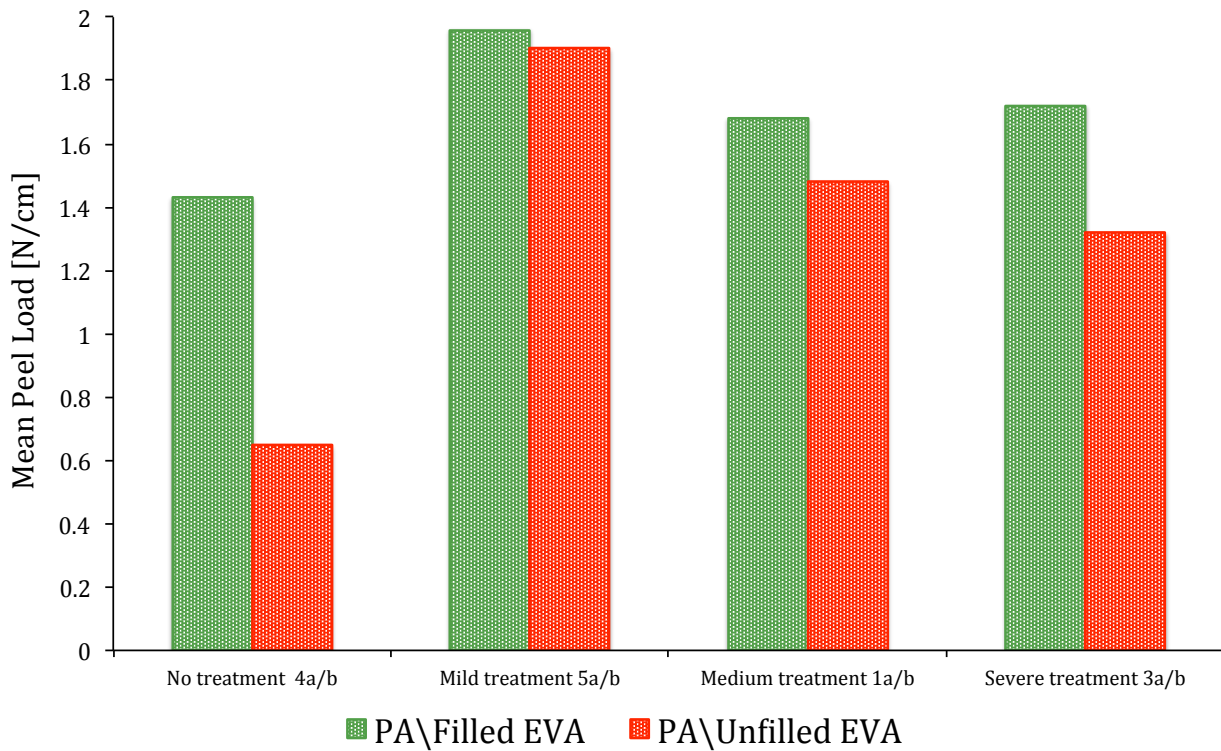
Graph V.10: histogram comparing mean peel loads of different joints.

V.4   Adhesive shear tests

Double lap joint samples have been prepared with the procedure explained in Chapter III using results outlined in Table V.13 where it has been proved that most effective plasma treatment to improve adhesion is performed with one pass at 10 mm distance. The double lap junctions named "unfoamed EVA" refer to the filled version of the blend.

The results of the Double Lap Joint tests are summarized in Table V.15:

n°	Junction	Junction area [mm^2]	Rupture Load [N]	Shear rupture stress [kPa]	Fracture type
2	PA 12 / Foamed EVA	681.0	385.5	565.3	Adhesive
3	PA 12 / Foamed EVA	756.3	(508.5)	-	Cohesive EVA
4	PA 12 / Foamed EVA	712.5	(444.5)	-	Cohesive EVA
5	PA 12 / Foamed EVA	737.5	(470.5)	-	Cohesive EVA
7	PA 12 / Unfoamed EVA	693.8	346.5	498.7	Adhesive
8	PA 12 / Unfoamed EVA	625.0	308.5	492.8	Adhesive
9	PA 12 / Unfoamed EVA	687.5	293.0	426.5	Adhesive
10	PA 12 / Unfoamed EVA	637.5	295.0	463.1	Adhesive

Table V.15: Double Lap Joint tests results.

Since not all the joints prepared with the foamed EVA broke with adhesive fracture but instead 3 out of 4 broke for tensile stress in the arm, Table V.16 shows the maximum shear stress held by the samples without breaking adhesively and the tensile stress which instead caused the rupture of the foamed arm of the double lap joint specimens.

n°	Junction	Junction area [mm^2]	Rupture Load [N]	Shear NON-rupture stress [kPa]	Tensile rupture stress [MPa]
3	PA 12 / Foamed EVA	756.3	(508.5)	671.1	3.450
4	PA 12 / Foamed EVA	712.5	(444.5)	623.8	3.016
5	PA 12 / Foamed EVA	737.5	(470.5)	637.8	3.192

Table V.16: foamed EVA double lap joints showing cohesive fracture results.

Table V.15 and Table V.16 confirm many interesting results:

- All of the DLJ specimens prepared with unfoamed EVA broke with adhesive fracture (since the adhesive left is highly deformed it is not possible to establish univocally which one is the weak interface).
- Only one of the DLJ prepared with the foamed EVA debonded: the others suffered tensile fracture of the EVA arm.
- The shear stresses held by the joints prepared with the foamed EVA are always higher (although comparable) than the ones causing adhesive fracture of the unfoamed EVA joints.

Peel tests confirmed that the weak interface in best performing joints was between the polyamide and the polyurethane adhesive. It has been proven that foamed EVA joints can withstand at least as much load as unfoamed EVA ones in shear stress conditions.

It has been said that adhesion is a surface phenomenon and it is therefore associated to surface-related mechanisms: this is not true for adhesive junctions. The mechanical performances of an adhesively bonded joint depend also on the adherends' (and adhesive's) mechanical behaviours. Since foamed EVA showed better shear adhesive resistance that its unfoamed counterpart it is highly probable it would outperform the unfoamed version also in peeling conditions, but additional investigation is required to prove it.

After mechanical tests established that the mildest plasma treatment was the most effective in improving adhesion, new surface energy analyses have been carried out to evaluate the surface energy increment caused by a 10mm-1pass plasma treatment. These new assessments have been performed with the same procedure outlined in Chapter II whose results have been explained in Chapter IV.
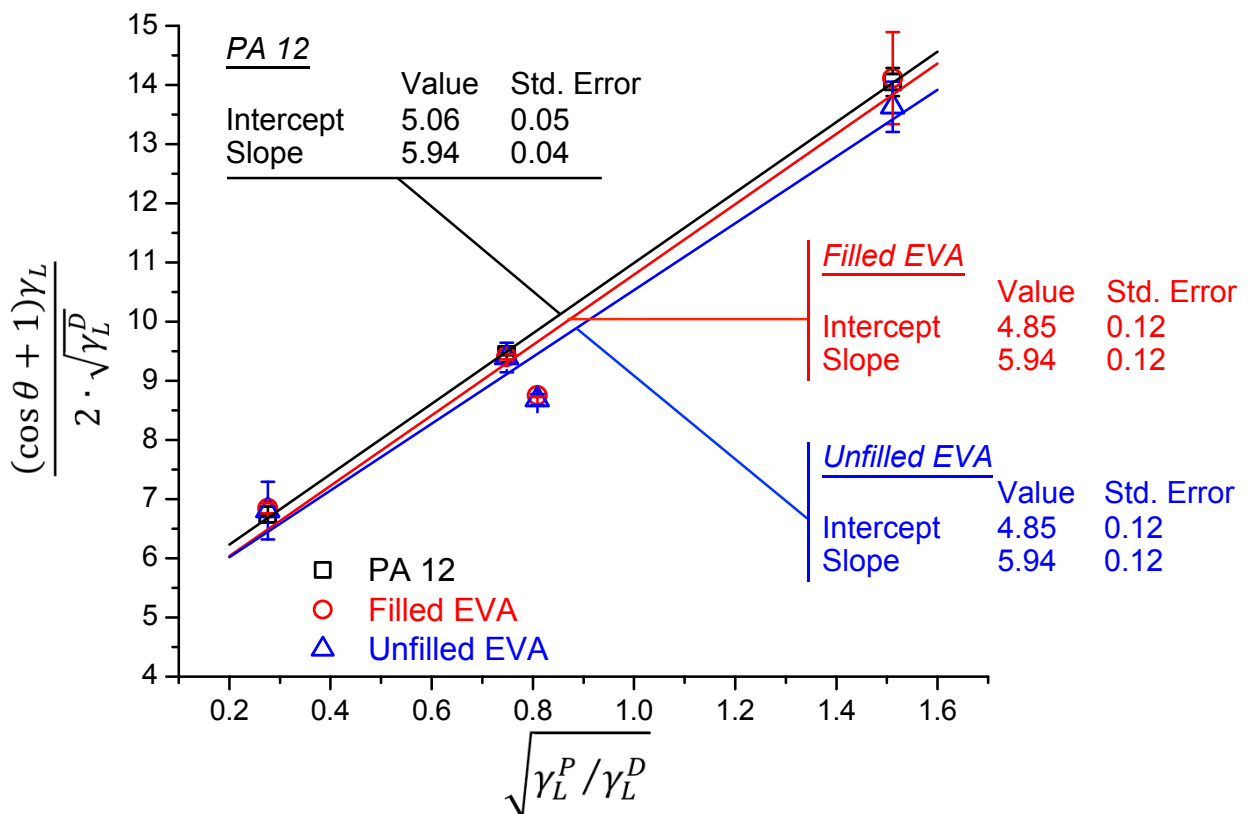
Graph V.11: PA 12, filled and unfilled EVA surface energy analysis OWRK method (plasma 10mm 1 pass).

In Graph V.11 the OWRK analyses for the three materials after mild plasma treatment are outlined. Graph V.11 shows only mean data for each point, but linear fitting have been

calculated on the entire set of data, as for the other OWRK analyses.

Table V.17 shows the results of new surface energy analyses.

10mm x 1 pass

	γ_S^P [mJ/m²]	γ_S^D [mJ/m²]	γ_S^{tot} [mJ/m²]
Polyamide 12	35.28 ± 0.95	25.59 ± 0.99	60.87 ± 1.88
Filled EVA	35.28 ± 2.70	23.52 ± 2.29	58.80 ± 3.72
Unfilled EVA	31.80 ± 2.94	23.91 ± 2.34	55.71 ± 3.75

Table V.17: results of OWRK analysis in all adherends after 10mm - 1 pass plasma treatment.

V.5   _Results comparison_

In Table V.18 is reported a comparison of surface energy values between the plasma treatment yielding the highest surface energy (named "medium plasma") and the one found to be the most effective by mechanical tests ("mild plasma");

	PA 12			Filled EVA			Unfilled EVA		
	γ_S^P [mJ/m²]	γ_S^D [mJ/m²]	γ_S^{tot} [mJ/m²]	γ_S^P [mJ/m²]	γ_S^D [mJ/m²]	γ_S^{tot} [mJ/m²]	γ_S^P [mJ/m²]	γ_S^D [mJ/m²]	γ_S^{tot} [mJ/m²]
No plasma	7.07	32.83	39.90	1.45	31.64	33.09	0.91	39.06	39.97
Mild plasma	35.28	25.59	60.87	35.28	23.52	58.80	31.80	23.91	55.71
Medium plasma	44.74	17.62	62.36	41.47	30.36	71.83	43.03	23.42	66.45

Table V.18: surface energies comparison between different plasma treatments.

In Table V.19 a recall of most important results obtained from peel tests, in the same plasma treatment conditions.

	PA 12 / Filled EVA		PA 12 / Unfilled EVA	
	Mean peel load [N/cm]	_Fracture energy_ [J/m²]	_Mean peel load_ [N/cm]	_Fracture energy_ [J/m²]
No plasma	1.43	82.86	0.647	47.20
Mild plasma	1.96	109.2	1.90	119.5
Medium plasma	1.68	94.95	1.48	92.79

Table V.19: adhesive fracture energies comparison between different plasma treatments.

A potential correlation between surface energy values and peel tests results should be found analysing data outlined in Table V.18 and Table V.19. To better understand possible correlations the different data are plotted in Graph V.12: adhesive fracture energies are reported on the ordinate while on the abscissa are plotted the total surface energies of the weak adherends of the joints. The fracture always propagated between the PU and one of the adherends: the EVA in the case of no plasma treatment and the PA 12 when surfaces have been treated.
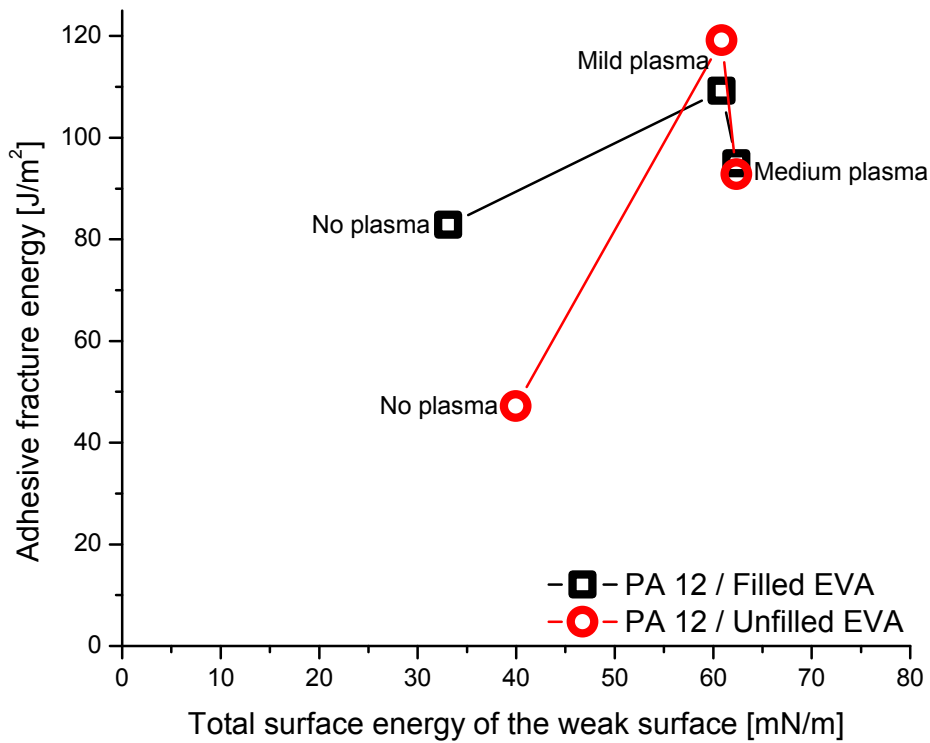
Graph V.12: adhesive fracture energy vs. total surface energy of the weak adherend; the labels indicate the plasma treatment adopted.

As shown in Graph V.12 there seems not to be a direct correlation in the data on the whole range; this is in agreement with what expressed by *Devries*: "A one-to-one correlation has never been established between the contact angle of an adhesive in a wetting test and the subsequent strength of the adhesive bond of the cured adhesive [18]"

It has been found that mild plasma treatment improves both adhesive fracture energy and surface energy of both polymers. This was not confirmed with the more intense treatment: an increment in surface energy did not correspond to an improvement in adhesive performances. This phenomenon might be due to the fact that the harsher plasma treatment started degrading the surface even if this did not result in any clear evidence. In this sense, further researches might include a chemical characterization of fracture surfaces to understand if what has been considered to be adhesive fracture between PA 12 and polyurethane adhesive has instead been cohesive fracture of a surface layer of PA 12.

VI. CHAPTER: CONCLUSIONS

The work investigated the many aspects concerning the establishment and improvement of adhesive phenomena in polymeric joints typically used in shoe production: polyamide and ethylene vinyl-acetate substrates have been jointed with polyurethane glue. Two different types of EVA have been investigated, and a third foamed version has been assessed with certain limitations.

The first part of the thesis concerned an adherends' surface energy investigation which determined polar and dispersive components through contact angle examinations and Owen-Wendt-Rabel-Kaelble analyses. First, polished polymers have been considered, finding that all materials exhibited surface energies as low as 30-40 mJ/m^2, with negligible polar components. A subsequent analysis investigated two different cleaning methods: a dry tissue wiping and a deep detergent cleaning. It has been found that different cleaning methods or surface polishing did not result in considerable surface energy dissimilarities.

A plasma treatment parameters optimization followed: by varying treatment distance and number of passes different conditions have been examined. Water contact angle has been used to establish which ones were best to obtain the strongest surface energy increment: 10 mm distance and 4 passes for the PA and 5mm - 2 passes for the EVA have been found to result in enhancing surface energies up to 60-70 mJ/m^2. OWRK analysis allowed confirming that this increment was due to a strong growth of the polar component, as expected.

The second part of the thesis involved mechanical tests to verify the effect of plasma on adhesion and to compare different treatment conditions. Fixed arm peel tests have been set up to assess the degree of adhesion in twelve different types of joints and tensile tests have been performed to evaluate certain mechanical features of the polymers. Three level of plasma intensity have been applied and assessed in joints prepared with polyurethane adhesive. The fundamentals of fracture mechanics have been exploited to calculate adhesive fracture energies in all cases. The junctions prepared with polyurethane glue demonstrated that the use of plasma has always been effective in increasing joint resistance, improving untreated bonding fracture energies from +15% to +150%, up to almost 120 J/m^2 with the mildest treatment.

Several tries have been carried out to obtain significant adhesion in junctions prepared with no glue, exploiting diffusive motes of polymer boosted by high temperature. These solutions resulted in minor or no adhesion, thus preventing them to be exploited in technological applications. To assess the adhesive properties of foamed EVA and to compare them with its unfoamed counterpart double lap shear tests have been performed. They allowed verifying

that foamed EVA displayed better shear adhesive properties that the unfoamed one, resisting to a shear stress up to almost 700 kPa.

Eventually, surface energy analysis and mechanical tests results have been merged. It has been found that although all plasma treatments resulted in both surface energy and fracture energy increment with respect to the base case, performing more intense plasma treatment after the mildest conditions causes a weakening of the junctions. This might have been due to surface degradation, although no experimental evidence proves it.

VI.1 *Further developments*

As explained, the results of surface energy analysis and the ones obtained from mechanical tests did not converge to the same results: although a certain plasma treatment led to the highest surface energies a milder treatment allowed obtaining tougher junctions. It would be interesting to understand the reasons for such discrepancy, which may be correlated to surface degradation. Further surface investigation would be required, to understand if polyamide fractured cohesively on a thin surface layer. X-ray or infrared analysis may be used, to verify if polyamide is present on the other side of the crack after the propagation.

VII. REFERENCES

1.   Comyn J., *Adhesion Science,* Royal Society of Chemistry Paperbaks, 1997.

2.   Singh S., *Effect of surface-treatment on adhesion of engineering materials*, in *Department of Mechanics*, Imperial college of London, 2010.

3.   Kinloch A.J., *Adhesion and adhesives, science and technology*: Chapman and Hall, 1987.

4.   Volland W., *Intermolecular forces*, available from: http://www.800mainstreet.com/08/0008-0012-interforce.html, 2005

5.   *"covalent bond"* and *"ionic bond"*, available from: http://hyperphysics.phy-astr.gsu.edu/hbase/chemical/bond.html.

6.   Adams R.D., *Adhesive Bonding; Science, technology and applications*: CRC Press, 2005.

7.   Young T., *An essay on the Cohesion of Fluids.* Phil. Trans. R. Soc. Lond., 1805.

8.   Bangham D.H. and Razouk R.I., *Adsorption and the wettability of solid surfaces.* Trans. of Faraday Society, 1937. **33**: p. 1459-1463.

9.   Li D., Cheng P., and Neumann A.W., *Contact angle measurement by axisymmetric drop shape analysis (ADSA).* Advanced Colloid and Interface Science, 1992. **39**.

10.   *The Zisman method*; Available from: http://www.kruss.de/en/theory/ measurements/contact- angle/models/zisman.html.

11.   Fox H.W., and Zisman W.A., *The spreading of liquids on low energy surfaces.* Journal of colloid science, 1950. **5**(6): p. 514 - 531.

12.   *The Equation of State model*; Available from: http://www.kruss.de/en/theory/ measurements/contact-angle/models/equation-of-state.html.

13.   Good J.R., *Contact angle, wetting and adhesion: a critical review.* Journal of Adhesion Science and Technology, 1992. **6**(12): p. 1269-1302.

14.   *The Owens-Wendt-Kaelble-Rabel method*; Available from: http://www.kruss.de/en/ theory/measurements/contact-angle/models/owrk.html.

15.   *The Wu method*; Available from: http://www.kruss.de/en/theory/measurements/ contact-angle/models/wu.html.

16.   Kinloch A.J., Kodokian G.K.A., Watts and J.F., *The adhesion of thermoplastic fibre composites.* Phil. Trans. R. Soc. Lond., 1992. **338**(1649): p. 83-112.

17.   *The Van Oss & Good method*; Available from: http://www.kruss.de/en/theory/ measurements/contact-angle/models/oss-good.html.

18.   Devries K.L., Adams D.O., (edited by Pocius A.V and Dillard D.A.), *Mechanical testing of adhesive joints (chapter 6 of "Adhesion science and engineering")*. 2002, Elsevier.

19.   *Adhesion theory*; Available from: http://www.chinahopson.com/en_Technical_3.asp.

20.   *Adhesion theories*; Available from: http://www.specialchem4adhesives.com/resources/adhesionguide/index.aspx.

21.   Kinlock A.J., *Interfacial fracture mechanical Aspects of adhesive Bonded Joints - A review.* Journal of adhesion, 1979. **10**(3): p. 193-219.

22.   Kim J. S., Kim Y. K. and Lee K. H., *Effect of atmospheric plasma treatment on the interfactial characteristics of ethylene-vinyl acetate/polyurethane composites.* Journal of colloid and interface science, 2004. **271**(2004): p. 187-192.

23.   Shenton M.J. and Stevens G.C., *Surface modification of polymer surfaces: atmospheric plasma versus vacuum plasma treatment.* Journal of applied physics, 2001. **34**(18).

24.   Stewart, R., et al., *Investigation and demonstration of the durability of air plasma pre-treatment on polypropylene autmotive bumpers.* International Journal of Adhesion and Adhesives, 2004. **4**(25): p. 93-99.

25.   Liston E.M., *Plasma treatment for improved bonding: a review.* Journal of adhesion, 1988. **30**(1-4): p. 199-218.

26.   Kaminska A., Kaczmarek H. and Kowalonek J., *The influence of side groups and polarity of polymers on the kind and effectiveness of their surface modification by air plasma action.* European Polymer Journal, 2002(38): p. 1915-1919.

27.   Steinbrecher, G., *Chracterization of the mode I fracture energy of adhesive joints.* International Journal of Adhesion and Adhesives, 2006. **26**: p. 644-650.

28.   Pavan A., *Notes of the course "Polymer Engineering"*, in *Dipartimento di Chimica, Materiali e Ingegneria Chimica "Giulio Natta"*, Politecnico di Milano: Milan, 2010.

29.   Caimmi F., *Sviluppo di una nuova prova per determinare la tenacità interlaminare di compositi polimerici in modo II a diverse velocità*, in *Dipartimento di Chimica, Materiali e Ingegneria Chimica "Giulio Natta"*, Politecnico di Milano: Milan, 2004

30.   Wang, C.H., *Introduction to fracture mechanics*, Airframe and Engines Division, Aeronautical and Maritime Research Laboratory, Australian department of defense, 1996.

31.   Kinloch A.J., Williams J.G., (edited by Pocius A.V and Dillard D.A.), *The mechanics of peel tests (*chapter 8 *"Adhesion science and engineering")* 2002: Elsevier.

32.   Moore D.R. and Williams J.G., *A Protocol for determination of the adhesive fracture toughness of flexible laminates by peel testing: Fixed arm and T-Peel methods*, 2007, ESIS.

33.   *ICPeel (digitised).* 2007; Available from:
        http://www3.imperial.ac.uk/meadhesion/testprotocols/peel.

34.   Mark F.H., *Encyclopedia of polymer science and engineering: volume 6* 1986: Wiley.

35.   Mascia L., *Thermoplastics: materials engineering.* Second edition, Applied Science
        Publisher, 1989.

36.   *Properties of polyamide 12.* Available from:
        http://cableorganizer.com/articles/materials-nylon12.html.

37.   Mark F.H. , *Encyclopedia of polymer science and engineering: volume 13* 1986: Wiley.

38.   ASTM International, *Standard Test Method for Measurement of the Surface Tension of
        Solid Cotings, Substrates and Pigment using Contact Angle Measurements*, 2008.

39.   *Surface Tension Table.* Available from: http://www.accudynetest.com/
        surface_tension_table.html?sortby=sort_st_disp.

40.   Van Oss C.J. and Good R.J., *Estimation of the polar surface tension parameters of
        glycerol and formamide, for use in contact angle measurements on polar solids.*
        Journal of Dispersion Science and Technology. **11**(1): p. 75-81.

41.   International Stardard Organization, *Peel test for a flexible-bonded-to-rigid specimen
        assembly, Part 1 90° peel*, in *ISO 8510-1 and ISO 8510-2*1990.

42.   ASTM International, *Standard Test Method for Tensile Properties of Plastics D638-10*,
        2010.

43.   British Standards InstitutionI, *Adhesives - Determination of tensile lap-shear strength
        of bonded assemblies*, 2009.

44.   Borcia G., Anderson C.A. and Brown N.M.D., *The surface oxidation of selected polymers
        using an atmospheric pressure air dielecttric barrier discharge. Part II.* Applied
        Surface Science, 2004(225).

45.   *Shoegoo data sheet.* Available from:
        http://eclecticproducts.com/_tds/sg_r01_tds.pdf.